**A Dissertation for the Degree of Doctor of Philosophy**

# Applications and Bactericidal Effects in Different Types of Plasma-Activated Water

## 플라즈마 활성수의 살균 효과 및 응용

**February 2021**

**Department of Agricultural Biotechnology**
**Graduate School**
**Seoul National University**

**Ki Ho Baek**

# Applications and Bactericidal Effects in Different Types of Plasma-Activated Water

Advisor: Cheorun Jo, Ph.D.

Submitting a Ph.D. Dissertation of Agriculture

December 2020

Department of Agricultural Biotechnology
Graduate School
Seoul National University

Ki Ho Baek

Confirming the Ph.D. Dissertation written by
Ki Ho Baek

December 2020

# 플라즈마 활성수의 살균 효과 및 응용

**Applications and Bactericidal Effects in Different Types of Plasma-Activated Water**

지도교수: 조 철 훈

이 논문을 농학박사 학위논문으로 제출함

2020년 12월

서울대학교 대학원

농생명공학부

백 기 호

백기호의 농학박사 학위논문을 인준함

2020년 12월

위 원 장 백 명 기 (인)

부위원장 조 철 훈 (인)

위 원 김 영 훈 (인)

위 원 김 갑 순 (인)

위 원 정 사 무 엘 (인)

# Overall Summary

A series of research results have been reported for the possible application of plasma-activated water (PAW) as a highly effective measure of pasteurization process. In the application perspective, there are various approaches including addition of chlorine, spray, micro- or nano-bubbles, and ultrasound-assisted synergy to make more effective and feasible. In addition, it is very important to understand the mechanism of action of the PAW in different forms of application. Therefore, the present experiments were conducted 1) to investigate the bactericidal effect and its mechanism of plasma-activated droplets generated from arc discharge plasma, 2) to identify the key reactive species and influence of organic matter for inactivating *Salmonella* Typhimurium by plasma bubbles, and 3) to confirm the possibility of synergistic bactericidal action between blue light and PAW against *Staphylococcus aureus* on stainless steel surfaces.

**Experiment I.**

**Antimicrobial effects and mechanism of plasma-activated droplets produced from arc discharge plasma on *Listeria monocytogenes* and *Escherichia coli* O157:H7**

In this study, the antimicrobial effects of plasma-activated droplet (PAD) produced from arc discharge plasma on planktonic *Listeria monocytogenes* and *Escherichia coli* O157:H7 was investigated. NaCl (0.9%, w/v) was used as the feeding solution for the plasma discharge. The inactivation mechanism of the PAD treatment was also investigated. PAD mainly contains $H_2O_2$ and $OCl^-$, which play a significant role in the inactivation process against *L. monocytogenes* and *E. coli* O157:H7. The population of *L. monocytogenes* and *E. coli* O157:H7 was significantly reduced by approximately 3 and 4 log units, respectively, within 5 min of PAD exposure. However, the bactericidal effects of PAD against *L. monocytogenes* and *E. coli* O157:H7 showed different trends by showing 0.58 and 4.13 log reductions, respectively, after 1 min of PAD exposure time. The change of membrane integrity was evaluated using two DNA-binding fluorescence dyes, SYTO 9 and propidium iodide (PI). The breakage of the cell wall and membrane of both microorganisms was evidenced by the uptake of PI by cells after 5 min of PAD exposure, but the effect was less in *L. monocytogenes* compared to *E. coli* O157:H7 after 1 min of PAD exposure time. The transmission electron microscopy results clearly showed morphological changes in both microorganisms, including denaturation or leakage of intracellular materials as a consequence of PAD treatment. These findings suggest that PAD-induced chemical species can

eventually affect the intracellular materials of bacterial cells by passing through or attacking the cell envelope. In addition, *L. monocytogenes* is less susceptible to PAD compared with *E. coli* O157:H7.

**Experiment II.**

**Inactivation of *Salmonella* Typhimurium by non-thermal plasma bubbles: Exploring the key reactive species and influence of organic matter**

The key reactive species generated by non-thermal plasma bubbles for the inactivation of *Salmonella* Typhimurium and the effects of organic matter on the inactivation efficacy were investigated. Plasma, which is primarily composed of ozone ($O_3$), was generated by dielectric barrier discharge and injected into a solution as a bubble. The population of viable *S.* Typhimurium decreased in proportion to the treatment time, resulting in a 5.29 log reduction after 5 min of treatment. Verification tests to specify key reactive species were conducted using an $O_3$ destruction unit and reactive oxygen species scavengers. The results indicated that singlet oxygen ($^1O_2$) contributes substantially to the inactivation of *S.* Typhimurium, and that the presence of superoxide anion radicals ($O_2^{\cdot-}$) from $O_3$ is essential for the production of $^1O_2$. When a *S.* Typhimurium suspension containing organic matter (final concentration: 0, 0.005, 0.05, 0.1, and 0.5 g/L), consisting of beef extract and peptone, was treated with plasma bubbles for 5, 10, 15, 20, 25, and 30 min, respectively, the potential of the plasma bubbles for inactivating *S.* Typhimurium successfully was verified with longer contact time, despite organic matter attenuating the inactivation efficiency in a dose-dependent manner.

**Experiment III.**

**Blue light promotes bactericidal action of plasma- activated water against *Staphylococcus aureus* on stainless steel surfaces**

The study was conducted to investigate the effects of blue light on the enhancement of bactericidal effect of plasma-activated water (PAW) against *Staphylococcus aureus* on stainless steel surfaces by inducing the photolysis of staphyloxanthin (STX). A light-emitting diode (LED; central emission wavelength, 466 nm; light intensity, 18.74 mW/cm$^2$) was used for blue light treatment, and encapsulated atmospheric pressure plasma generator (2.2 kHz, 4.2 kV) was applied for PAW treatment. When STX extract was treated with blue light (0, 30, 60, 90, and 150 J/cm$^2$), the absorbance value at 460 nm significantly decreased in a dose-dependent manner, and became completely transparent at dose of 150 J/cm$^2$. After combined treatment with blue light (150 J/cm$^2$) and PAW (10 min), the surviving population of *S. aureus* decreased by 2.70 log CFU/mL, which was about 40 times higher than that after plasma single treatment. In addition, 10 min of post plasma treatment in combined treatment group showed more than 6.66 log CFU/mL reduction compared to the control group, resulting in non-detectable levels (detection limit: 1 log CFU/mL). Blue light (150 J/cm$^2$) treatment increased the absorbance values at 260 and 280 nm, indicating the possibility of damage to cell membranes, which was also identified by an increase in the SYTOX$^{TM}$ green fluorescence signal. The synergistic bactericidal effect of blue light (150 J/cm$^2$) and PAW (15 min) against *S. aureus* was also observed in stainless steel coupons.

**Keyword:** Atmospheric-pressure plasma, Plasma-activated water, Plasma activated-droplet, Plasma bubble, Reactive oxygen species, Bactericidal effect, Pathogenic bacteria, Blue light

**Student number:** 2017-37213

# Contents

# List of Tables

**Chapter I.**



**Chapter II.**



**Chapter III.**

# List of Figures

**Chapter I.**



**Chapter II.**

**Chapter III.**

**Chapter IV.**

# List of Abbreviations

| | | |
|---|---|---|
| AC | : | Alternating current |
| APP | : | Atmospheric pressure plasma |
| CFU | : | Colony forming unit |
| DBD | : | Dielectric barrier discharge |
| FWHM | : | Full width at half maximum |
| PAD | : | Plasma-activated droplet |
| PAW | : | Plasma-activated water |
| PBS | : | Phosphate-buffered saline |
| PI | : | Propidium iodide |
| PTFE | : | Polytetrafluoroethylene |
| RNS | : | Reactive nitrogen species |
| ROS | : | Reactive oxygen species |
| RONS | : | Reactive oxygen/nitrogen species |
| SFP | : | Staphylococcal food poisoning |
| STX | : | Staphyloxanthin |
| TEM | : | Transmission electron microscopy |
| TEMP | : | 2,2,6,6-tetramethylpiperidine |
| TSA | : | Tryptic soy agar |
| TSB | : | Tryptic soy broth |
| UV/Vis | : | Ultraviolet visible |

# Chapter I.

# General introduction

## 1.1. Food safety

### *1.1.1. Definition*

Safe food is a product that is rich in health-enhancing substances that can be consumed without becoming ill (Hansen et al., 2002) (Table 1). Food safety is a factor that should be considered in all aspects, from the production of food to the final consumption.

Table 1. Definition of food safety (modified from Hansen et al., 2002)

| **Food safety** |
|---|
| **Product safety** |
| Safety, non-toxicity of the food |
| Safety, nutritious food |
| Safety of the declaration (all components are shown on a declaration[1]) |
| Safety of the label (the organic food is truly organic) |
| **Agri-food-system safety** |
| Safety of supply |
| Safety of distribution |
| Safety of transparency and proximity |
| Safety of consumer influence on food production |
| Safety of information on the whole food production process |
| Safety, no negative impacts of production practices on humans and other living organisms, the environment, climate etc. |

[1]Danish authorities

*1.1.2. Foodborne disease*

Foodborne pathogens have had a tremendous impact on food safety due to health risks caused by consumption of food contaminated with pathogenic bacteria (Ma et al., 2018). During 2009-2015, Foodborne Disease Outbreak Surveillance Systems (FDOSS) received reports of 1,906 outbreaks, resulting in 42,546 illnesses, 4,731 hospitalizations, and 131 deaths caused by bacterial etiology (Dewey-Mattia et al., 2018) (Table 2). In addition, cases of foodborne illnesses caused by pathogenic bacteria have been consistently reported around the world until recently (Lee and Yoon, 2020) (Table 3). Major pathogenic bacteria include *Escherichia coli* O157:H7, *Salmonella* sp., *Listeria monocytogenes*, and *Staphylococcus aureus*, and in particular *E. coli* O157:H7 and *L. monocytogenes* are known as fatal pathogenic bacteria because they are highly toxic and can cause disease at low doses (Hyun et al., 2020). In addition, *Salmonella* is the most common microorganism in the United States that can cause foodborne illness, hospitalization, and death (Park et al., 2017) (Table 2). *S. aureus* can also be contaminated with food and produce Staphylococcal enterotoxin, which can lead to Staphylococcal Food Poisoning (SFP) (Fetsch and Johler, 2018), and about 240,000 cases per year in the United States are reported to occur, resulting in 1,000 hospitalizations (Scallan et al., 2011). Therefore, proper control of these pathogenic microorganisms is the most important aspect in terms of food safety.

Table 2. Number of foodborne disease outbreaks, outbreak-associated illnesses, hospitalizations, and deaths by bacterial etiology in the United States and Puerto Rico (2009-2015) (modified from Dewey-Mattia et al., 2018)

| Bacterial etiology | Outbreaks | Illnesses | Hospitalizations | Deaths |
|---|---|---|---|---|
| | No. | No. | No. | No. |
| *Bacillus cereus* | 65 | 839 | 6 | 0 |
| *Campylobacter* | 201 | 2,309 | 151 | 1 |
| *Clostridium perfringens* | 198 | 7,834 | 18 | 4 |
| *Escherichia coli* (STEC[1]) | 203 | 2,465 | 693 | 13 |
| *Listeria monocytogenes* | 36 | 388 | 341 | 75 |
| *Salmonella* | 949 | 24,172 | 3,207 | 29 |
| *Shigella* | 39 | 1,226 | 110 | 1 |
| *Staphylococcus aureus* | 75 | 1,681 | 86 | 0 |
| *Vibrio parahaemolyticus* | 49 | 280 | 20 | 0 |
| Other | 91 | 1,352 | 99 | 8 |
| Total | 1,906 | 42,546 | 4,731 | 131 |

[1]Shiga toxin-producing *E. coli*

Table 3. Number of foodborne illnesses in the United States (2017), European Union (2016), Korea (2018), and Japan (2018) (modified from Lee and Yoon, 2020)

| Hazards | United States | European Union | Korea | Japan |
|---|---|---|---|---|
| | 2017 | 2016 | 2018 | 2018 |
| *Bacillus cereus* | 341 | NA[1] | NA | NA |
| *Campylobacter* | 147 | 246,307 | 453 | 1,995 |
| *Clostridium botulinum* | 17 | NA | NA | NA |
| *Clostridium perfringens* | 843 | NA | 679 | 2,319 |
| Pathogenic *Escherichia coli* | 562 | 6,378 | 2,715 | 860 |
| *Listeria monocytogenes* | 32 | 2,536 | NA | NA |
| Non-typhoidal *Salmonella* | 3,061 | 94,530 | 3,516 | 640 |
| *Shigella* | 54 | NA | NA | NA |
| *Staphylococcus aureus* | 128 | NA | 52 | 405 |
| *Yersinia enterocolitica* | 0 | 6,861 | NA | NA |
| Total | 5,185 | 356,612 | 7,415 | 6,219 |

[1]Not applicable

## 1.2. Plasma-activated water (PAW)

### *1.2.1. Definition*

PAW is defined as 'the product of atmospheric plasma reacting with water, whereby the ionized gas reacts within or with the surface of water to create reactive species within the water' (Darmanin et al., 2020). Various approaches have been applied to generate PAW or to treat plasma directly for specific targets (such as bacteria, organic matter, etc.) present in water (Esua et al., 2020; Ke et al., 2018; Ma et al., 2017; Rahimpour et al., 2019; Zhou et al., 2019) (Fig. 1). Various reactive molecules, commonly called reactive oxygen and nitrogen species (RONS), can be generated by gas-phase discharges and can dissolve or penetrate the liquid to produce secondary reactive species (Lukes et al., 2014). Secondary aqueous RONS, such as hydroxyl radicals ($OH^{\bullet}$), hydrogen peroxide ($H_2O_2$), singlet oxygen ($^1O_2$), superoxide anion/perhydroxyl radical ($O_2^{\bullet-}/HO_2^{\bullet}$), ozone ($O_3$), nitrite/nitrate ($NO_2^-/NO_3^-$) and peroxynitrites/peroxynitrous acid ($ONOO^-$/ONOOH), can initiate chemical and biocidal processes in the liquid (Machala et al., 2018). Therefore, PAW could be utilized to increase the rate of biofilm removal, bacteria/viruses inactivation, and cancer therapy in biomedicine (Zhou et al., 2019). In terms of agriculture, application of PAW span promotion of seed and plant growth, inactivation of pathogenic organisms, and curing fungus-infected plants (Zhou et al., 2020). PAW is considered an economical and eco-friendly green technology because it can be generated using air without the need to use any chemical agents and water can be recycled continuously (Zhou et al., 2020).

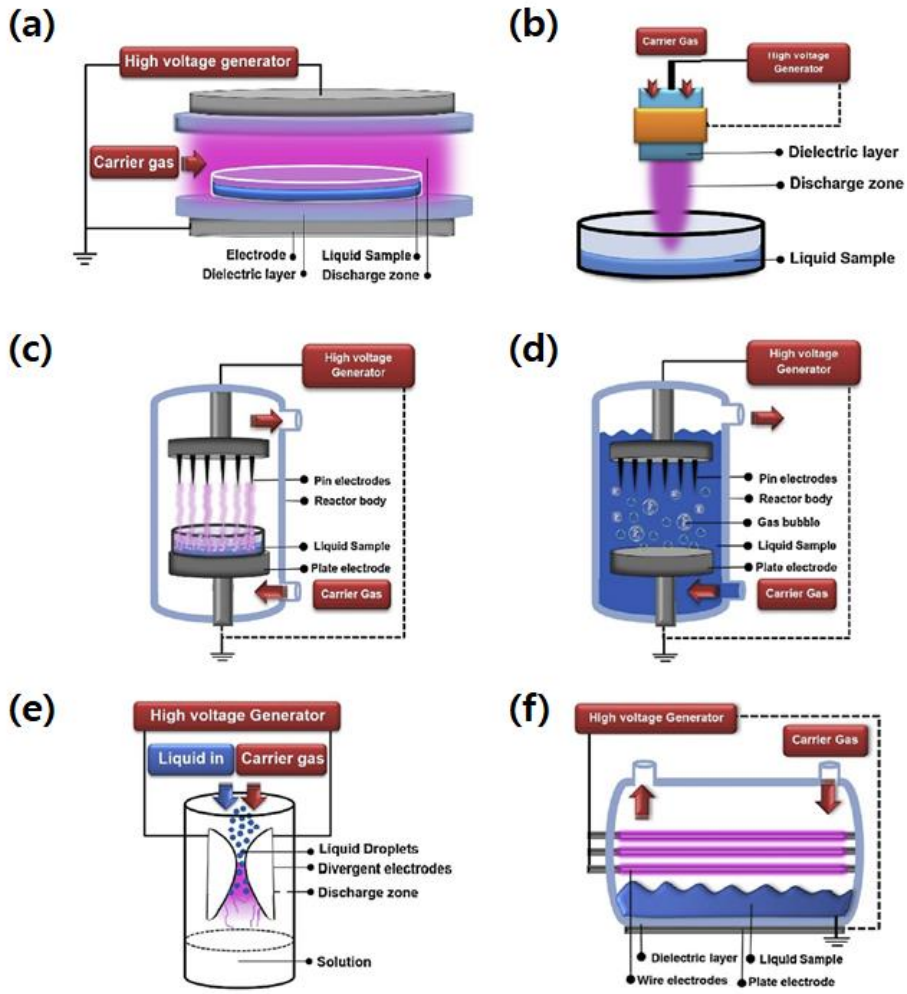


Figure 1. Various plasma-activated water (PAW) generation systems (modified from Rahimpour et al., 2019). (a) flat plate dielectric barrier discharge plasma; (b) radio frequency driven plasma jet; (c, d) pin-to-plate corona discharge; (e) gliding arc discharge; (f) pulsed corona discharge.

*1.2.2. PAW for microbial inactivation*

*1.2.2.1 Factors involved in microbial inactivation*

Many researchers have conducted studies to inactivate pathogenic bacteria that exist in water by activating plasma into water using various devices and conditions (Table 4). Ji et al., (2018) suggested that plasma bubble treatment for water mainly produce a certain level of $H_2O_2$ and $NO_3^-$, which enabled the pasteurization of *S. aureus* and *E. coli* present in the water by 3.6 and 6.3 log CFU/mL respectively. Ma et al. (2020) confirmed that *E. coli* can be inactivated by more than 6 log CFU/mL through PAW treatment, and suggested that peroxynitric acid ($O_2NOOH$) produced by the reaction of peroxynitrous acid (ONOOH) and $H_2O_2$ can eventually be decomposed into $O_2^{\cdot-}$ and $^1O_2$, contributing to the bactericidal action. They suggested the possibility that short-lived reactive species could be generated through subsequent reactions even after the discharge was terminated. Xiang et al. (2018) confirmed that exposure of *Pseudomonas deceptionensis* CM2 to PAW for 10 min showed bactericidal effect of more than 5 log accompanied by cell membrane damage. They also demonstrated that $H_2O_2$, $NO_2^-$, and $NO_3^-$ contained in PAW play a key role for inactivation of bacteria in acidic pH. These studies show that plasma can be applied to water in various ways, and that PAW can contribute to inactivation of microorganisms in the short or long term, and its efficiency differs from those contributing to inactivation of microorganisms under detailed conditions such as plasma type, discharge condition, and target samples.

Table 4. Bactericidal effect on pathogenic or spoilage bacteria by plasma treatment in solution (liquid-gas interface or underwater treatment)

| Plasma types | Conditions | PAW parameters | Log reduction | References |
|---|---|---|---|---|
| DBD[1] | Air, 20 kHz, 5.74 kV, 3 min | pH: 4.4, $H_2O_2$: 13.68 μM, $NO_3$: 138 μM | *E. coli*: 6.30<br>*S. aureus*: 3.60 | Ji et al. (2018) |
| DBD | $N_2$ gas, 15 kVpp, 60 min | ROS (volume, $\times 10^5$): 104 | *P*[2]*. aeruginosa* PA01: >8.0<br>*S. aureus*: >8.0 | Kim et al. (2018) |
| DBD | Air, 20 kHz, 18 kV, 2 min | $H_2O_2$: $2.5\times10^{-6}$ M,<br>·OH formation rate: $2.35\times10^{-8}$ M/s | *E. coli*: 6.0 | Khan et al. (2015) |
| DBD | Air, 4 kV, 40 W, 15 min | - | *E. coli* biofilm: ~83%<br>(biomass reduction) | Zhou et al. (2019) |
| DC[3] plasma | Air, 18 kV, 5 min | pH: 2.8, $H_2O_2$: 827 μM, $NO_2^-$: 60 μM, $NO_3^-$: 1954 μM, $ONOO^-$: ~30 μM | *E. coli*: >6.0 | Ma et al. (2020) |
| DC plasma | Air, 10 kV, 20 min | $H_2O_2$: 79.56 mg/L, $NO_2^-$: 48.17 mg/L, $NO_3^-$: 27.95 mg/L, $O_3$: 2.99 mg/L | *E. coli*: 6.56<br>*S. aureus*: 5.35 | Xu et al. (2018) |
| Plasma arc | Air, 3 kV, 200 W, 30 min | pH: 7.18, $H_2O_2$: 20 mg/L | *E. coli*: >6.0 | Hwang et al. (2018) |
| Plasma jet | Air, 750 W, 1 min | pH: 2.80, $H_2O_2$: 24.33 μM,<br>$NO_2^-$: 1162.67 μM, $NO_3^-$: 1384.49 μM | *P. deceptionensis* CM2: 5.78<br>(PAW treatment time: 10 min) | Xiang et al. (2018) |

[1]Dielectric barrier discharge

[2]*Pseudomonas*

[3]Direct current

*1.2.2.2 Mechanisms of microbial inactivation*

Various reactive species are involved in the interaction between plasma and organisms, which is a complex process (Wu et al., 2017). Inactivation of microorganisms by plasma may result in different efficiency depending on the properties of plasma or target microorganisms. In this regard, many researchers have suggested that extracellular structural differences between Gram-positive and negative bacteria can have a significant impact on the sensitivity of bacteria to plasma. Reactive species can react with both lipopolysaccharide and peptidoglycan, leading to damage the molecular structure by decomposing C-C, C-N, and C-O bonds (Han et al., 2016). Since Gram-positive bacteria have a relatively thick peptidoglycan layer compared to Gram-negative bacteria (Mai-Prochnow et al., 2016), two different mechanisms are proposed for these two types of bacteria. For Gram-negative bacteria, reactive species can directly damage cell walls and membranes, leading to death, while in the case of Gram-positive bacteria, reactive species must penetrate cell walls and membranes or do relatively more damage to react with intracellular materials (Huang et al., 2020) (Fig. 2). In addition, many researchers have studied biofilms that show strong resistance to a variety of external factors. Zhou et al. (2019) suggested that plasma-induced ·NO species interact with cell receptors, reducing the intracellular second messenger and biofilm regulator cyclic-di-guanosine monophosphate, thereby weakening the antibacterial resistance to PAW (Fig. 3). Thus, the inactivation mechanism of pathogenic bacteria by reactive species has been presented in various aspects, which can contribute to the improvement of the applicability

and efficiency of PAW.

Therefore, the objective of this study was to enhance the application of PAW for microbial inactivation by applying various techniques, and to identify each mechanism.

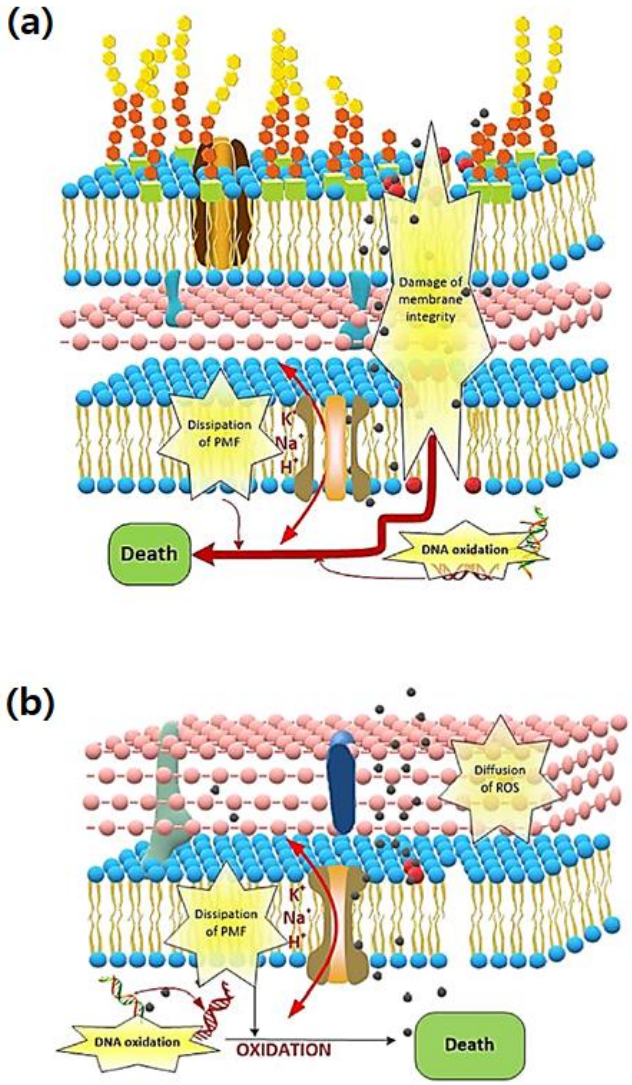


Figure 2. Plasma-related (a) *S.* Typhimurium and (b) *S. aureus* inactivation (reprinted from Huang et al., 2020).

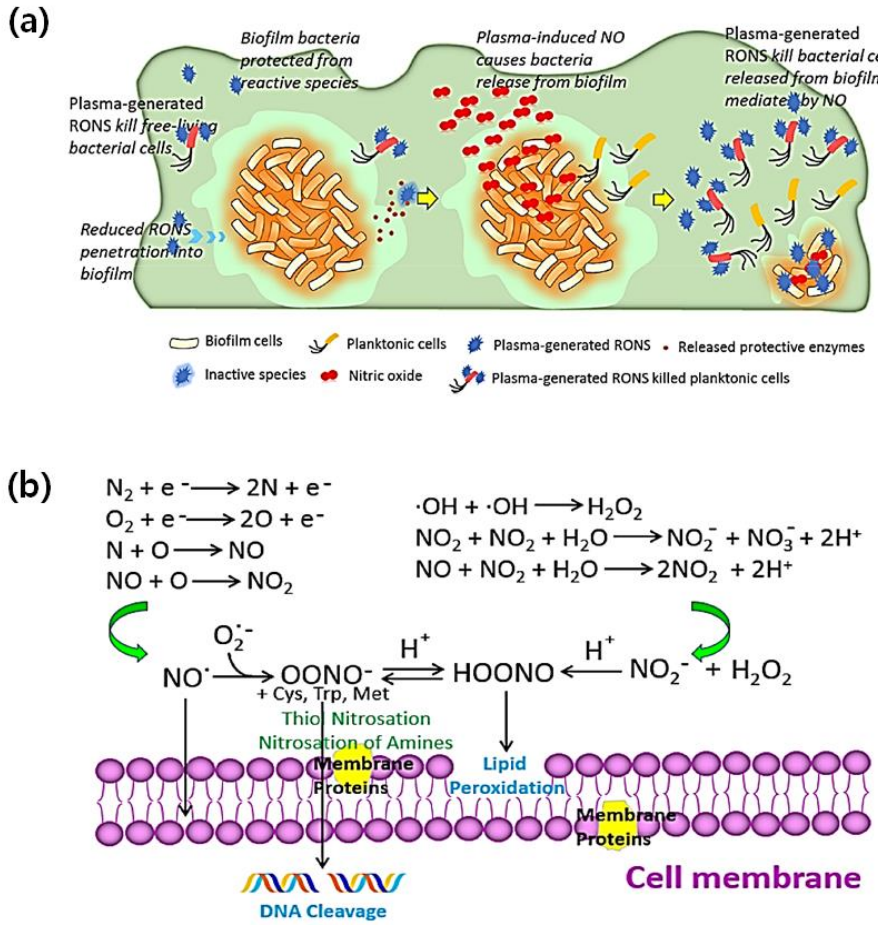


Figure 3. (a) Plasma-derived NO in biofilm dispersal and (b) antibacterial mechanisms of NO and its byproducts lead to decreased bacterial viability (modified from Zhou et al., 2019).

**References**


Becker, T. (2000). Consumer perception of fresh meat quality: A framework for analysis. *British Food Journal*, *102*, 158-176.

Calkins, C. R., & Hodgen, J. M. (2007). A fresh look at meat flavor. *Meat Science*, *77*, 63-80.

Darmanin, M., Kozak, D., de Oliveira Mallia, J., Blundell, R., Gatt, R., & Valdramidis, V. P. (2020). Generation of plasma functionalized water: Antimicrobial assessment and impact on seed germination. *Food Control*, *113*, 107168.

Dewey-Mattia, D., Manikonda, K., Hall, A. J., Wise, M. E., & Crowe, S. J. (2018). Surveillance for foodborne disease outbreaks—United States, 2009–2015. *MMWR Surveillance Summaries*, *67*, 1-11.

Esua, O. J., Cheng, J. H., & Sun, D. W. (2020). Functionalization of water as a nonthermal approach for ensuring safety and quality of meat and seafood products. *Critical Reviews in Food Science and Nutrition*, 1-19.

Fetsch, A., & Johler, S. (2018). *Staphylococcus aureus* as a foodborne pathogen. *Current Clinical Microbiology Reports*, *5*, 88-96.

Han, L., Patil, S., Boehm, D., Milosavljević, V., Cullen, P. J., & Bourke, P. (2016). Mechanisms of inactivation by high-voltage atmospheric cold plasma differ for *Escherichia coli* and *Staphylococcus aureus*. *Applied and Environmental Microbiology*, *82*, 450-458.

Hansen, B., Alrøe, H. F., Kristensen, E. S., & Wier, M. (2002). Assessment of food safety in organic farming. *DARCOF Working Papers*, *52*, 1-24.

Huang, M., Zhuang, H., Zhao, J., Wang, J., Yan, W., & Zhang, J. (2020). Differences in cellular damage induced by dielectric barrier discharge plasma between *Salmonella* Typhimurium and *Staphylococcus aureus*. *Bioelectrochemistry*, *132*, 107445.

Hwang, I., Jeong, J., You, T., & Jung, J. (2018). Water electrode plasma discharge to enhance the bacterial inactivation in water. *Biotechnology & Biotechnological Equipment*, *32*, 530-534.

Hyun, J. E., Moon, S. K., & Lee, S. Y. (2020). Antibacterial activity and mechanism of 460–470 nm light-emitting diodes against pathogenic bacteria and spoilage bacteria at different temperatures. *Food Control*, 107721.

Ji, S. H., Ki, S. H., Ahn, J. H., Shin, J. H., Hong, E. J., Kim, Y. J., & Choi, E. H. (2018). Inactivation of *Escherichia coli* and *Staphylococcus aureus* on contaminated perilla leaves by dielectric barrier discharge (DBD) plasma treatment. *Archives of Biochemistry and Biophysics*, *643*, 32-41.

Ke, Z., Chen, Z., & Huang, Q. (2018). Effect of chloride on bacterial inactivation by discharge plasma at the gas-solution interface: Potentiation or attenuation?. *Plasma Processes and Polymers*, *15*, 1700153.

Khan, M. S. I., Lee, E. J., & Kim, Y. J. (2015). Roles of individual radicals generated by a submerged dielectric barrier discharge plasma reactor during *Escherichia coli* O157:H7 inactivation. *AIP Advances*, *5*, 107111.

Kim, T., Seo, H., Bae, H., Kim, T., Yang, S., & Moon, E. (2018). Generation of active species and antimicrobial efficacy of an underwater plasma

device equipped with a porous bubbler. *Plasma Processes and Polymers*, *15*, 1700229.

Lee, H., & Yoon, Y. (2020). Etiological Agents Implicated in Foodborne Illness World Wide. *Food Science of Animal Resources*.

Lukes, P., Dolezalova, E., Sisrova, I., & Clupek, M. (2014). Aqueous-phase chemistry and bactericidal effects from an air discharge plasma in contact with water: evidence for the formation of peroxynitrite through a pseudo-second-order post-discharge reaction of $H_2O_2$ and $HNO_2$. *Plasma Sources Science and Technology*, *23*, 015019.

Ma, D. S., Tan, L. T. H., Chan, K. G., Yap, W. H., Pusparajah, P., Chuah, L. H., Ming, L. C., Khan, T. M., Lee, L. H., & Goh, B. H. (2018). Resveratrol—potential antibacterial agent against foodborne pathogens. *Frontiers in Pharmacology*, *9*, 102.

Ma, M., Zhang, Y., Lv, Y., & Sun, F. (2020). The key reactive species in the bactericidal process of plasma activated water. *Journal of Physics D: Applied Physics*, *53*, 185207.

Ma, S., Kim, K., Huh, J., & Hong, Y. (2017). Characteristics of microdischarge plasma jet in water and its application to water purification by bacterial inactivation. *Separation and Purification Technology*, *188*, 147-154.

Machala, Z., Tarabová, B., Sersenová, D., Janda, M., & Hensel, K. (2018). Chemical and antibacterial effects of plasma activated water: correlation with gaseous and aqueous reactive oxygen and nitrogen species, plasma

sources and air flow conditions. *Journal of Physics D: Applied Physics*, *52*, 034002.

Mai-Prochnow, A., Clauson, M., Hong, J., & Murphy, A. B. (2016). Gram positive and Gram negative bacteria differ in their sensitivity to cold plasma. *Scientific Reports*, *6*, 38610.

Rahimpour, M., Taghvaei, H., Zafarnak, S., Rahimpour, M. R., & Raeissi, S. (2019). Post-discharge DBD plasma treatment for degradation of organic dye in water: A comparison with different plasma operation methods. *Journal of Environmental Chemical Engineering*, *7*, 103220.

Scallan, E., Hoekstra, R. M., Angulo, F. J., Tauxe, R. V., Widdowson, M. A., Roy, S. L., Jones, J. L., & Griffin, P. M. (2011). Foodborne illness acquired in the United States—major pathogens. *Emerging Infectious Diseases*, *17*, 7-15.

Xiang, Q., Kang, C., Niu, L., Zhao, D., Li, K., & Bai, Y. (2018). Antibacterial activity and a membrane damage mechanism of plasma-activated water against *Pseudomonas deceptionensis* CM2. *LWT*, *96*, 395-401.

Wu, S., Zhang, Q., Ma, R., Yu, S., Wang, K., Zhang, J., & Fang, J. (2017). Reactive radical-driven bacterial inactivation by hydrogen-peroxide-enhanced plasma-activated-water. *The European Physical Journal Special Topics*, *226*, 2887-2899.

Xu, Z., Cheng, C., Shen, J., Lan, Y., Hu, S., Han, W., & Chu, P. K. (2018). In vitro antimicrobial effects and mechanisms of direct current air-liquid discharge plasma on planktonic *Staphylococcus aureus* and *Escherichia coli* in liquids. *Bioelectrochemistry*, *121*, 125-134.

Zhou, R., Zhou, R., Wang, P., Luan, B., Zhang, X., Fang, Z., Xian, Y., Lu, X., Ostrikov, K. K., & Bazaka, K. (2019). Microplasma bubbles: reactive vehicles for biofilm dispersal. *ACS Applied Materials & Interfaces*, *11*, 20660-20669.

Zhou, R., Zhou, R., Wang, P., Xian, Y., Mai-Prochnow, A., Lu, X., Cullen, P. J., Ostrikov, K. K., & Bazaka, K. (2020). Plasma-activated water: generation, origin of reactive species and biological applications. *Journal of Physics D: Applied Physics*, *53*, 303001.

This chapter comprises a part of a paper published in Journal of Physics D: Applied Physics as a partial fulfillment of Ki Ho Baek's Ph.D. program

# Chapter II.

# Antimicrobial effects and mechanism of plasma-activated droplets produced from arc discharge plasma on *Listeria monocytogenes* and *Escherichia coli* O157:H7

## 2.1. Introduction

In recent years, with the increasing consumption of various food products, foodborne outbreaks have been constantly reported (Yong et al., 2015; Seo et al., 2016; Karyotis et al., 2017). These outbreaks can occur from every step of production through farms, post harvesting, transportation, slaughtering, storage, distribution, and finally consumption. In practice, contaminated livestock transport vehicles can be sources of various disease pathogens, infecting other abattoirs and animals (Ni et al., 2016). Furthermore, cross-contamination can occur when the food comes into contact with contaminated equipment during the production process (An et al., 2019). Thus, the amount and occurrence of pathogens varies depending on the management of the food distribution channel, and it is especially important to control *Listeria monocytogenes* and *Escherichia coli* O157:H7, which are major foodborne

pathogens that can potentially lead to foodborne infections (Huang et al., 2019).

*L. monocytogenes*, a Gram-positive bacterium, is a pathogenic agent causing listeriosis; the disease can be fatal to humans and has a high mortality rate of 20-40% (Alsheikh et al., 2014). One of the characteristics of *L. monocytogenes* is that it can adapt to refrigerated environments and can even form biofilms, which is a concern for the contemporary food industry, particularly in slaughterhouses (Oliveira et al., 2018). *E. coli* O157:H7, a Gram-negative bacterium, can mainly cause bloody diarrhea and hemolytic-uremic syndrome occasionally (Abuladze et al., 2008), and there is a significant risk of contamination of meat from livestock animals by *E. coli* O157:H7 (Huang et al., 2019). Despite technological advances, foodborne disease outbreaks by these pathogens have continuously occurred, requiring efficient pasteurization techniques to effectively control the growth of microorganisms in various environments.

Plasma, especially atmospheric pressure plasma (APP), has attracted attention as a non-thermal pasteurization technology (Misra and Jo, 2017; Yong et al., 2019). Because of the presence of primary and secondary species, plasma possess bactericidal (Gavahian et al., 2019), fungicidal (Yong et al., 2017; Misra et al., 2019), and virucidal (Puligundla and Mok, 2016) effects. However, plasma technology has spatial limitations because it is difficult to apply to environments where plasma is difficult to access, such as deep inside pipes and areas of equipment or devices (An et al., 2019). To overcome these limitations and to apply plasma to a wide area, research has recently been conducted on applying plasma to water, which is called plasma-treated water

(Yong et al., 2018a; Hozák et al., 2018; Machala et al., 2018).

Recently, plasma-treated water has gained increasing attention as an environment friendly and cost-effective aqueous disinfectant (Ji et al., 2018). Because some plasma-induced chemical species can dissolve or penetrate into water to produce primary and secondary species (Shen et al., 2016), plasma-treated water exhibits antibacterial and anti-biofilm activities (Park et al., 2017; Wu et al., 2017). It is generally agreed that the existence of reactive species such as ·OH, $H_2O_2$, $O_3$, $NO_2^-$, and $NO_3^-$ may contribute to the antibacterial activity of plasma-treated water (Shen et al., 2016; Xu et al., 2018), and plasma-treated water is known to be effective even when applied in different ways, such as a spray (Hong et al., 2018) or mist (Bingyan et al., 2016; Ranieri et al., 2018). Therefore, plasma-treated water has the potential to be applied to various environments because it can overcome spatial limitations of other approaches. Therefore, studies on the antibacterial effects for various uses of plasma-treated water should be carried out, and optimal pasteurization conditions for new applications should be established.

In this study, we produced plasma-activated droplet (PAD), a type of plasma-treated water, as an aqueous disinfectant using arc discharge plasma without any gas injection. The aim of this study was to clarify the antimicrobial effects and the mechanisms of PAD on planktonic *L. monocytogenes* and *E. coli* O157:H7, which are representative Gram-positive and -negative foodborne pathogens, respectively.

## 2.2. Material and methods

### *2.2.1. Plasma source and preparation of PAD*

Fig. 4 and Table 5 show a schematic diagram of the experimental apparatus and conditions used in this study. Plasma discharge was generated between cylindrical tungsten and titanium electrodes separated by ceramic plates. Electric power for plasma generation was provided by an alternating current (AC) power supply (IPS-1500, Insung Heavy Industry Co., Ltd., Busan, Korea). The electrical discharge was formed in electrically conductive liquid without additional gas injection, and the PAD was spurted through a hole (2 mm). A petri dish was used to collect PAD for 10 s, and the distance between the end of the hole and the petri dish was 15 cm. Distilled water containing NaCl (0.9% w/v) was used as the feeding solution to provide conductive characteristics of liquid for the plasma discharge. Current and voltage profiles during the plasma discharge were acquired by a current probe (Model 110, Pearson Electronics, Inc., Palo Alto, CA, USA) and a voltage probe (P6015A, Tektronix, Beaverton, OR, USA), respectively, using a digital oscilloscope (DPO 2024, Tektronix, Beaverton, OR, USA).

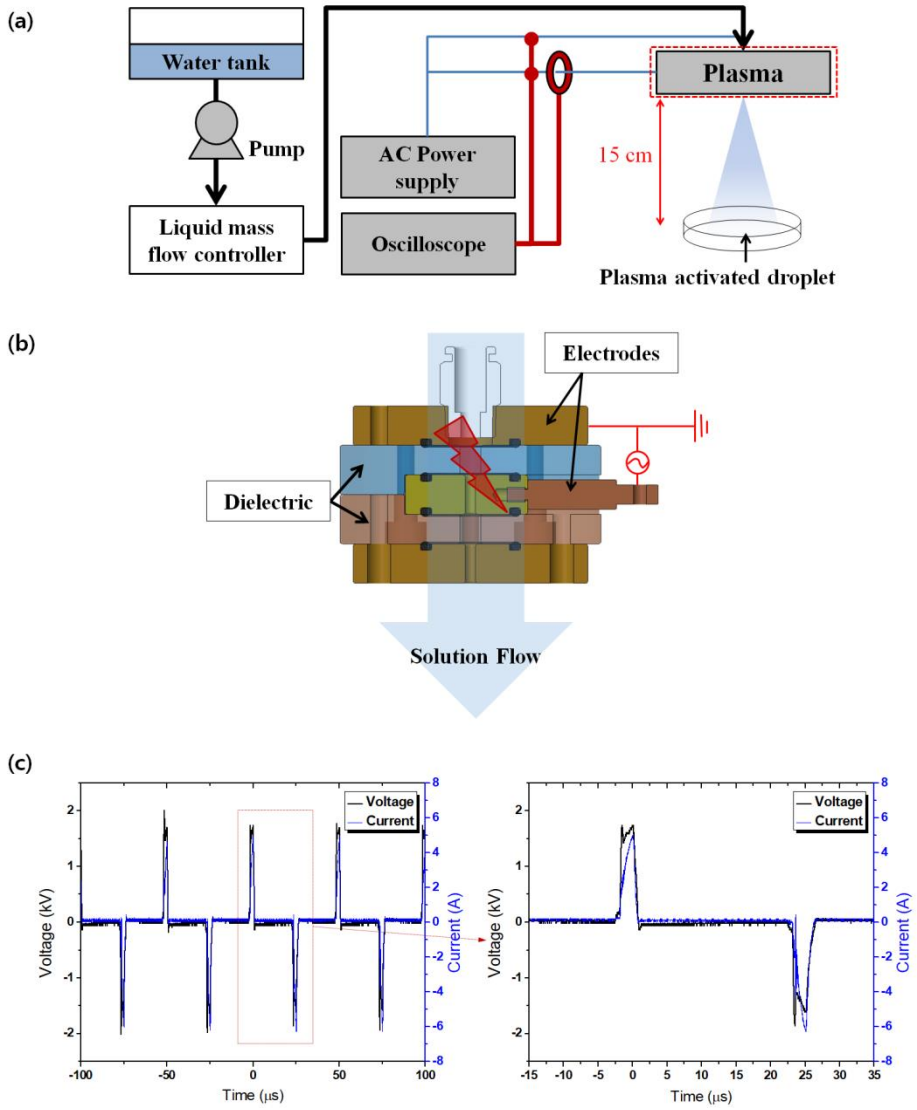


Figure 4. Schematic diagram showing (a) the generation of plasma-activated droplet (b) produced from arc discharge and (c) current and voltage profile during discharge.

Table 5. Conditions of arc discharge

| Parameter | Conditions |
|---|---|
| Peak voltage | 2 kV |
| Peak current | 1.5 A |
| Frequency | 20 kHz |
| Pulse width | 3 $\mu s$ |
| Feeding solution | 0.9% w/v NaCl |
| Solution flow rate | 40-70 mL/min |
| Hole diameter | 2 mm |
| Dielectric composition | Ceramic |
| Powered electrode composition | Tungsten |
| Ground electrode composition | Titanium |

*2.2.2. Chemical measurements in PAD*

The chemical properties of PAD produced from different liquid flow rates (40, 50, 60, and 70 mL/min) were determined immediately, including temperature, pH, electric conductivity, and the concentrations of hydrogen peroxide ($H_2O_2$), free available chlorine (FAC; HOCl or $OCl^-$), nitrate anions ($NO_3^-$), and nitrite anion ($NO_2^-$). Temperature was measured using a digital thermometer (YF-160 Type-K, YFE, Hsinchu City, Taiwan), and the pH value was measured using a pH meter (SevenGo2, Mettler-Toledo International Inc., Schwerzenbach, Switzerland). The electric conductivity was measured using an Orion conductivity meter (VSTAR52, Thermo Scientific, Waltham, MA, USA) equipped with a conductivity probe (Orion 013005MD, Thermo Scientific, USA). $H_2O_2$ was analyzed based on a previous method (Park et al., 2017) with slight modifications by using ammonium metavanadate (99%; Sigma-Aldrich GmbH, Steinheim, Germany). The reaction is based on a red-orange color change caused by peroxovanadium cation, which is formed by the reaction between $H_2O_2$ and metavanadate under acidic conditions. To measure the $H_2O_2$ concentration in PAD, one milliliter of the 10 mM ammonium metavanadate and 0.3 mL of 5 M sulfuric acid (95%; Junsei Chemical Co. Ltd., Chuo-ku, Japan) were added to 1 mL of PAD. After 2 min, the absorbance was measured at 450 nm by using a UV/Vis spectrophotometer (X-ma 3100, Human Co. Ltd., Seoul, Korea). A standard curve was used to calculate the concentration of $H_2O_2$ in samples. The concentration of FAC was analyzed using the colorimetric method based on the N,N-diethyl-p-phenylenediamine (DPD) chemistry using a free chlorine

assay kit (HS-$Cl_2$, Humas, Daejeon, Korea). The concentration of $NO_2^-$ was analyzed by measuring nitrite-nitrogen ($NO_2$-N) using test kits (TNT840, HACH Co., Loveland, CO, USA), and the concentration of $NO_3^-$ was analyzed by measuring the nitrate-nitrogen ($NO_3$-N) using the HACH Test 'N Tube Reactor/Cuvette Tubes with NItraVer X Reagent (Chromotropic Acid method). A spectrophotometer (DR 1900, HACH Co., Loveland, CO, USA) was used for absorbance measurements to analyze FAC, $NO_3^-$, and $NO_2^-$. Each three (Ca, Mg, and Si) and seven (Al, Cu, Fe, Mo, Ni, W, and Zn) mineral elements were quantified by using inductively coupled plasma-absorption emission spectrometry (ICP-AES, ICP-730ES, Varian, Victoria, Australia) and inductively coupled plasma-mass spectrometry (ICP-MS, 7900, Agilent Technologies, Inc., CA, USA), respectively. ICP-AES was operated with the following instrument settings: radio frequency power, 1.35 kW; plasma flow, 15 L/min; auxiliary flow, 1.5 L/min; nebulizer gas flow, 0.73 L/min; pump rate, 15 rpm. ICP-MS was operated with the following instrument settings: radio frequency power, 1.55 kW; radio frequency matching, 1.72 V; nebulizer gas flow, 1.05 L/min; scan sweep, 100; integration time/mass, 0.3.

*2.2.3. Bacterial strain and culture conditions*

The Gram-positive bacterium *L. monocytogenes* (ATCC 19111) and Gram-negative bacterium *E. coli* O157:H7 (NCCP 15739) for this study were provided by the Korean Culture Center of Microorganisms (Seoul, Korea) and the National Culture Collection for Pathogen (Osong, Korea), respectively. *L. monocytogenes* was cultivated in fresh sterile tryptic soy broth (TSB; Difco,

Becton Dickinson Co., Sparks, MD, USA) containing 0.6% yeast extract, and *E. coli* O157:H7 was cultivated in fresh sterile TSB medium. They were incubated at 37℃ and 120 rpm orbital agitation for 24 h. The cells were harvested by centrifugation at 2,265 *g* for 15 min at 4℃ in a refrigerated centrifuge (UNION 32R, Hanil Science Industrial, Co., Ltd. Korea) and washed twice with sterile 0.85% saline solution. The final pellets were resuspended in 0.85% saline solution, corresponding to approximately $10^8$ to $10^9$ CFU/mL.

*2.2.4. Analysis of the antibacterial ability of PAD*

A volume of 4.5 mL of PAD or sterile 0.85% saline solution was transferred into sterile 50 mL tubes containing 0.5 mL of each bacterial suspension. The volume ratio of PAD and bacterial suspension in this study was consistent with other research using plasma treated water or electrolyzed water (Xiang et al., 2018; Abadias et al., 2008). The obtained bacterial suspensions were mixed thoroughly for 5 s and incubated at room temperature for different time intervals (1, 2, 3, 4, and 5 min). Following each incubation, tenfold serial dilution of the 100 μL bacterial suspensions were plated onto agar plates and incubated at 37℃ for 24 h. The medium used for *L. monocytogenes* was tryptic soy agar (TSA; Difco, Becton Dickinson Co., Sparks, MD, USA) containing 0.6% yeast extract, and the medium used for *E. coli* O157:H7 was TSA. All colonies were counted, and the number of microorganisms was expressed as log CFU/mL.

*2.2.5. Determination of cell membrane integrity*

A BacLight™ Live/Dead Bacterial viability kit (L-7012; Molecular Probes, Eugene, OR, USA) was used to evaluate cell membrane integrity. The kit contains two DNA-binding dyes, SYTO 9 (green fluorescence) and propidium iodide (PI, red fluorescence). Green fluorescence indicates membrane intact bacteria, whereas red fluorescence of PI indicates membrane damaged bacteria. Therefore, PAD-induced cellular membrane disruption could be successfully evaluated.

After PAD treatment (0, 1, and 5 min), the planktonic bacteria in suspension were immediately separated from PAD after centrifugation at 13,200 g for 2 min and resuspended in 0.1 M phosphate-buffered saline (PBS, pH 7.4). The dye mixture (3 μL) was dripped into 1 mL of the PAD-treated bacterial suspension and incubated for 20 min at room temperature in the darkness. Each sample (5 μL) was then dripped onto a slide glass (Paul Marienfeld GmbH & Co. KG, Laud-Königshofen, Germany) which had a thickness of 1 mm and covered for examination on a confocal laser scanning microscope (Leica TCS SP8 X, Wetzlar, Germany) using appropriate filters with excitation/emission wavelengths at 483/490-540 nm for SYTO 9 and excitation/emission wavelengths at 535/590-680 nm for PI.

*2.2.6. Transmission electron microscopy*

To evaluate the morphological changes in *L. monocytogenes* and *E. coli* O157:H7 resulting from PAD treatment, transmission electron microscopy (TEM) analysis was performed. The planktonic bacteria in suspension were

immediately separated from PAD and resuspended in 0.1 M PBS (pH 7.4). The cell pellets were collected by centrifugation at 8,000 *g* for 10 min and fixed at 4℃ for 2 h in modified Karnovsky's fixative, consisting of 2% paraformaldehyde and 2% glutaraldehyde in 0.05 M sodium cacodylate buffer (pH 7.2). After primary fixation, each sample was washed three times with 0.05 M sodium cacodylate buffer at 4℃ for 10 min and postfixed in 1% osmium tetroxide in 0.05 M sodium cacodylate buffer at 4℃ for 2 h. The fixed sample was rinsed twice with distilled water and stained with 0.5% uranyl acetate at 4℃ for 24 h. The stained sample was dehydrated at room temperature with a graded ethanol series (15 min each) of 30, 50, 70, 80, and 90% and finally repeated thrice at 100%. Transition was performed twice with 100% propylene oxide for 15 min each, and then, the sample was infiltrated with a 1:1 solution of 100% propylene oxide and Spurr's resin for 2 h. The sample was immersed into Spurr's resin for 24 h and then re-immersed in Spurr's resin for 2 h for the final infiltration. The sample was polymerized at 70℃ for 24 h and sectioned using an ultramicrotome (MT-X, RMC, Tucson, AZ, USA) before TEM analysis. The microstructure of each bacterial cell was observed using a transmission electron microscope (JEM-1010, JEOL, Tokyo, Japan) at 80 kV.

*2.2.7. Statistical analysis*

Each experiment was performed in triplicate. The data were analyzed using SAS statistical software program (version 9.4, SAS Institute Inc., Cary, NC, USA). Statistical analysis was performed by one-way analysis of variance

(ANOVA), with a completely randomized design, using the general linear model. Significant differences among the mean values were determined using the Tukey's multiple comparison test at a significance level of $p<0.05$.

## 2.3. Results and discussion

### *2.3.1. Chemical characterization of PAD*

Table 6 shows the temperature, pH, and electric conductivity of the untreated solution (0.9% w/v NaCl) and PAD produced from different liquid flow rates (40, 50, 60, and 70 mL/min). The temperature of PAD was 47.10℃ at 40 mL/min of liquid flow rate, and it increased in proportion with the liquid flow rate. This is attributed to the accumulation of high temperature PAD as the liquid flow rate is increased. The pH of the PAD increased from 6.52 before discharge to 8.08-8.26, and no difference was observed depending on the liquid flow rate. Kondeti et al. (2018) reported a large pH increase in saline solution by applying atmospheric pressure plasma jet with air in Ar or 1% $O_2$, and Jirásek and Lukeš (2019) suggested that plasma-induced pH increase in saline solution is due to the alkaline characteristics of hypochlorite ions ($OCl^-$) and its capturing of hydrogen ions ($H^+$) (see equation 13). In our previous studies (Jung et al., 2015; Yong et al., 2018b), the pH of the plasma treated water dramatically decreased during plasma treatment. In the case of atmospheric air discharge, nitrogen oxides (such as NO, $NO_2$, and $N_2O_3$) are mainly produced and react with water molecules, resulting in the formation of $HNO_2$ and $HNO_3$ (Park et al., 2017). These molecules release hydrogen ions through deprotonation reactions, thus acidifying water. However, air was not injected for plasma discharge in the present system; therefore, the generation of reactive nitrogen species (RNS) can be negligible. The increase in electric conductivity was the largest up to 17.99 mS/cm at 40 mL/min of liquid flow rate possibly because of the formation of chemical species, but the electric

conductivity decreased with increasing liquid flow rate.

The concentration of metal ions in the PAD is depicted in Table 7. The devices used in this study have the possibility for corrosion or elution of electrodes as arc discharge occurs in narrow spaces. As a result, various components of the electrode were detected in PAD (40 mL/min). Chen et al. (2017) confirmed that metal ions in the solution could only exhibit synergistic antibacterial effect with plasma-activated water under acidic pH, so it is estimated that there was no additional bactericidal effect from metal ions in this study.

Fig. 5 shows the concentrations of $H_2O_2$, $NO_2^-$, $NO_3^-$, and FAC in the untreated solution (0.9% w/v NaCl) and PAD produced from different liquid flow rates (40, 50, 60, and 70 mL/min). Here, we considered $H_2O_2$ as an indicator of ROS formation because it is stable with a relatively long lifetime, up to 10 h (at pH 7.0) in aqueous environments (Burns et al., 2012) and it can be dissociated into hydroxyl radicals (·OH), which are the strongest oxidants (Shang et al., 2016) but are difficult to detect because of their short lifetime (Burns et al., 2012). In Fig. 5a, the highest concentration of $H_2O_2$, 29.3 mg/L, was found at the lowest liquid flow rate (40 mL/min), which was consistent with our observation of the highest electric conductivity at 40 mL/min of liquid flow rate. Burlica et al (2010) also found the same trends for the formation of $H_2O_2$ from water spray produced by pulsed gliding arc plasma with different carrier gases and water flow rates.

In plasma generated in the confined area between the electrodes, a higher increase in ·OH and ·H can occur because of the high temperature thermal

dissociation of water caused by the collision of water molecules in the confined spaces. This reaction can be given by the following equation (Mededovic and Locke, 2007).

(1) $H_2O + M \rightarrow \cdot OH + \cdot H + M$

where M = $H_2O$.

Moreover, direct water dissociation may occur according to equations 2-3, and both $H_2O_2$ and $H_2$ may be formed through an overall reaction 4, including possible ·OH recombination and other pathways (Burlica et al., 2010).

(2) $H_2O + e^- \rightarrow H + \cdot OH + 2e^-$

(3) $H_2O + e^- \rightarrow 2H + O + e^-$

(4) $2H_2O \rightarrow H_2O_2 + H_2$

$H_2O_2$ can be dissociated to ·OH by the reactions 5-9 (An et al., 2019; Shang et al., 2016).

(5) $H_2O_2 \rightarrow \cdot OH + \cdot OH$

(6) $H_2O_2 + \cdot H \rightarrow H_2O + \cdot OH$

(7) $H_2O_2 + \cdot O \rightarrow HO_2 + \cdot OH$

(8) $H_2O_2 + e^- \rightarrow \cdot OH + OH^-$

(9) $H_2O_2 + \cdot HO_2 \rightarrow H_2O + O_2 + \cdot OH$

As shown in Fig. 5b and 5c, the concentration of $NO_2^-$ in PAD was lower than the minimum detection limit (0.6 mg/L) for all treatment groups, and there was no significant difference in $NO_3^-$ content. Because air was not injected for plasma discharge in this system, the generation of reactive nitrogen species (RNS) can be assumed to be negligible, which shows similar trends with the previous study using underwater capillary discharge system

(Hong et al., 2018).

The plasma discharge showed the formation of FAC in the PAD, and the concentrations of FAC were 0.58 and 0.54 mg/L at liquid flow rates of 40 and 50 mL/min, respectively (Fig. 5d). We expected that hypochlorous acid (HOCl) and hypochlorite ion ($OCl^-$) could be produced by the reactions 10-13 when the saline solution was exposed to plasma as follows (Lee et al., 2018).

(10) $H_2O \leftrightarrow H^+ + \cdot OH + e^-$

(11) $Cl^- \leftrightarrow \cdot Cl + e^-$

(12) $\cdot Cl + \cdot OH \leftrightarrow HOCl$

(13) $HOCl \leftrightarrow H^+ + OCl^-$

Because $OCl^-$ is more stable in alkaline water (Jirásek and Lukeš, 2019; Kim and Chung, 2012), the major component of FAC in our system could be $OCl^-$. The antimicrobial effects of $OCl^-$ are relatively poorer than those of HOCl, but it can also exert an oxidizing action from outside of the cell (Fukuzaki, 2006). As mentioned before, ROS with a lifetime in the order of nanoseconds can exist in the PAD, resulting in microbial inactivation. However, measuring of the short-lived ROS in the PAD is difficult and beyond the scope of the present research. In this regard, we considered that long-lived ROS, short-lived ROS that may have been generated, and FAC mainly composed of $OCl^-$ were significantly responsible for the bactericidal effects in the current system. For measuring the bactericidal activities of PAD, a liquid flow rate of 40 mL/min was chosen for the optimal condition corresponding to the highest $H_2O_2$ and FAC formation (Fig. 5).

Table 6. Temperature, pH, and electric conductivity of PAD

| Liquid flow rate (mL/min) | Temperature (℃) | pH | Conductivity (mS/cm) |
|---|---|---|---|
| Before discharge | 20.93±0.29$^{d}$ | 6.52±0.13$^{b}$ | 15.84±0.01$^{e}$ |
| 40 | 47.10±0.82$^{c}$ | 8.26±0.07$^{a}$ | 17.99±0.27$^{a}$ |
| 50 | 49.47±1.38$^{bc}$ | 8.13±0.16$^{a}$ | 17.61±0.04$^{b}$ |
| 60 | 50.47±1.14$^{b}$ | 8.08±0.20$^{a}$ | 17.39±0.05$^{c}$ |
| 70 | 53.13±0.12$^{a}$ | 8.15±0.10$^{a}$ | 17.14±0.03$^{d}$ |

Data represent the mean ± standard deviation.

$^{a\text{-}e}$Different letters within the same column differ significantly ($p$<0.05).

Table 7. Concentration of metal ions in the PAD

| Components | Concentration | |
|---|---|---|
| | Before discharge | After discharge |
| Ca (mg/L) | 0.00±0.00 | 0.10±0.17 |
| Mg (mg/L) | 0.02±0.02 | 0.01±0.01 |
| Si (mg/L) | 0.08±0.02 | 0.09±0.01 |
| Al (μg/L) | 5.57±0.28 | 15.87±1.55* |
| Cu (μg/L) | 3.26±0.40 | 1,870.66±30.07* |
| Fe (μg/L) | 0.01±0.02 | 2.86±0.43* |
| Mo (μg/L) | 0.03±0.02 | 0.38±0.02* |
| Ni (μg/L) | 0.00±0.00 | 12.27±0.92* |
| W (μg/L) | 0.00±0.00 | 3,007.41±228.07* |
| Zn (μg/L) | 7.36±0.33 | 2,697.49±124.06* |

PAD was generated at 40 mL/min of liquid flow rate.

Data represent the mean ± standard deviation.

Student's *t*-test; *, $p<0.05$ with respect to the untreated control.

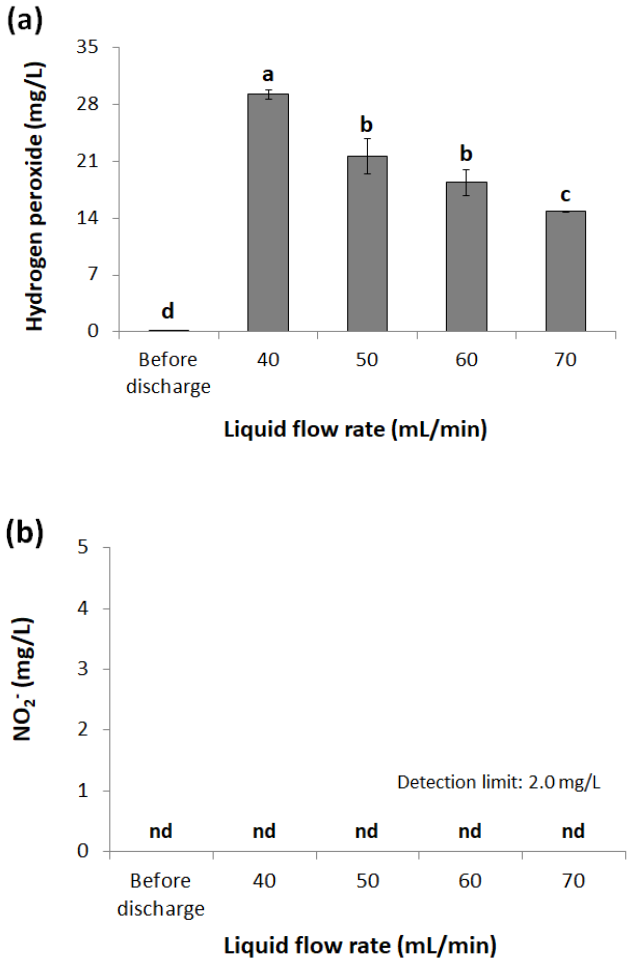


Figure 5. (a) Hydrogen peroxide, (b) nitrite ($NO_2^-$), (c) nitrate ($NO_3^-$), and (d) free available chlorine concentration of PAD according to the liquid flow rate (0, 40, 50, 60, and 70 mL/min).

nd, not detected.

Error bars denote standard deviation.

[a-d]Different letters differ significantly ($p$<0.05).

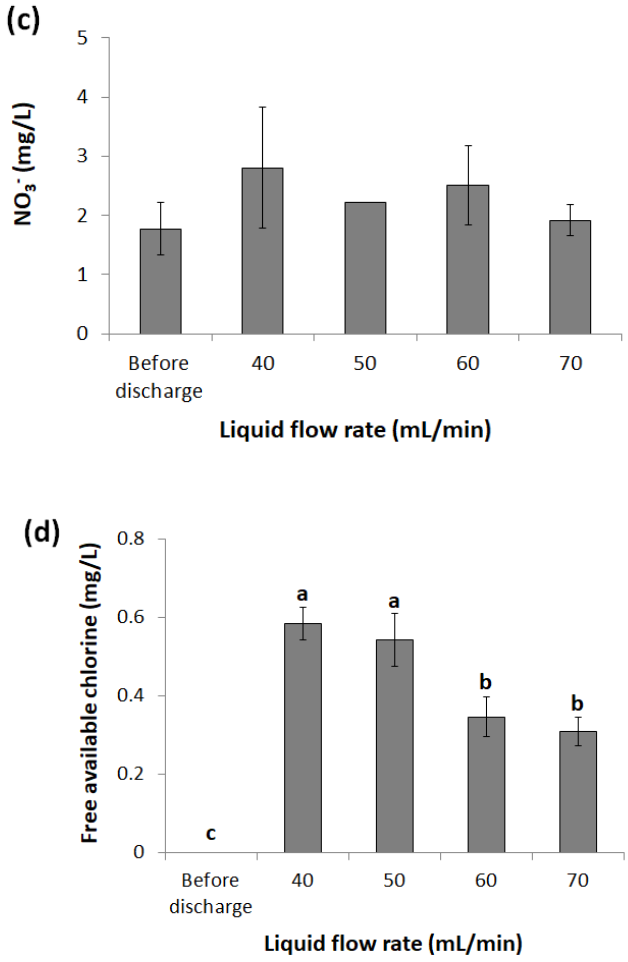


Figure 5. Continued.

*2.3.2. Bacterial viable count*

The inactivation patterns of PAD-treated *L. monocytogenes* and *E. coli* O157:H7 cells are depicted in Fig. 6. The surviving population of *L. monocytogenes* significantly reduced by 0.58 log CFU/mL after 1 min of exposure to PAD and further decreased in proportion to the treatment time (Fig. 6a). As a result, the surviving population of *L. monocytogenes* significantly reduced by 3.10 log CFU/mL after 5 min of exposure to PAD. However, *E. coli* O157:H7 inactivation required a shorter treatment time compared to that needed to inactivate *L. monocytogenes*. The surviving population of *E. coli* O157:H7 significantly reduced by 4.13 log CFU/mL after 1 min of treatment time (Fig. 6b), but no additional antimicrobial effects were observed as the treatment time increased. These data indicate that PAD has antimicrobial effects against both *L. monocytogenes* and *E. coli* O157:H7 cells and are especially more potent for *E. coli* O157:H7, which is a Gram-negative bacterium. Several studies have shown the different antimicrobial effects of plasma treatment against Gram-positive and Gram-negative bacteria (Ji et al., 2018; Han et al., 2016). The relative ineffectiveness of PAD against Gram-positive bacteria can be explained by the relatively dense peptidoglycan structures, leading to less PAD sensitivity. Gram-positive bacteria have a thick (20-80 nm) cell wall as the outer shell of the cell (Mai-Prochnow et al., 2016). In contrast, Gram-negative bacteria have a relatively thin peptidoglycan layer (<10 nm) of cell wall and an outer membrane consisting of lipopolysaccharides and phospholipids (Amro et al., 2000). Our results show that the Gram-negative *E. coli* O157:H7 with a thin cell wall had a significant

higher susceptibility to PAD treatment compared with Gram-positive *L. monocytogenes* with a thick cell wall. As Gram-positive bacteria are less susceptible to chemical oxidation (Yong et al., 2015; Xu et al., 2018), more active exposure is required from aqueous ROS to break down the thick cell wall of *L. monocytogenes*.

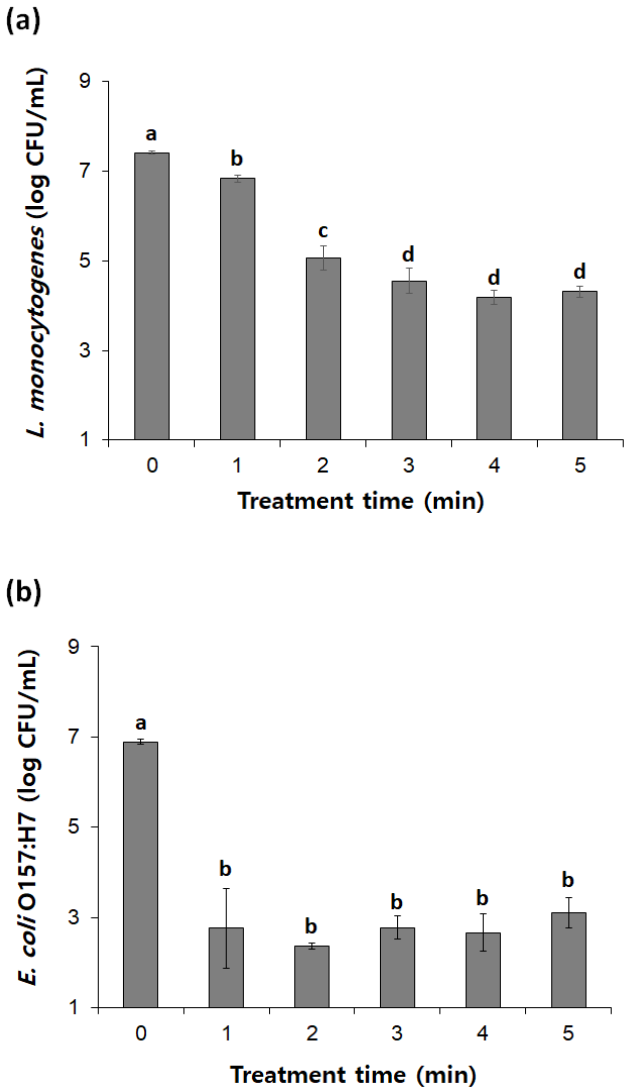


Figure 6. Surviving population (log CFU/mL) of (a) *L. monocytogenes* and (b) *E. coli* O157:H7 after being exposed to the PAD (0, 1, 2, 3, 4, and 5 min).

Error bars denote standard deviation.

[a-d]Different letters differ significantly ($p$<0.05).

*2.3.3. Membrane integrity*

The fluorescence images of the counterstained PAD-treated planktonic *L. monocytogenes* and *E. coli* O157:H7 are depicted in Fig. 7. SYTO 9 can penetrate the intact cell membrane of bacteria, thus staining all bacteria to green, while PI can penetrate only membrane-damaged bacteria, resulting in a reduction of SYTO 9 stain fluorescence (Stiefel et al., 2015). The untreated cells of both bacterial species mostly have intact cell membranes, and the membrane permeability of *L. monocytogenes* was slightly increased when exposed to 1 min of PAD. More cells were stained with PI when exposed to 5 min of PAD compared with 1 min PAD-treated cells. However, the membrane permeability of *E. coli* O157:H7 to PI increased dramatically after only 1 min exposure to PAD. These results supported the fact that *E. coli* O157:H7 could be more effectively inactivated than *L. monocytogenes* by PAD-induced membrane damages. According to Xu et al (2018) who compared the plasma-driven antimicrobial effects against to *Staphylococcus aureus* (NCTC-8325) and *E. coli* (ATCC-25922), more *E. coli* cells lost their membrane integrity than *S. aureus* cells, suggesting the susceptibility difference between Gram-positive and Gram-negative bacteria to plasma. In our results, formation of pores in the membrane of *L. monocytogenes* and *E. coli* O157:H7 was evidenced by uptake of PI by cells after 5 min of exposure to PAD.

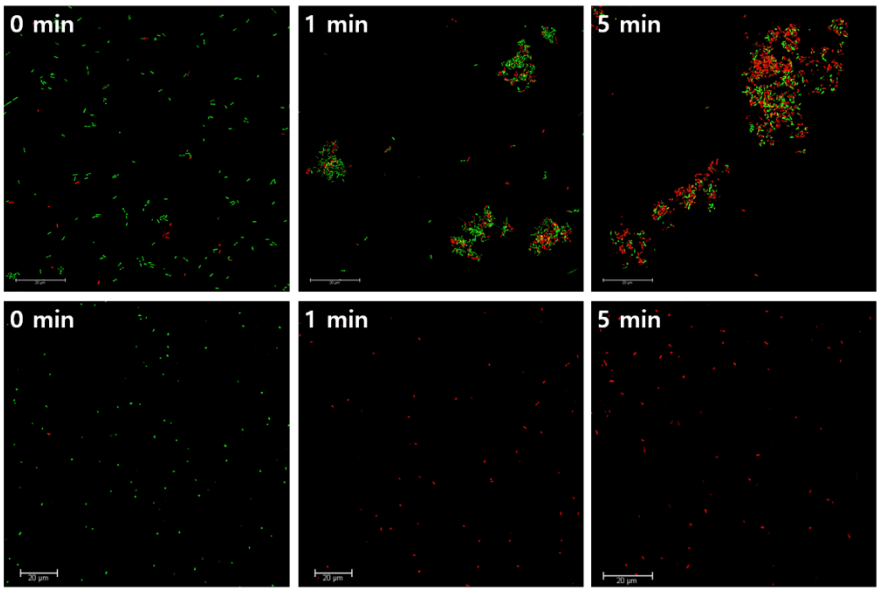


Figure 7. Fluorescence images of bacterial cells without or with PAD treatment. *L. monocytogenes* (upper) and *E. coli* O157:H7 (bottom) after 0, 1, and 5 min of exposure to PAD, respectively.

Live bacteria appeared as green (SYTO 9 stain fluorescence) and dead bacteria appeared as red (propidium iodide stain fluorescence).

*2.3.4. Morphological analysis*

PAD-induced morphological changes of *L. monocytogenes* and *E. coli* O157:H7 were examined by TEM (Fig. 8). The untreated cells of both bacterial species showed intact cell membranes. In *L. monocytogenes* cells treated with PAD for 1 min, the outer shell was slightly damaged, and deformation of intracellular materials was observed. However, when *L. monocytogenes* cells were exposed to PAD for 5 min, obvious morphological changes were observed, including leakage of intracellular materials and breakage of cell wall. In the case of *E. coli* O157:H7, dramatic structural changes were observed only 1 min after exposure to PAD. These results also suggest, as previously discussed, that *E. coli* O157:H7 was more susceptible to PAD than *L. monocytogenes*, and the outer cell structure of both bacterial species can be damaged by PAD-induced chemical attacks, which results in cell damage or cell death. Ji et al (2018) suggest that reactive species produced from the plasma can eventually damage the intracellular DNA and RNA by attacking the chemical bonds of the cell membrane, which are mainly composed of proteins, fatty acids, lipids, and phospholipids. Moreover, the bactericidal action of plasma can be possibly explained by diffusion, in which reactive species can pass through the cell membrane and attack intracellular nucleic acids and proteins, leading to cell death (Ziuzina et al., 2013).

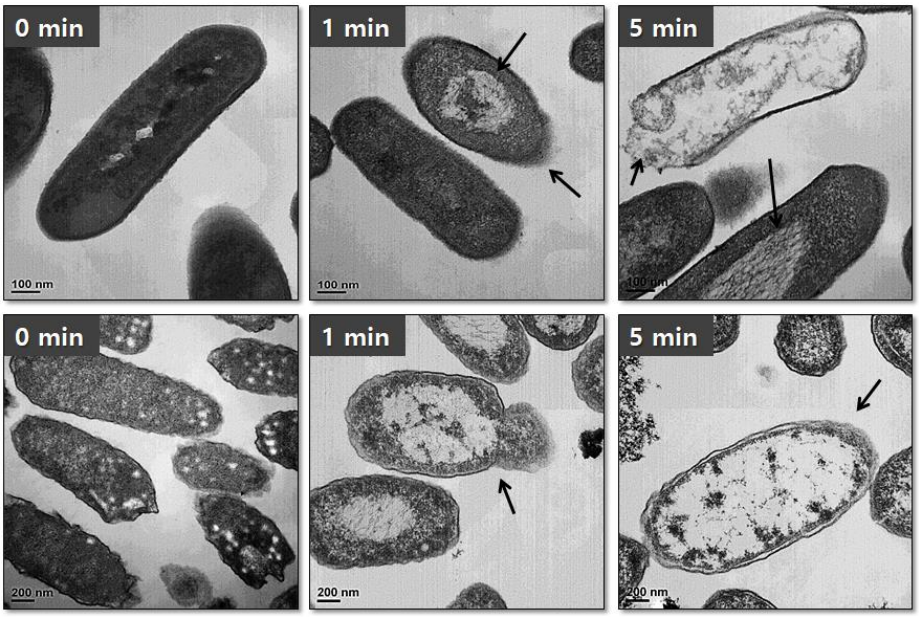


Figure 8. TEM images of bacterial cells without or with PAD treatment. *L. monocytogenes* (upper) and *E. coli* O157:H7 (bottom) after 0, 1, and 5 min of exposure to PAD, respectively.

The deformation and efflux of intracellular materials of membrane-damaged cells were observed (black arrows).

## 2.4. Conclusion

PAD produced from arc discharge plasma mainly contains $H_2O_2$ as ROS and $OCl^-$, which play a significant role in the inactivation process against both *L. monocytogenes* and *E. coli* O157:H7 cells. PAD reduced the number of both pathogenic bacteria, but *L. monocytogenes* was less susceptible to PAD than *E. coli* O157:H7 possibly because of the different outer structures of the cells. Nevertheless, PAD treatment can disrupt both the outer cell walls and membranes of *L. monocytogenes* and *E. coli* O157:H7, which is accompanied by the denaturation or leakage of intracellular nucleic acids and proteins. These findings suggest that PAD-induced chemical species can eventually affect the intracellular materials of bacterial cells by passing through or attacking the cell envelope.

**References**

Abadias, M., Usall, J., Oliveira, M., Alegre, I., & Viñas, I. (2008). Efficacy of neutral electrolyzed water (NEW) for reducing microbial contamination on minimally-processed vegetables. *International Journal of Food Microbiology*, *123*, 151-158.

Abuladze, T., Li, M., Menetrez, M. Y., Dean, T., Senecal, A., & Sulakvelidze, A. (2008). Bacteriophages reduce experimental contamination of hard surfaces, tomato, spinach, broccoli, and ground beef by *Escherichia coli* O157:H7. *Applied and Environmental Microbiology*, *74*, 6230-6238.

Alsheikh, A. D. I., Mohammed, G. E., Abdalla, M. A., & Bakhiet, A. O. (2014). First isolation and identification of *Listeria monocytogenes* isolated from frozen and shock frozen dressed broiler chicken in Sudan. *Microbiology Research Journal International*, *4*, 28-38.

Amro, N. A., Kotra, L. P., Wadu-Mesthrige, K., Bulychev, A., Mobashery, S., & Liu, G. Y. (2000). High-resolution atomic force microscopy studies of the *Escherichia coli* outer membrane: structural basis for permeability. *Langmuir*, *16*, 2789-2796.

An, J. Y., Yong, H. I., Kim, H. J., Park, J. Y., Lee, S. H., Baek, K. H., Choe, W., & Jo, C. (2019). Estimation of inactivation effects against *Escherichia coli* O157:H7 biofilm by different plasma-treated solutions and post-treatment storage. *Applied Physics Letters*, *114*, 073703.

Bingyan, C. H. E. N., Changping, Z. H. U., Juntao, F. E. I., Xiang, H., Cheng, Y., Yuan, W., Yongfeng, J., Longwei, C., Yuan, G., & Qingbang, H.

(2016). Water content effect on oxides yield in gas and liquid phase using DBD arrays in mist spray. *Plasma Science and Technology*, *18*, 41.

Burlica, R., Shih, K. Y., & Locke, B. R. (2010). Formation of $H_2$ and $H_2O_2$ in a water-spray gliding arc nonthermal plasma reactor. *Industrial & Engineering Chemistry Research*, *49*, 6342-6349.

Burns, J. M., Cooper, W. J., Ferry, J. L., King, D. W., DiMento, B. P., McNeill, K., Miller, C. J., Miller, W. L., Peake, B. M., Rusak, S. A., Rose, A. L., & Waite, T. D. (2012). Methods for reactive oxygen species (ROS) detection in aqueous environments. *Aquatic Sciences*, *74*, 683-734.

Chen, T. P., Liang, J., & Su, T. L. (2018). Plasma-activated water: antibacterial activity and artifacts?. *Environmental Science and Pollution Research*, *25*, 26699-26706.

Fukuzaki, S. (2006). Mechanisms of actions of sodium hypochlorite in cleaning and disinfection processes. *Biocontrol Science*, *11*, 147-157.

Gavahian, M., Chu, Y. H., & Jo, C. (2019). Prospective applications of cold plasma for processing poultry products: Benefits, effects on quality attributes, and limitations. *Comprehensive Reviews in Food Science and Food Safety*, *18*, 1292-1309.

Han, L., Patil, S., Boehm, D., Milosavljević, V., Cullen, P. J., & Bourke, P. (2016). Mechanisms of inactivation by high-voltage atmospheric cold plasma differ for *Escherichia coli* and *Staphylococcus aureus*. *Applied and Environmental Microbiology*, *82*, 450-458.

Hong, Y. C., Huh, J. Y., Ma, S. H., & Kim, K. I. (2018). Inactivation of microorganisms by radical droplets from combination of water discharge and electro-spraying. *Journal of Electrostatics*, *91*, 56-60.

Hozák, P., Scholtz, V., Khun, J., Mertová, D., Vaňková, E., & Julák, J. (2018). Further contribution to the chemistry of plasma-activated water: influence on bacteria in planktonic and biofilm forms. *Plasma Physics Reports*, *44*, 799-804.

Huang, L., Hwang, C. A., & Fang, T. (2019). Improved estimation of thermal resistance of *Escherichia coli* O157: H7, *Salmonella* spp., and *Listeria monocytogenes* in meat and poultry–The effect of temperature and fat and a global analysis. *Food Control*, *96*, 29-38.

Ji, S. H., Ki, S. H., Ahn, J. H., Shin, J. H., Hong, E. J., Kim, Y. J., & Choi, E. H. (2018). Inactivation of *Escherichia coli* and *Staphylococcus aureus* on contaminated perilla leaves by dielectric barrier discharge (DBD) plasma treatment. *Archives of Biochemistry and Biophysics*, *643*, 32-41.

Jirásek, V., & Lukeš, P. (2019). Formation of reactive chlorine species in saline solution treated by non-equilibrium atmospheric pressure $He/O_2$ plasma jet. *Plasma Sources Science and Technology*, *28*, 035015.

Jung, S., Kim, H. J., Park, S., Yong, H. I., Choe, J. H., Jeon, H. J., Choe, W., & Jo, C. (2015). Color developing capacity of plasma-treated water as a source of nitrite for meat curing. *Korean Journal for Food Science of Animal Resources*, *35*, 703.

Karyotis, D., Skandamis, P. N., & Juneja, V. K. (2017). Thermal inactivation of *Listeria monocytogenes* and *Salmonella* spp. in sous-vide processed marinated chicken breast. *Food Research International*, *100*, 894-898.

Kim, H. W., & Chung, N. Y. (2012). Effectiveness of the electrochemical sensor for the free chlorine measurement. *Journal of the Korean Society of Manufacturing Technology Engineers*, *21*, 720-725.

Kondeti, V. S. K., Phan, C. Q., Wende, K., Jablonowski, H., Gangal, U., Granick, J. L., Hunter, R. C., & Bruggeman, P. J. (2018). Long-lived and short-lived reactive species produced by a cold atmospheric pressure plasma jet for the inactivation of *Pseudomonas aeruginosa* and *Staphylococcus aureus*. *Free Radical Biology and Medicine*, *124*, 275-287.

Lee, S. J., Ma, S. H., Hong, Y. C., & Choi, M. C. (2018). Effects of pulsed and continuous wave discharges of underwater plasma on *Escherichia coli*. *Separation and Purification Technology*, *193*, 351-357.

Lu, H., Patil, S., Keener, K. M., Cullen, P. J., & Bourke, P. (2014). Bacterial inactivation by high-voltage atmospheric cold plasma: influence of process parameters and effects on cell leakage and DNA. *Journal of Applied Microbiology*, *116*, 784-794.

Machala, Z., Tarabová, B., Sersenová, D., Janda, M., & Hensel, K. (2018). Chemical and antibacterial effects of plasma activated water: correlation with gaseous and aqueous reactive oxygen and nitrogen species, plasma sources and air flow conditions. *Journal of Physics D: Applied Physics*, *52*, 034002.

Mai-Prochnow, A., Clauson, M., Hong, J., & Murphy, A. B. (2016). Gram positive and Gram negative bacteria differ in their sensitivity to cold plasma. *Scientific Reports*, *6*, 38610.

Medodovic, S., & Locke, B. R. (2009). Primary chemical reactions in pulsed electrical discharge channels in water. *Journal of Physics D: Applied Physics*, *42*, 049801.

Misra, N. N., & Jo, C. (2017). Applications of cold plasma technology for microbiological safety in meat industry. *Trends in Food Science & Technology*, *64*, 74-86.

Misra, N. N., Yadav, B., Roopesh, M. S., & Jo, C. (2019). Cold plasma for effective fungal and mycotoxin control in foods: mechanisms, inactivation effects, and applications. *Comprehensive Reviews in Food Science and Food Safety*, *18*, 106-120.

Ni, L., Zheng, W., Zhang, Q., Cao, W., & Li, B. (2016). Application of slightly acidic electrolyzed water for decontamination of stainless steel surfaces in animal transport vehicles. *Preventive Veterinary Medicine*, *133*, 42-51.

Oliveira, T. S., Varjão, L. M., da Silva, L. N. N., Pereira, R. D. C. L., Hofer, E., Vallim, D. C., & de Castro Almeida, R. C. (2018). *Listeria monocytogenes* at chicken slaughterhouse: Occurrence, genetic relationship among isolates and evaluation of antimicrobial susceptibility. *Food Control*, *88*, 131-138.

Park, J. Y., Park, S., Choe, W., Yong, H. I., Jo, C., & Kim, K. (2017). Plasma-functionalized solution: A potent antimicrobial agent for biomedical

applications from antibacterial therapeutics to biomaterial surface engineering. *ACS Applied Materials & Interfaces*, *9*, 43470-43477.

Pradeep, P., & Chulkyoon, M. (2016). Non-thermal plasmas (NTPs) for inactivation of viruses in abiotic environment. *Research Journal of Biotechnology*, *11*, 91-96.

Ranieri, P., McGovern, G., Tse, H., Fulmer, A., Kovalenko, M., Nirenberg, G., Miller, V., Fridman, A., Rabinovich, A., & Fridman, G. (2018). Microsecond-Pulsed Dielectric Barrier Discharge Plasma-Treated Mist for Inactivation of *Escherichia coli In Vitro*. *IEEE Transactions on Plasma Science*, *47*, 395-402.

Seo, J., Seo, D. J., Oh, H., Jeon, S. B., Oh, M. H., & Choi, C. (2016). Inhibiting the growth of *Escherichia coli* O157:H7 in beef, pork, and chicken meat using a bacteriophage. *Korean Journal for Food Science of Animal Resources*, *36*, 186.

Shang, K., Li, J., Wang, X., Yao, D., Lu, N., Jiang, N., & Wu, Y. (2015). Evaluating the generation efficiency of hydrogen peroxide in water by pulsed discharge over water surface and underwater bubbling pulsed discharge. *Japanese Journal of Applied Physics*, *55*, 01AB02.

Shen, J., Tian, Y., Li, Y., Ma, R., Zhang, Q., Zhang, J., & Fang, J. (2016). Bactericidal effects against *S. aureus* and physicochemical properties of plasma activated water stored at different temperatures. *Scientific Reports*, *6*, 28505.

Stiefel, P., Schmidt-Emrich, S., Maniura-Weber, K., & Ren, Q. (2015). Critical aspects of using bacterial cell viability assays with the fluorophores SYTO9 and propidium iodide. *BMC Microbiology*, *15*, 36.

Wu, S., Zhang, Q., Ma, R., Yu, S., Wang, K., Zhang, J., & Fang, J. (2017). Reactive radical-driven bacterial inactivation by hydrogen-peroxide-enhanced plasma-activated-water. *The European Physical Journal Special Topics*, *226*, 2887-2899.

Xiang, Q., Kang, C., Niu, L., Zhao, D., Li, K., & Bai, Y. (2018). Antibacterial activity and a membrane damage mechanism of plasma-activated water against *Pseudomonas deceptionensis* CM2. *LWT*, *96*, 395-401.

Xu, Z., Cheng, C., Shen, J., Lan, Y., Hu, S., Han, W., & Chu, P. K. (2018). In vitro antimicrobial effects and mechanisms of direct current air-liquid discharge plasma on planktonic *Staphylococcus aureus* and *Escherichia coli* in liquids. *Bioelectrochemistry*, *121*, 125-134.

Yong, H. I., Kim, H. J., Park, S., Kim, K., Choe, W., Yoo, S. J., & Jo, C. (2015). Pathogen inactivation and quality changes in sliced cheddar cheese treated using flexible thin-layer dielectric barrier discharge plasma. *Food Research International*, *69*, 57-63.

Yong, H. I., Lee, H., Park, S., Park, J., Choe, W., Jung, S., & Jo, C. (2017). Flexible thin-layer plasma inactivation of bacteria and mold survival in beef jerky packaging and its effects on the meat's physicochemical properties. *Meat Science*, *123*, 151-156.

Yong, H. I., Han, M., Kim, H. J., Suh, J. Y., & Jo, C. (2018a). Mechanism underlying green discolouration of myoglobin induced by atmospheric pressure plasma. *Scientific Reports*, *8*, 1-9.

Yong, H. I., Park, J., Kim, H. J., Jung, S., Park, S., Lee, H. J., Choe, W., & Jo, C. (2018b). An innovative curing process with plasma-treated water for production of loin ham and for its quality and safety. *Plasma Processes and Polymers*, *15*, 1700050.

Yong, H. I., Lee, S. H., Kim, S. Y., Park, S., Park, J., Choe, W., & Jo, C. (2019). Color development, physiochemical properties, and microbiological safety of pork jerky processed with atmospheric pressure plasma. *Innovative Food Science & Emerging Technologies*, *53*, 78-84.

Ziuzina, D., Patil, S., Cullen, P. J., Keener, K. M., & Bourke, P. (2013). Atmospheric cold plasma inactivation of *Escherichia coli* in liquid media inside a sealed package. *Journal of Applied Microbiology*, *114*, 778-787.

This chapter comprises a part of a paper published in Foods

as a partial fulfillment of Ki Ho Baek's Ph.D. program

# Chapter III.

# Inactivation of *Salmonella* Typhimurium by non-thermal plasma bubbles: Exploring the key reactive species and the influence of organic matter

## 3.1. Introduction

As the food industry continues to develop, consumers are demanding safer, fresher, and higher-quality foods (Ji et al., 2018). However, despite technological advances, food products can still become contaminated with pathogenic bacteria at any point from production to final consumption, including farming, harvesting, processing, transportation, and storage, which can cause serious health problems and global economic losses (Baek et al., 2020; Yoo et al., 2021). Therefore, it is necessary to develop a technology that can effectively inactivate pathogenic microorganisms without compromising food quality. In this regard, it is important to prevent food spoilage in advance and reduce the risk of food poisoning through proper cleaning and sanitization (Xiang et al., 2019). Many previous studies have been conducted into the development of effective sanitizers and disinfectants by utilizing various

substances, including chlorine-containing chemicals (Chen et al., 2017; Jung et al., 2018), electrolyzed water (Cao et al., 2009; Ovissipour et al., 2015), organic acid (Huang and Chen, 2011; Lee et al., 2010; Qian et al., 2019), ozone ($O_3$) (Fan et al., 2020; Lee et al., 2011), and plasma-activated solutions (Ke et al., 2018; Lin et al., 2019; Zhao et al., 2020), and have verified that these substances can effectively inactivate microorganisms. Among the various disinfectants, plasma activated water (PAW) has attracted significant attention due to its properties, which include virus inactivation, wound healing, the promotion of plant growth, and microbial inactivation (Zhou et al., 2020).

PAW, which is easy to operate, safe, and highly efficient (Qian et al., 2019), is usually produced by the treatment of non-thermal (non-equilibrium, cold) plasma in water. Various reactive molecules, commonly called reactive oxygen and nitrogen species (RONS), can be formed by gas-phase discharges and can dissolve or penetrate the liquid (at the gas-liquid interface) to produce secondary reactive species (Lukes et al., 2014). Secondary aqueous RONS, such as hydroxyl radicals (OH·), hydrogen peroxide ($H_2O_2$), singlet oxygen ($^1O_2$), superoxide anion/perhydroxyl radical ($O_2^{\cdot-}$/$HO_2^{\cdot}$), $O_3$, nitrite/nitrate ($NO_2^-$/$NO_3^-$) and peroxynitrites/peroxynitrous acid ($ONOO^-$/ONOOH), can initiate chemical and biocidal processes in the liquid (Machala et al., 2018). Each reactive species has a different oxidative potential and lifetime (Burns et al., 2012), and the type and concentration of the reactive species produced in the liquid depend on the discharge conditions, gas types, solution types, etc. (Zhou et al., 2020). In this regard, PAW can be considered in two aspects, depending on the application method: 1) Short- and long-lived reactive

species, which are generated in the liquid at the same time as plasma treatment, react with the target in real-time, and 2) short- and long-lived reactive species, which are produced and remain in the liquid during plasma treatment (mainly long-lived reactive species) and newly-generated by post-discharge reactions after plasma treatment, are used separately to react with the target. In fact, Ma et al. (2020) demonstrated that short-lived reactive species can also be subsequently produced after discharge through the following reactions (reaction 1-5). Therefore, it is important to consider appropriate PAW generation and application methods, depending on the purpose.

(1) $ONOOH + H_2O_2 \rightarrow O_2NOOH + H_2O$

(2) $O_2NOOH \rightarrow O_2NOO^-$

(3) $O_2NOO^- \rightarrow {}^1O_2 + NO_2^-$

(4) $O_2NOO^- \rightarrow NO_2 + O_2^-$

(5) $2O_2^- + 2H^+ \rightarrow {}^1O_2 + H_2O_2$

Since most reactive species have a significantly short half-life and can react with a variety of organic substances (Table 8) (Møller et al., 2007), there are some possible limitations to the effective pasteurization of bacteria present on food surfaces or in solutions containing organic matter (Xiang et al., 2019), as can be found in other sanitizers or disinfectants (Huo et al., 2018; Jo et al., 2018). To overcome some of these limitations, previous studies have aimed to improve the efficiency of plasma treatment for solutions by incorporating plasma into various technologies (Baek et al., 2020; Hong et al., 2018; Ma et al., 2017), one of which involves using bubbles as a potential means of

improving the efficiency of mass transfer (Liu et al., 2018; Zhou et al., 2019). However, few studies have revealed the clear pasteurization mechanism of plasma bubbles.

In this study, a non-thermal plasma bubble was applied for the direct plasma treatment of liquid, and *Salmonella* Typhimurium was used as a model pathogenic bacterium. The inactivation efficacy of plasma bubbles against *S.* Typhimurium was examined, and the mechanism of its bactericidal action was investigated by exploring the key reactive species in PAW. In addition, the effects of organic matter on the *S.* Typhimurium inactivation efficiency of plasma bubbles were investigated.

Table 8. Basic properties of reactive oxygen species in plant tissues (modified from Møller et al., 2007)

| Property | Hydroxyl radical | Singlet oxygen | Superoxide | Hydrogen peroxide |
|---|---|---|---|---|
| Half-life (in biological system) | 1 ns | 1 μs | 1 μs | 1 ms |
| Penetration depth | 1 nm | 30 nm | 30 nm | 1 μm |
| Reacts with | | | | |
| Lipids | Rapidly | PUFA[1] | Hardly | Hardly |
| DNA | Rapidly | Mainly guanine | No | No |
| Carbohydrates | Rapidly | No | No | No |
| Proteins | Rapidly | Trp, His, Tyr, Met, Cys | Fe-S centers | Cysteines |

[1]Polyunsaturated fatty acids

## 3.2. Material and methods

### *3.2.1. Plasma generator and plasma-bubbling system*

Fig. 9 and 10 shows a schematic diagram of the dielectric barrier discharge (DBD) plasma generator and plasma-bubbling system used in this study. The DBD apparatus consisted of four aluminum oxide plates (100 × 100 × 0.635 mm) with two nickel-chromium sheets attached back and forth as electrodes (Fig. 9). The major components of the plasma bubbling system included a function generator (Agilent 33500B series; Agilent Technologies, Loveland, CO, USA), high-voltage amplifier (model 5/80; Trek, Inc., Lockport, NY, USA), plasma generator, air pump, air flow controller, and bubbler (SL-03; Sang-A Pneumatic Co., Ltd., Daegu, Korea) (Fig. 10).

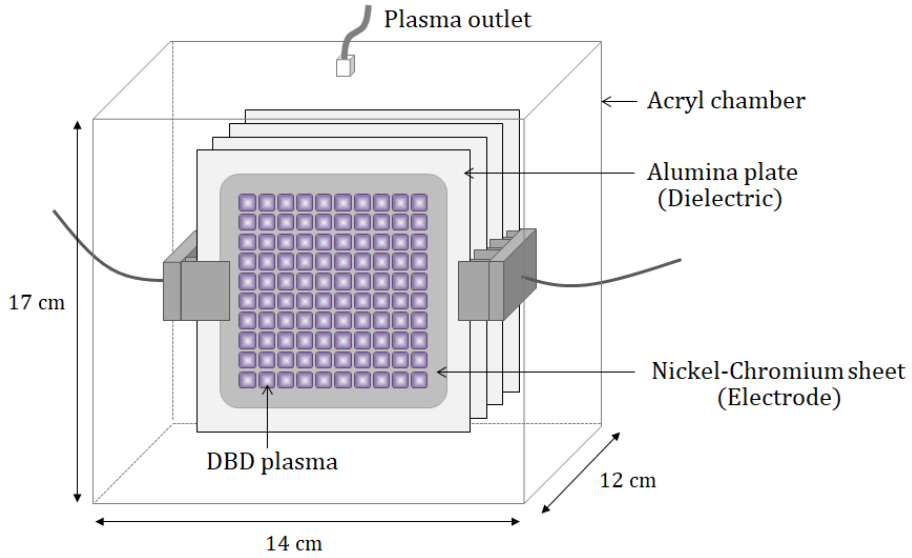


Figure 9. Schematic diagram of dielectric barrier discharge (DBD) plasma generator.

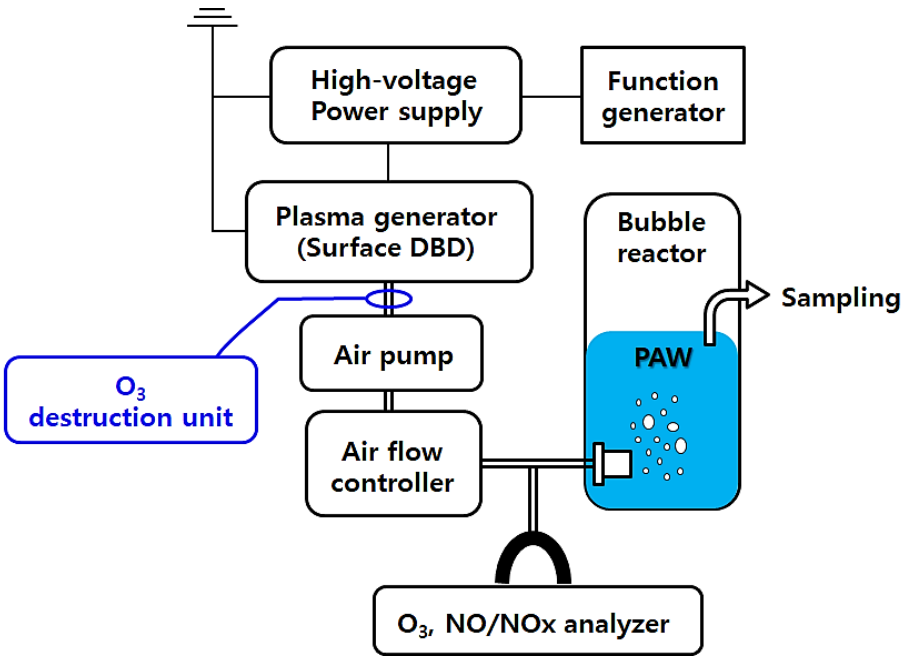


Figure 10. Schematic diagram of plasma-bubbling system ($O_3$ destruction unit was optionally applied according to experimental conditions).

*3.2.2. The generation of plasma bubbles*

Table 9 shows the operating conditions for generating the plasma bubbles used in this study. Plasma was generated between two electrodes separated by an aluminum oxide plate (Fig. 9) and was injected into deionized water (400 mL) at a gas flow rate of 4 L/min through a bubbler. The specific voltage and current waveform generated from the DBD are presented in Fig. 11. Voltage and current profiles were obtained using a digital oscilloscope (DPO 2024, Tektronix, Beaverton, OR, USA) equipped with a voltage probe (P6015A, Tektronix, Beaverton, OR, USA) and current probe (Pearson 411, Pearson Electronics, Inc., Pal Alto, CA, USA).

Table 9. Operating conditions for generating plasma bubbles

| Parameter | Conditions |
|---|---|
| Frequency | 2.5 kHz |
| Peak voltage | 3.0 kV |
| Working gas | Air |
| Gas flow rate | 4 L/min |
| Electrode composition | Nickel-Chromium |
| Dielectric composition | Aluminum oxide |
| Bubble reactor composition | Acryl |
| Sample volume | 400 mL |

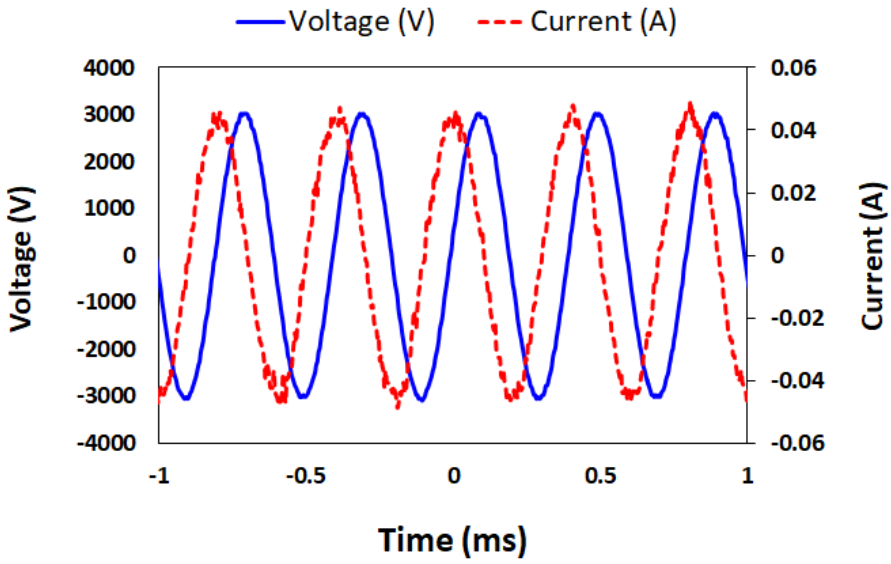


Figure 11. Voltage and current waveforms during discharge.

*3.2.3. Measurement of gaseous $O_3$ and nitrogen oxides (NO/NOx)*

To measure the actual amount of gaseous reactive species injected into the bubble reactor, the gas generated under the same operating conditions was collected and analyzed just before the gas was injected into the bubble reactor. The concentrations of gaseous $O_3$ and NO/NOx were measured using an $O_3$ analyzer (106-M, 2B Technologies, Boulder, USA) and NO/NOx gas analyzer (nCLD 63, Eco Physics AG, Duernten, Switzerland), respectively.

*3.2.4. Chemical measurement in PAW*

The chemical properties of PAW were analyzed simultaneously with plasma bubble treatment (0-5 min). Temperature and pH were measured using a thermometer (YF-160 Type-K, YFE, Hsinchu City, Taiwan) and pH meter (SevenGo2, Mettler-Toledo International Inc., Schwerzenbach, Switzerland), respectively. The concentration of dissolved $O_3$ was analyzed using the indigo method (standard method 4500-$O_3$ B) (APHA, 1992). $NO_2^-$ and $NO_3^-$ were analyzed using test kits (TNT840, HACH Co., Loveland, CO, USA) and HACH Test 'N Tube Reactor/Cuvette Tubes with NItraVer X Reagent (Chromotropic Acid method), respectively. A spectrophotometer (DR 1900, HACH Co., Loveland, Co, USA) was used to measure $NO_2^-$ and $NO_3^-$. The concentration of $^1O_2$ in PAW (0 and 5 min, respectively) was measured using an electron spin resonance spectroscope (JES-X320, Jeol, Ltd., Tokyo, Japan). A final concentration of 10 mM 2,2,6,6-tetramethylpiperidine (TEMP) was used as a spin trap reagent for trapping $^1O_2$. In addition, to verify the contribution of superoxide anions ($O_2^{\cdot-}$) to the production of $^1O_2$, the

concentration of $^1O_2$ in PAW containing 10 mM tiron (a scavenger of $O_2^{\cdot-}$) was also analyzed. All scans were carried out with the following instrument settings: sweep range, 7.5 mT; microwave power, 1 mW; modulation width, 0.3 mT; time constant, 0.03 s; central magnetic field, 336 mT; scanning time, 30 s. Each sample was measured three times and averaged. Hyperfine coupling constants of the signal were obtained using isotropic simulation software (Jeol, Ltd., Tokyo, Japan).

*3.2.5. Bacterial strain and culture conditions*

The Gram-negative bacterium *S.* Typhimurium (ATCC 13311) used in this study was provided by the Korean Culture Center of Microorganisms (Seoul, Korea). *S.* Typhimurium was cultivated in fresh sterile nutrient broth (NB; Difco, Becton Dickinson Co., Sparks, MD, USA) at 37℃ and 120 rpm orbital agitation for 24 h. The cells were washed twice with sterile 0.85% saline solution by centrifugation at 2,265 *g* for 15 min at 4℃ using a refrigerated centrifuge (UNION 32R, Hanil Science Industrial, Co., Ltd., Gimpo, Korea). The pellets were re-suspended in sterile 0.85% saline solution at a final concentration of $10^8$ to $10^9$ colony-forming unit (CFU)/mL.

*3.2.6. Plasma bubble treatment of the bacterial suspension and assessment of bacterial inactivation*

For the bacterial inactivation assay, sterile deionized water was inoculated by adding a prepared bacterial suspension to a final concentration of $10^6$-$10^7$ CFU/mL. Then, 400 mL of bacterial suspension was treated with plasma

bubbles for 1, 2, 3, 4, and 5 min. NB (Difco) consisting of 37.5% beef extract and 62.5% peptone by weight was used to evaluate the effect of organic matter on the inactivation efficacy of plasma bubbles against *S*. Typhimurium suspension. Different final concentrations (0, 0.005, 0.05, 0.1, and 0.5 g/L) of NB-containing bacteria were treated with plasma bubbles for 5, 10, 15, 20, 25, and 30 min, respectively. After treatment, an aliquot (1 mL) of the sample was immediately transferred to 9 mL Dey-Engley neutralizing broth (Difco), mixed well, and decimally diluted. To enumerate both uninjured and injured *S*. typhimurium, the thin agar layer (TAL) method (Wu and Fung, 2001) was applied to recover injured cells. The selective and nonselective media used for TAL were xylose lysine deoxycholate agar (Difco) and nutrient agar (Difco), respectively. To prepare TAL plates, solidified selective medium was overlaid with 7 mL of melted nonselective medium (48℃), and another 7 mL of melted nonselective medium was overlaid (7 + 7 mL; two times overlay) after solidification of the first layer. The top layer solidifies within minutes. Each diluent (100 μL) was plated onto the TAL plates and incubated at 37℃ for 24 h.

*3.2.7. Application of reactive oxygen species (ROS) scavengers and $O_3$ destruction unit*

To evaluate the roles of OH·, $H_2O_2$, $^1O_2$, and $O_2^{\cdot-}$ in the bactericidal action of plasma bubbles, a final concentration of 200 mM D-mannitol (OH· scavenger), 10 mM sodium pyruvate ($H_2O_2$ scavenger), 5 mM sodium azide ($^1O_2$ scavenger), 10 mM L-histidine ($^1O_2$ scavenger), or 10 mM tiron ($O_2^{\cdot-}$

scavenger) was added to the bacterial suspension before plasma bubble treatment. The types and concentrations of these scavengers have already been proven to be effective through various previous studies (Aboubakr et al., 2016; Guo et al., 2018; Kim et al., 2018). The bacterial suspension with or without scavengers was treated with plasma bubbles for 5 min, and the inactivation rates were determined as described above. In addition, dissolved $O_3$ analysis and bacterial inactivation assays were conducted after artificially removing $O_3$ gas using an $O_3$ destruction unit (ODS-2P, Ozone Solutions, Hull, IA, USA), which can remove up to 1% of $O_3$ gas, to verify its contribution to the antibacterial action of plasma bubbles.

*3.2.8. Statistical analysis*

All experiments were conducted in triplicates. SAS statistical software (version 9.4, SAS Institute Inc., Cary, NC, USA) was used to analyze the data. Student's *t*-test and Tukey's multiple comparison test were used for statistical analyses. Significant differences among the mean values were established at a significance level of $p<0.05$.

### 3.3. Results and discussion

*3.3.1. Physicochemical characterization of plasma*

During discharge, gaseous $O_3$ continuously increased from 0 to 240 ppm over 5 min, whereas NO/NOx did not occur (detection limit: 0.05 ppm) (Fig. 12a). As a result, the dissolved $O_3$ concentration in PAW increased with treatment time, and was 0.11 ± 0.008 ppm after 5 min treatment (Fig. 12b). On the other hand, after 5 min of plasma bubble treatment, the concentration of $NO_2^-$ in PAW was below the detection limit (2.00 ppm) (Fig. 13a), and the concentration of $NO_3^-$ was only 1.39 ± 0.051 ppm (Fig. 13b). At this point, short-lived gas-phase reactive species were excluded, as plasma produced in the plasma generator was injected into the water in a secondary manner. Park et al. (2018) reported that the rapidly generated $O_3$ at the early stage of discharge was eventually quenched by NO, resulting in the dominance of NO and $NO_2$, and that gas temperature ($N_2$ vibrational temperature) was one of the important factors in this transition. However, our discharge in air-based surface DBD plasma systems was a condition in which no aforementioned transition occurred, and $O_3$ was mainly formed and acted as a major chemical. Therefore, in this study, as the plasma bubble treatment time increased, the concentration of dissolved $O_3$ in the water increased. During plasma bubble treatment, the liquid temperature and pH remained at 24.12 ± 0.032℃ (Fig. 14a) and 6.30 ± 0.042 (Fig. 14b), respectively, until 5 min. For atmospheric air discharge (Yong et al., 2018; Ma et al., 2020), the pH of the liquid generally decreased during plasma treatment due to the production of $HNO_2$ and $HNO_3$. These molecules release hydrogen ions through deprotonation

reactions, thus, acidifying water. However, the current DBD condition did not generate enough NOx to drastically lower the pH of the water within 5 min (Fig. 12a and 14a).

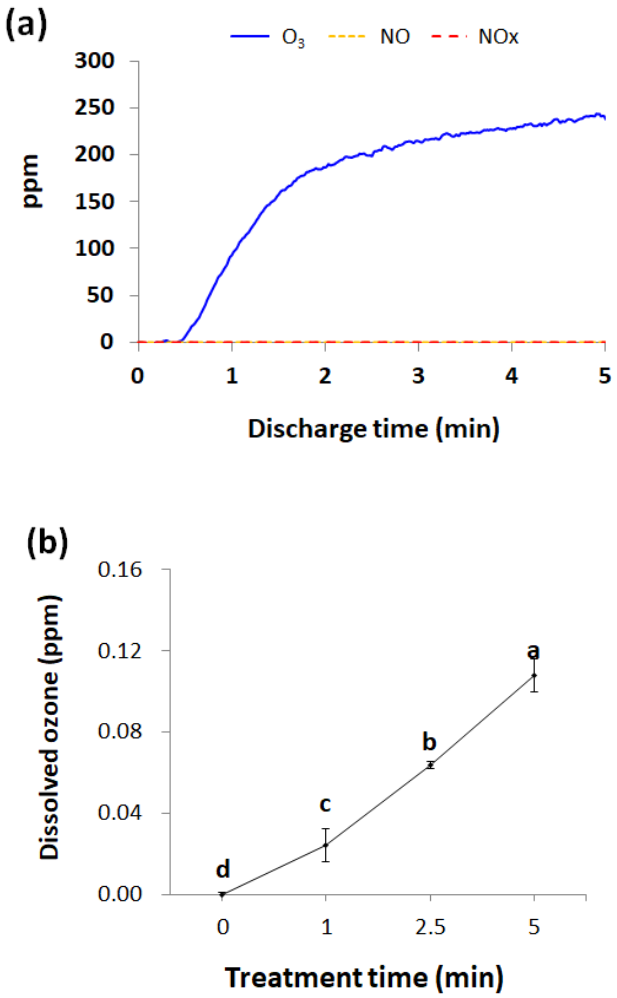


Figure 12. (a) Gaseous $O_3$ and NO/NOx concentrations during discharge and (b) dissolved $O_3$ concentration in PAW during 5 min of plasma bubble treatment.

Error bars denote standard deviation.

[a-d]Different letters indicate significant differences ($p$<0.05).

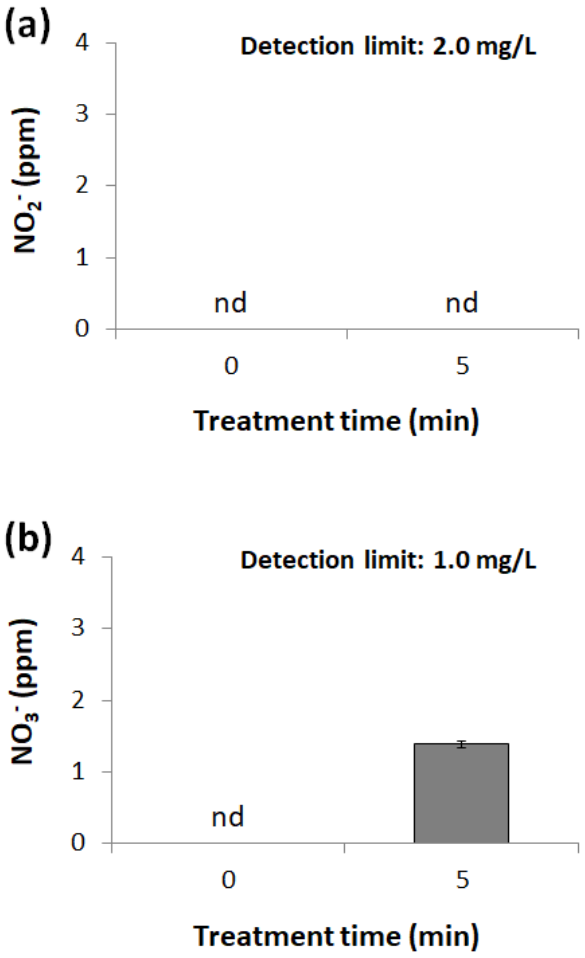


Figure 13. (a) $NO_2^-$ and (b) $NO_3^-$ concentrations in PAW after 5 min of plasma bubble treatment.

nd, not detected.

Error bars denote standard deviation.

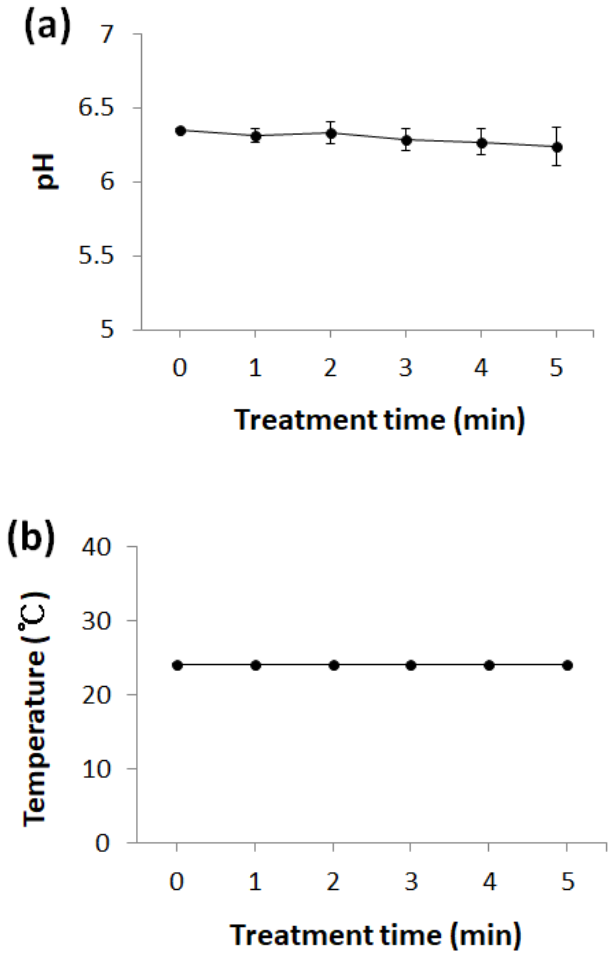


Figure 14. (a) Temperature and (b) pH values of PAW according to the plasma bubble treatment time (0, 1, 2, 3, 4, and 5 min).

Error bars denote standard deviation.

*3.3.2. Bactericidal effects of plasma bubbles and contributions of reactive species*

The inactivation efficacy of plasma bubbles against *S.* Typhimurium is depicted in Fig. 15a. The number of viable cells decreased significantly in proportion with the treatment time ($p<0.05$). The results indicate that plasma bubble treatment effectively inactivated *S.* Typhimurium floating in the solution, and that certain reactive species produced by plasma bubbles contributed to bactericidal action. At this time, ROS should be considered more important than reactive nitrogen species because it has already been verified that the generation and contribution of NOx may be negligible through the results of gaseous NO/NOx concentrations and solutions pH (Fig. 12a and 13).

Many studies have been conducted involving the application of $O_3$ generators for the injection of $O_3$ gas into water to inactivate microorganisms or decompose organic matter (Lee et al., 2011; Puyate and Rim-Rukeh, 2008; Skowron et al., 2019). Since $O_3$ can directly oxidize various organic substances and microbial components (Fan et al., 2020), previous studies have suggested that concentrations of gas-phase or dissolved $O_3$ in solution are important as an oxidative indicators (Puyate and Rim-Rukeh, 2008; Chung et al., 2010). However, not only the concentration of gaseous or aqueous $O_3$, but also the specific reactive species that contribute substantially to the degradation of organic matter or inactivation of microorganisms should be considered. Therefore, a series of ROS scavengers, such as D-mannitol for OH·, sodium pyruvate for $H_2O_2$, sodium azide and L-histidine for $^1O_2$, and

tiron for $O_2^{\cdot-}$ were used to evaluate the possible roles in the bacterial inactivation process of plasma bubbles (Fig. 15b). As a result of the experiment, sodium azide, L-histidine, and tiron almost completely eliminated the bactericidal effects of plasma bubbles. These data suggest that $^1O_2$ and $O_2^{\cdot-}$ were the main functional species of the plasma bubble in the inactivation of *S.* Typhimurium.

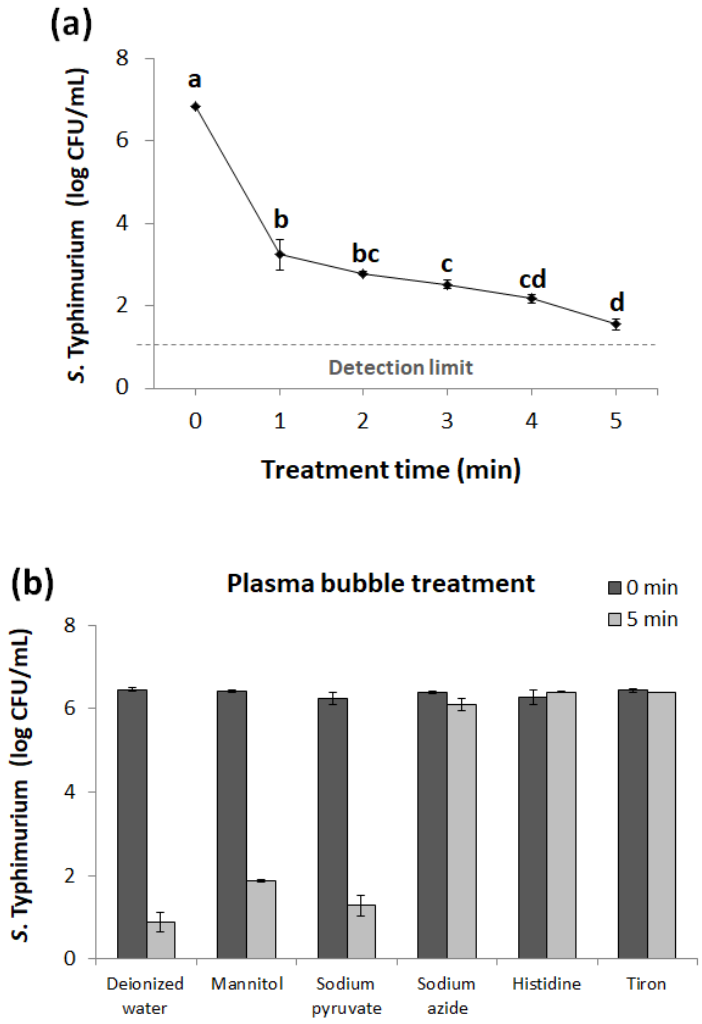


Figure 15. (a) Surviving population (log CFU/mL) of *S.* Typhimurium after different plasma bubble treatment times (0, 1, 2, 3, 4, and 5 min) and (b) *S.* Typhimurium inactivation results by 5 min plasma bubble treatment with the addition of different ROS scavengers.

Error bars denote standard deviation.

[a-d]Different letters indicate significant differences ($p$<0.05).

*3.3.3. The role of gaseous $O_3$ on the bactericidal action of plasma bubbles and generation of key reactive species*

Under the DBD conditions applied in this study, gaseous $O_3$ was produced the most and was injected into the water as a bubble (Fig. 12). In the present study, the reactive species contributing most to the bactericidal action of plasma bubbles were $^1O_2$ and $O_2^{\cdot-}$ (Fig. 15b). Hence, the first consideration was to verify the relationship between gaseous $O_3$ and the key reactive species ($^1O_2$ and $O_2^{\cdot-}$). The $O_3$ destruction unit was used to artificially eliminate $O_3$ gas produced from plasma generators, and the concentration of dissolved $O_3$ in solution was measured to assess whether $O_3$ gas was completely removed. Fig. 16a shows the dissolved $O_3$ concentration in the solution according to the $O_3$ filtration, which confirmed that there was no dissolved $O_3$ in the water under the $O_3$ gas destruction unit during the 5 min treatment of plasma bubbles. The results of applying the same conditions to *S.* Typhimurium inactivation experiments are presented in Fig. 16b. Since the filtration of gaseous $O_3$ completely eliminated the bactericidal action of plasma bubbles against *S.* Typhimurium for 5 min of treatment (Fig. 16b), it was confirmed that the production of $O_3$ gas and injection into the solution must be preceded to the inactivation of *S.* Typhimurium by plasma bubbles.

The production of $^1O_2$ in PAW was analyzed because the role of $^1O_2$ in the bactericidal action of *S.* Typhimurium by plasma bubbles is important (Fig. 15b). The amount of accumulated $^1O_2$ after 5 min of plasma bubble treatment was approximately 168.40 ± 14.812 μM (Fig. 17a). Since it was necessary to identify which reactive species mainly contributed to the formation of $^1O_2$

during plasma bubble treatment, whether $O_2^{\cdot-}$, which plays a role in *S.* Typhimurium inactivation at a level equivalent to $^1O_2$, could affect the formation of $^1O_2$ was first considered. After 5 min of plasma bubble treatment with the addition of tiron (a scavenger of $O_2^{\cdot-}$), it was confirmed that no $^1O_2$ was produced in the PAW (Fig. 17b). These results indicate that $O_2^{\cdot-}$ is fully involved in the final production of $^1O_2$, which, in turn, has a direct effect on *S.* Typhimurium inactivation.

$^1O_2$ and $O_2^{\cdot-}$ are major ROS and have the potential to improve the bactericidal and virucidal effects of PAW (Ma et al., 2020; Guo et al., 2018). Guo et al. (2018) reported that $^1O_2$ effectively inactivated bacteriophages (double- and single-stranded DNA as well as RNA bacteriophages) in water by attacking both proteins and nucleic acids, resulting in the aggregation of bacteriophages (Guo et al., 2018). Ma et al. (2020) also proved that $^1O_2$ and $O_2^{\cdot-}$ induced the antibacterial effects of PAW against *Escherichia coli* DH5α., and that both species were generated by post-discharge reactions (reaction 1-5) due to their short half-life. In order for the aforementioned reaction (reaction 1-5) to occur, sufficiently generated $NO_2^-$ and $H_2O_2$ must react with each other to produce ONOOH, which can further interact with $H_2O_2$ to produce peroxynitric acid ($O_2NOOH$). Finally, $O_2NOOH$ decomposes into $^1O_2$ and $O_2^{\cdot-}$. However, in the current system, it is difficult for $^1O_2$ or $O_2^{\cdot-}$ to be produced through these reactions because $NO_2^-$ is not detected in PAW (detection limit: 2.00 ppm) due to insufficient NOx generation in DBD plasma, and sodium pyruvate (a scavenger of $H_2O_2$) does not eliminate the bactericidal effect of plasma bubbles.

In our plasma bubble system, it was confirmed that the injection of $O_3$ gas must precede for generating the source of the antimicrobial action, and the presence of $O_2^{\cdot-}$ is necessary for the production of $^1O_2$. Once $O_3$ enters the water, it becomes highly unstable and rapidly decomposes through a complex series of reactions. At this time, hydroxide ions ($HO^-$) can initiate a chain reaction, which is sustained by $HO_2^{\cdot}$ as follows (Silva and Jardim, 2006):

(6) $O_3 + HO^- \rightarrow HO_2^{\cdot} + O_2^{\cdot-}$

The $HO_2^{\cdot}$ generated by the above reaction may initiate further reactions and contribute to the production of $^1O_2$. The possible reactions that have been proposed for converting $O_2^{\cdot-}$ to $^1O_2$ are as follows (Tarr and Valenzeno, 2003):

(7) $HO_2^{\cdot} + HO_2^{\cdot} \rightarrow {}^1O_2 + H_2O_2$

(8) $HO_2^{\cdot} + O_2^{\cdot-} + H^+ \rightarrow {}^1O_2 + H_2O_2$

In reaction (7), two $HO_2^{\cdot}$ molecules react together to produce $^1O_2$ (rate constant of $8.6 \times 10^5$ $M^{-1}s^{-1}$) (Tarr and Valenzeno, 2003). Reaction (8) shows the spontaneous dismutation reaction for superoxide, in which $O_2^{\cdot-}$ reacts with $HO_2^{\cdot}$ to produce $^1O_2$ and $H_2O_2$ (rate constant of $9.7 \times 10^7$ $M^{-1}s^{-1}$) (Tarr and Valenzeno, 2003). As $O_2^{\cdot-}$ is essential for the production of $^1O_2$ in this study, it is worth considering the possibility that the reaction (8) is the main path for $^1O_2$ production. In addition, since the solution pH remained at $6.30 \pm 0.042$ during the 5 min plasma bubble treatment, the reaction rate of reaction (7) is relatively lower than that of reaction (8) as the $HO_2^{\cdot}/O_2^{\cdot-}$ ratio falls 10-fold for each unit rise in pH above a p$K_a$ of 4.8.

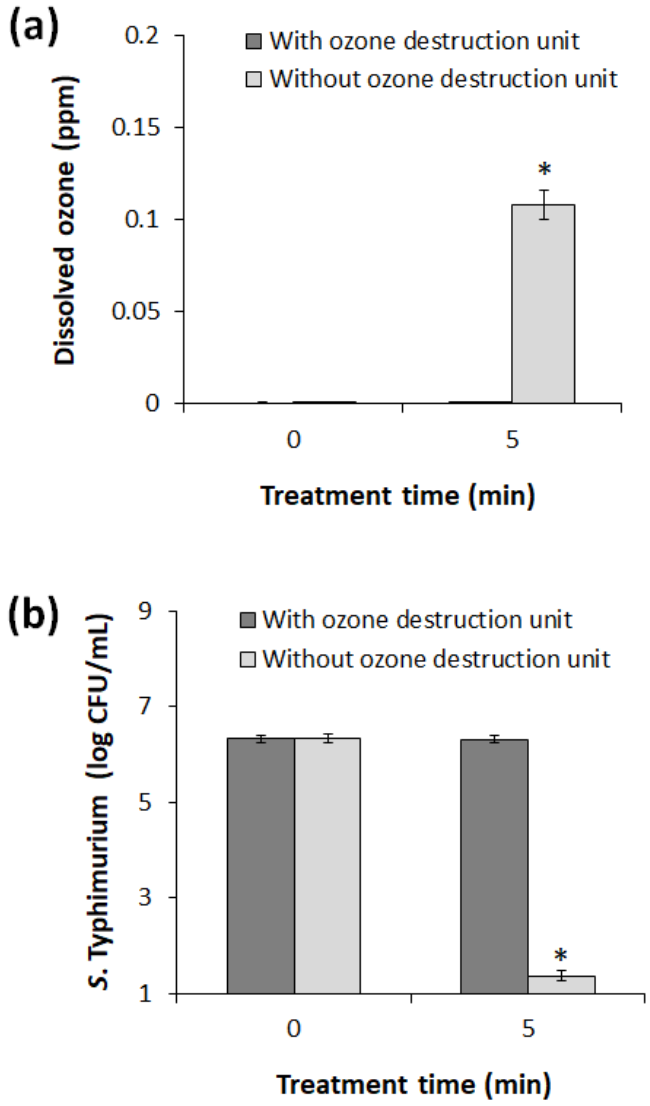


Figure 16. (a) Concentrations of dissolved $O_3$ in PAW; (b) the surviving population (log CFU/mL) of *S.* Typhimurium after 5 min of plasma bubble treatment according to $O_3$ filtration.

Error bars denote standard deviation.

Student's *t*-test; $^{*}$, $p<0.05$ with respect to the untreated control.

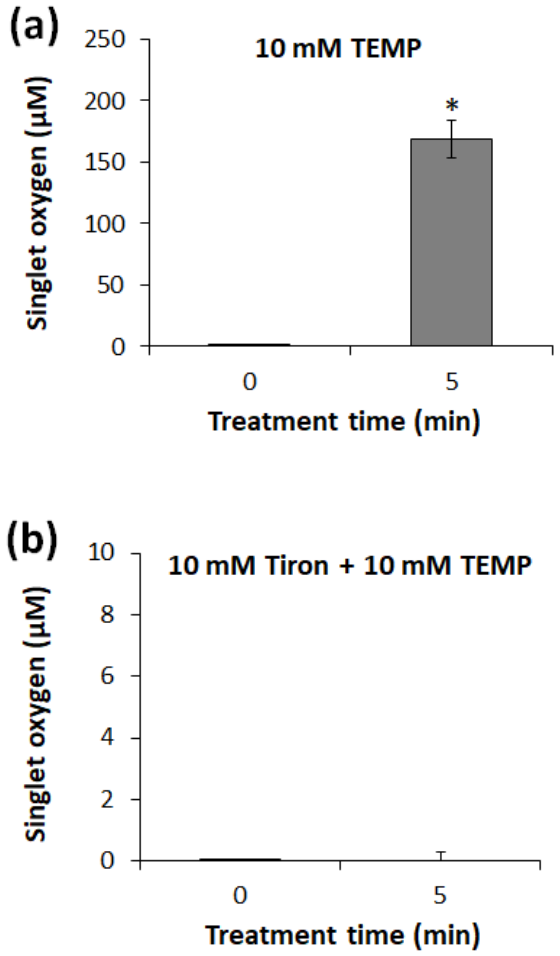


Figure 17. Concentrations of accumulated $^1O_2$ in PAW (a) without or (b) with the addition of 10 mM tiron (a scavenger of $O_2^{\cdot-}$) during 5 min plasma bubble treatment.

TEMP: 2,2,6,6-tetramethylpiperidine (a spin trap reagent for trapping $^1O_2$.

Error bars denote standard deviation.

Student's *t*-test; $^*$, $p<0.05$ with respect to the untreated control.

*3.3.4. Effects of organic matter on the inactivation efficacy of plasma bubbles*

The effects of organic matter on the inactivation efficacy of plasma bubbles against *S.* Typhimurium are presented in Fig. 18. First, plasma bubble treatment in the absence of organic matter effectively inactivated *S.* Typhimurium, resulting in a reduction of more than 5.86 log CFU/mL within 10 min ($p<0.05$). On the other hand, *S.* Typhimurium inactivation efficiency in organic mixtures (0.005-0.5 g/L) according to plasma bubble treatment time decreased as the concentration of organic matter increased. When plasma bubbles were treated for 10 and 20 min with 0.005 g/L organic matter, the surviving population of *S.* Typhimurium decreased by 4.21 and 5.59 log CFU/mL ($p < 0.05$), respectively, and no surviving bacteria were detected when treated for more than 25 min (detection limit: $10^1$ CFU/mL; Fig.18). The bacterial inactivation efficiency of the plasma bubbles after 10 min of treatment decreased in the 0.05 g/L organic matter compared to 0.005 g/L, but the survival population of *S.* Typhimurium decreased by 3.06 and 4.77 log CFU/mL ($p<0.05$) as plasma bubbles were treated for 10 and 20 min, respectively, and the bactericidal effect of approximately 5.47 log CFU/mL was shown after 30 min of plasma bubble treatment ($p<0.05$; Fig. 18). However, in organic matter at a 0.1 g/L concentration, the inactivation efficiency of the plasma bubbles for *S.* Typhimurium decreased dramatically, and the 10 min treatment of plasma bubbles did not show any significant bactericidal effect ($p>0.05$). Under the same conditions, the number of *S.* Typhimurium decreased by 1.17, 1.72, and 2.96 log CFU/mL ($p<0.05$), respectively, when plasma bubbles were treated for 20, 25, and 30 min (Fig.

18). When the concentration of organic matter was 0.5 g/L, the bactericidal effect of the plasma bubbles against *S.* Typhimurium was completely eliminated, and no significant reduction was observed even when the plasma bubbles were treated for up to 30 min ($p$>0.05) (Fig. 18). These results indicate that organic matter severely attenuated the inactivation effect of plasma bubbles against *S.* Typhimurium in a dose-dependent manner.

Various sanitizers and disinfectants being less effective in the presence of organic matter, including beef extract, peptone, tryptone, and cellulose, has previously been suggested in a number of studies (Xiang et al., 2019; Huo et al., 2018; Jo et al., 2018). Chen et al. (2017) demonstrated that organic loads affect the chlorine requirements of produce (romaine lettuce, iceberg lettuce, strawberries, and grapes) wash water, especially as organic loads increase. Jo et al. (2018) found that proteins have the greatest negative effect on the antibacterial efficacy of slightly acidic electrolyzed water against *Bacillus cereus* (ATCC 14579; 10987), *Listeria monocytogenes* (ATCC 19118 and Scott A), *Escherichia coli* O157:H7 (ATCC 35150; 43894), and *S. enterica* (*S. enteritidis* ATCC 13076 and *S.* Typhimurium ATCC 14028) compared to lipids and carbohydrates. Xiang et al. (2019) also reported that high concentrations of organic matter affected the physicochemical properties of PAW, such as pH, ORP, and $NO_2^-$, thereby reducing the antibacterial properties of PAW. Similarly, in this study, organic matter attenuated the antibacterial property of plasma bubbles in a dose-dependent manner, but PAW is still highly available because longer contact times have allowed it to eventually inactivate microorganisms successfully (except for the highest

organic matter concentrations).

Particularly for PAW, since reactive species have a remarkably short half-life and can react with a variety of organic materials (Table 8) (Møller et al., 2007), there are some limitations in the pasteurization of microorganisms present on the surfaces of food or in mixture solutions. To overcome some of these limitations, we applied bubble technology, which has the potential to increase the efficiency of mass transfer (Liu et al., 2018; Zhou et al., 2019), but unfortunately, the characteristics of bubbles (such as bubble size and density) and the efficiency of mass transfer have not yet been considered in depth.

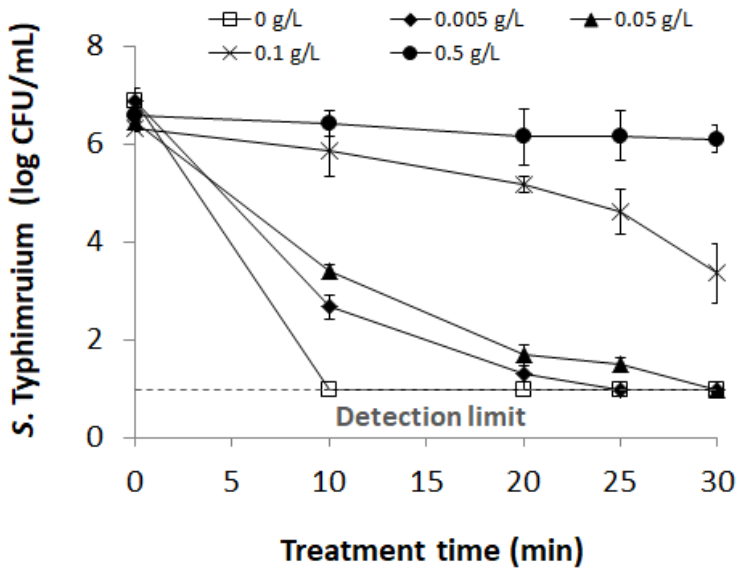


Figure 18. Effects of different concentrations of organic matter (final concentration: 0, 0.005, 0.05, 0.1, and 0.5 g/L) on the inactivation efficacy of plasma bubbles against *S*. Typhimurium according to plasma bubble treatment times (0, 10, 20, 25, and 30 min).

The organic matter consisted of 37.5% beef extract and 62.5% peptone by weight.

Error bars denote standard deviation.

### 3.4. Conclusion

This study was conducted to determine the key reactive species generated by non-thermal plasma bubbles for the inactivation of *S.* Typhimurium and to examine the effects of organic matter on inactivation efficacy. Plasma bubble treatment effectively inactivated *S.* Typhimurium floating in water, and $^{1}O_2$ originating mainly from $O_3$ and $O_2^{\cdot-}$ contributed substantially to the bactericidal action. Organic matter attenuated the bactericidal action of plasma bubbles in a dose-dependent manner, but the potential for inactivating *S.* Typhimurium was confirmed successfully with longer contact times. In future, it will be necessary to consider the types and contents of organic matter contained in the target (solid, semisolid, or liquid phase) for practical applications in food-related materials, and the specific pasteurization mechanism of plasma bubbles through bubble characterization will need to be identified.

**References**


Aboubakr, H. A., Gangal, U., Youssef, M. M., Goyal, S. M., & Bruggeman, P. J. (2016). Inactivation of virus in solution by cold atmospheric pressure plasma: identification of chemical inactivation pathways. *Journal of Physics D: Applied Physics*, *49*, 204001.

APHA. (1992). APHA Method 4500-$O_3$: *Standard methods for the examination of water and wastewater*, *18th ed*.

Baek, D. Y., Park, J. H., Cho, S. C., & Lee, Y. D. (2020). Rapid detection of shiga-toxin producing *E. coli* by bacteriophage amplification assay. *Korean Journal of Food Science and Technology*, *52*, 103-108.

Baek, K. H., Yong, H. I., Yoo, J. H., Kim, J. W., Byeon, Y. S., Lim, J., Yoon, S. Y., Ryu, S., & Jo, C. (2020). Antimicrobial effects and mechanism of plasma activated fine droplets produced from arc discharge plasma on planktonic *Listeria monocytogenes* and *Escherichia coli* O157:H7. *Journal of Physics D: Applied Physics*, *53*, 124002.

Burns, J. M., Cooper, W. J., Ferry, J. L., King, D. W., DiMento, B. P., McNeill, K., Miller, C. J., Miller, W. L., Peake, B. M., Rusak, S. A., Rose, A. L., & Waite, T. D. (2012). Methods for reactive oxygen species (ROS) detection in aqueous environments. *Aquatic Sciences*, *74*, 683-734.

Cao, W., Zhu, Z. W., Shi, Z. X., Wang, C. Y., & Li, B. M. (2009). Efficiency of slightly acidic electrolyzed water for inactivation of *Salmonella* Enteritidis and its contaminated shell eggs. *International Journal of Food Microbiology*, *130*, 88-93.

Chen, X., & Hung, Y. C. (2017). Effects of organic load, sanitizer pH and initial chlorine concentration of chlorine-based sanitizers on chlorine demand of fresh produce wash waters. *Food Control*, *77*, 96-101.

Chung, J. W., Park, J. W., & Lee, C. S. (2010). Effects of operating parameters on dissolved ozone and phenol degradation in ozone contact reactor. *Journal of Korean Society of Environmental Engineers*, *32*, 241-247.

Fan, W., An, W. G., Huo, M. X., Yang, W., Zhu, S. Y., & Lin, S. S. (2020). Solubilization and stabilization for prolonged reactivity of ozone using micro-nano bubbles and ozone-saturated solvent: A promising enhancement for ozonation. *Separation and Purification Technology*, *238*, 116484.

Guo, L., Xu, R., Gou, L., Liu, Z., Zhao, Y., Liu, D., Zhang, L., Chen, H., & Kong, M. G. (2018). Mechanism of virus inactivation by cold atmospheric-pressure plasma and plasma-activated water. *Applied and Environmental Microbiology*, *84*, e00726-18.

Hong, Y. C., Huh, J. Y., Ma, S. H., & Kim, K. I. (2018). Inactivation of microorganisms by radical droplets from combination of water discharge and electro-spraying. *Journal of Electrostatics*, *91*, 56-60.

Huang, Y., & Chen, H. (2011). Effect of organic acids, hydrogen peroxide and mild heat on inactivation of *Escherichia coli* O157:H7 on baby spinach. *Food Control*, *22*, 1178-1183.

Huo, Z. Y., Li, G. Q., Yu, T., Lu, Y., Sun, H., Wu, Y. H., Yu, C., Xie, X., & Hu, H. Y. (2018). Impact of water quality parameters on bacteria

inactivation by low-voltage electroporation: mechanism and control. *Environmental Science: Water Research & Technology*, *4*, 872-881.

Ji, S. H., Ki, S. H., Ahn, J. H., Shin, J. H., Hong, E. J., Kim, Y. J., & Choi, E. H. (2018). Inactivation of *Escherichia coli* and *Staphylococcus aureus* on contaminated perilla leaves by dielectric barrier discharge (DBD) plasma treatment. *Archives of Biochemistry and Biophysics*, *643*, 32-41.

Jo, H. Y., Tango, C. N., & Oh, D. H. (2018). Influence of different organic materials on chlorine concentration and sanitization of slightly acidic electrolyzed water. *LWT*, *92*, 187-194.

Jung, S. J., Park, S. Y., & Ha, S. D. (2018). Synergistic effect of X-ray irradiation and sodium hypochlorite against *Salmonella enterica* serovar Typhimurium biofilms on quail eggshells. *Food Research International*, *107*, 496-502.

Ke, Z., Chen, Z., & Huang, Q. (2018). Effect of chloride on bacterial inactivation by discharge plasma at the gas-solution interface: Potentiation or attenuation?. *Plasma Processes and Polymers*, *15*, 1700153.

Kim, T., Seo, H., Bae, H., Kim, T., Yang, S., & Moon, E. (2018). Generation of active species and antimicrobial efficacy of an underwater plasma device equipped with a porous bubbler. *Plasma Processes and Polymers*, *15*, 1700229.

Lee, I., Lee, E., Lee, H., & Lee, K. (2011). Removal of COD and color from anaerobic digestion effluent of livestock wastewater by advanced oxidation using microbubbled ozone. *Applied Chemistry for Engineering*, *22*, 617-622.

Lee, S. Y., Rhee, M. S., Dougherty, R. H., & Kang, D. H. (2010). Antagonistic effect of acetic acid and salt for inactivating *Escherichia coli* O157:H7 in cucumber puree. *Journal of Applied Microbiology*, *108*, 1361-1368.

Lin, C. M., Chu, Y. C., Hsiao, C. P., Wu, J. S., Hsieh, C. W., & Hou, C. Y. (2019). The optimization of plasma-activated water treatments to inactivate *Salmonella* Enteritidis (ATCC 13076) on shell eggs. *Foods*, *8*, 520.

Liu, Y., Zhang, H., Sun, J., Liu, J., Shen, X., Zhan, J., Zhang, A., Ognier, S., Cavadias, S., & Li, P. (2018). Degradation of aniline in aqueous solution using non-thermal plasma generated in microbubbles. *Chemical Engineering Journal*, *345*, 679-687.

Lukes, P., Dolezalova, E., Sisrova, I., & Clupek, M. (2014). Aqueous-phase chemistry and bactericidal effects from an air discharge plasma in contact with water: evidence for the formation of peroxynitrite through a pseudo-second-order post-discharge reaction of $H_2O_2$ and $HNO_2$. *Plasma Sources Science and Technology*, *23*, 015019.

Ma, S., Kim, K., Huh, J., & Hong, Y. (2017). Characteristics of microdischarge plasma jet in water and its application to water purification by bacterial inactivation. *Separation and Purification Technology*, *188*, 147-154.

Machala, Z., Tarabová, B., Sersenová, D., Janda, M., & Hensel, K. (2018). Chemical and antibacterial effects of plasma activated water: correlation with gaseous and aqueous reactive oxygen and nitrogen species, plasma

sources and air flow conditions. *Journal of Physics D: Applied Physics*, *52*, 034002.

Ma, M., Zhang, Y., Lv, Y., & Sun, F. (2020). The key reactive species in the bactericidal process of plasma activated water. *Journal of Physics D: Applied Physics*, *53*, 185207.

Møller, I. M., Jensen, P. E., & Hansson, A. (2007). Oxidative modifications to cellular components in plants. *Annual Review of Plant Biology*, *58*, 459-481.

Ovissipour, M., Al-Qadiri, H. M., Sablani, S. S., Govindan, B. N., Al-Alami, N., & Rasco, B. (2015). Efficacy of acidic and alkaline electrolyzed water for inactivating *Escherichia coli* O104:H4, *Listeria monocytogenes*, *Campylobacter jejuni*, *Aeromonas hydrophila*, and *Vibrio parahaemolyticus* in cell suspensions. *Food Control*, *53*, 117-123.

Park, S., Choe, W., & Jo, C. (2018). Interplay among ozone and nitrogen oxides in air plasmas: Rapid change in plasma chemistry. *Chemical Engineering Journal*, *352*, 1014-1021.

Puyate, Y. T., & Rim-Rukeh, A. (2008). Biocidal efficacy of dissolved ozone, formaldehyde and sodium hypochlorite against total planktonic microorganisms in produced water. *Journal of Applied Sciences*, *8*, 860-865.

Qian, J., Zhuang, H., Nasiru, M. M., Muhammad, U., Zhang, J., & Yan, W. (2019). Action of plasma-activated lactic acid on the inactivation of inoculated *Salmonella* Enteritidis and quality of beef. *Innovative Food Science & Emerging Technologies*, *57*, 102196.

Silva, L. M. D., & Jardim, W. F. (2006). Trends and strategies of ozone application in environmental problems. *Química Nova*, *29*, 310-317.

Skowron, K., Wałecka-Zacharska, E., Grudlewska, K., Białucha, A., Wiktorczyk, N., Bartkowska, A., Kowalska, M., Kruszewski, S., & Gospodarek-Komkowska, E. (2019). Biocidal Effectiveness of Selected Disinfectants Solutions Based on Water and Ozonated Water against *Listeria monocytogenes* Strains. *Microorganisms*, *7*, 127.

Tarr, M., & Valenzeno, D. P. (2003). Singlet oxygen: the relevance of extracellular production mechanisms to oxidative stress in vivo. *Photochemical & Photobiological Sciences*, *2*, 355-361.

Wu, V. C. H., & Fung, D. Y. C. (2001). Evaluation of thin agar layer method for recovery of heat-injured foodborne pathogens. *Journal of Food Science*, *66*, 580-583.

Xiang, Q., Kang, C., Zhao, D., Niu, L., Liu, X., & Bai, Y. (2019). Influence of organic matters on the inactivation efficacy of plasma-activated water against *E. coli* O157: H7 and *S. aureus*. *Food Control*, *99*, 28-33.

Yong, H. I., Han, M., Kim, H. J., Suh, J. Y., & Jo, C. (2018). Mechanism underlying green discolouration of myoglobin induced by atmospheric pressure plasma. *Scientific reports*, *8*, 1-9.

Yoo, J. H., Baek, K. H., Heo, Y. S., Yong, H. I., & Jo, C. (2020). Synergistic bactericidal effect of clove oil and encapsulated atmospheric pressure plasma against *Escherichia coli* O157: H7 and *Staphylococcus aureus* and its mechanism of action. *Food Microbiology*, *93*, 103611.

Zhao, Y., Chen, R., Tian, E., Liu, D., Niu, J., Wang, W., Qi, Z., Xia, Y., Song, Y., & Zhao, Z. (2018). Plasma-activated water treatment of fresh beef: Bacterial inactivation and effects on quality attributes. *IEEE Transactions on Radiation and Plasma Medical Sciences*, *4*, 113-120.

Zhou, R., Zhou, R., Wang, P., Luan, B., Zhang, X., Fang, Z., Xian, Y., Lu, X., Ostrikov, K. K., & Bazaka, K. (2019). Microplasma bubbles: reactive vehicles for biofilm dispersal. *ACS Applied Materials & Interfaces*, *11*, 20660-20669.

Zhou, R., Zhou, R., Wang, P., Xian, Y., Mai-Prochnow, A., Lu, X., Cullen, P. J., Ostrikov, K. K., & Bazaka, K. (2020). Plasma-activated water: generation, origin of reactive species and biological applications. *Journal of Physics D: Applied Physics*, *53*, 303001.

# Chapter IV.

# Blue light promotes bactericidal action of plasma-activated water against *Staphylococcus aureus* on stainless steel surfaces

## 4.1. Introduction

Plasma-activated water (PAW), which is mainly produced by applying atmospheric-pressure plasma to water, has drawn interest from various fields such as biomedicine, food hygiene, and wastewater treatment (El Shaer et al., 2020; Liu et al., 2016; Zhao et al., 2018; Zhou et al., 2019). The generation of plasma-induced reactive oxygen and nitrogen species (RONS) depends on electrode composition, gas type, gas flow, discharge condition (applied voltage), and so on (Zhou et al., 2020). Various RONS can penetrate or dissolve into the liquid to produce secondary RONS (Baek et al., 2020a). Therefore, PAW contains a variety of reactive species, such as hydrogen peroxide, nitric oxide, nitrite/nitrate ions, and peroxynitrites (Liao et al., 2020), which can contribute to organic matter degradation, plant growth promotion, and antiviral and antibacterial action (Liu et al., 2019; Zhou et al., 2020). Studies have recently been conducted to control pathogenic bacteria by applying PAW, and many researchers have suggested that the use of PAW can enhance food safety (Baek et al., 2020b; Liao et al., 2020; Royintarat et al.,

2020).

A number of microbial control studies using PAW have been carried out successfully, but various studies have shown that the bactericidal efficiency of PAW may vary depending on the target (surface roughness, organic matter composition, microbial type, and so on). Zhang et al. (2015) demonstrated that during liquid-based treatment, air pockets could form on rough surfaces, resulting in more opportunities to protect bacteria from sanitization. Xiang et al. (2019) suggested that the presence of organic materials could affect the chemical properties of PAW, reducing the bactericidal effect of PAW. Many researchers have demonstrated that the sensitivity of microorganisms to chemical oxidation by PAW differs owing to the structural differences between Gram-positive and Gram-negative bacteria (Baek et al., 2020b; Ji et al., 2018; Xu et al., 2018). Gram-positive bacteria, which have relatively thick extracellular structures (Mai-Prochnow et al., 2016), may be less sensitive to PAW than that are Gram-negative bacteria. Meanwhile, it has recently been suggested that various microorganisms have their own virulence factors that can resist oxidative stress (Krewing et al., 2019; Yang et al., 2020). Krewing et al. (2019) demonstrated that a molecular chaperone in *Escherichia coli*, heat shock protein 33, was converted to active chaperone by oxidative stress, preventing protein aggregation and consequently protecting bacteria from PAW. Staphyloxanthin (STX), a golden carotenoid pigment condensed into functional membrane microdomains (FMM) of bacterial cells, is produced by over 90% of *Staphylococcus aureus* clinical isolates (Chen et al., 2016; Hui et al., 2020). This pigment can contribute to protect the *S. aureus* against plasma

treatment by maintaining the integrity of the membrane and resisting reactive oxygen species (ROS) (Jusuf et al., 2020; Yang et al., 2020). Therefore, the study of these virulence factors can be very important to understand the exact mechanisms of various applications for controlling bacteria and promoting bactericidal efficiency. In particular, *S. aureus* is a representative Gram-positive bacterium that must be properly controlled for food hygiene (Wang et al., 2020; Yoo et al., 2021) and/or medical applications (mainly methicillin-resistant *S. aureus*) (Bekeschus et al., 2019; Ben Belgacem et al., 2017; Hu et al., 2019; Liao et al., 2018). Studies have recently suggested that blue light of wavelength near 460 nm may increase the sensitivity of *S. aureus* to oxidative stress. In this regard, it is worth investigating the promotion of the bactericidal efficiency of PAW against *S. aureus* using synergistic oxidative stress.

The light-emitting diode (LED), which uses semiconductor technology, is a diode that generates light on its own and is gaining recognition as a non-thermal technology (Do and Bang, 2013). LEDs at 405-470 nm wavelengths exhibit antibacterial activity, and their effects vary depending on the wavelength, power density, contact time, and target microorganism (Hyun et al., 2020). Interestingly, a recent study found that the entire wavelength range (400-490 nm) of blue light could induce the photolysis of STX, which is present in the functional membrane microdomains of *S. aureus* (Hui et al., 2020). Such STX decomposition reduces the inherent antioxidant properties of *S. aureus* and induces the perturbation of cell membranes, thus increasing the sensitivity to oxidative stress or antibiotics (Dong et al., 2019; Hui et al., 2020). Therefore, there is a possibility that the photolysis of STX by blue light

may enhance the bactericidal effects of PAW on *S. aureus*; however, no research has been conducted to ascertain this.

*S. aureus* can exist on food or food-related materials by adhering onto surfaces and produce staphylococcal enterotoxins, which can cause staphylococcal food poisoning (SFP) by ingestion (Fetsch and Johler, 2018). These bacteria can be contaminated in any process in food production, such as the vehicles carrying livestock or the equipment used in food preparation (Baek et al., 2020b). Therefore, in terms of food safety, it is important to properly clean and disinfect not only the food itself, but also all factors that may cause contamination by contacting the food, and many researchers have applied stainless steel surfaces as model samples (Choi et al., 2020; Ni et al., 2016; Kim and Kang, 2020).

In this study, we induced STX photolysis by applying a 466 nm blue light LED and investigated whether the bactericidal action of PAW on *S. aureus* could be enhanced. In addition, stainless steel surfaces were used as model samples for various equipment and materials in food preparation that are likely to be contaminated in the food industry and medical fields.

## 4.2. Material and methods

### *4.2.1. Bacterial strains, culture, and preparation*

The Gram-positive bacterium, *S. aureus* (ATCC 27213), used in this study was obtained from the bacterial culture collection of the Department of Food Science and Biotechnology at the Seoul National University (Seoul, Korea). *S. aureus* was cultivated in fresh sterile tryptic soy broth (TSB; Difco, Becton Dickinson Co., Sparks, MD, USA) at 37℃ and 120 rpm orbital agitation for 24 h. The cells were washed twice with sterile 0.85% saline solution by centrifugation at 4,000 *g* for 10 min at 4℃ using a refrigerated centrifuge (Combi R515, Hanil Scientific Inc., Gimpo, Korea). The pellets were re-suspended in sterile 0.85% saline solution at a final concentration of $10^8$-$10^9$ colony-forming unit (CFU)/mL ($OD_{600}$=0.2). The prepared bacterial suspension was used for various experiments by placing 3 or 5 mL in a petri-dish (35 × 10 mm) for each purpose.

### *4.2.2. Blue light source*

Fig. 19 presents the LED array used in this study. Three LEDs (LG Innotek Co., Ltd., Korea) with a central emission wavelength of 466 nm and a full width at half maximum (FWHM) of 27 nm were attached to the center of the heat sink (7 × 7 × 2.3 cm) (Fig. 20). The distance of the LED from the sample was 4 cm, and the irradiance was 18.74 ± 1.627 mW/cm$^2$ (Fig. 21). The irradiances were uniformly measured using a fiber optic spectrometer (AvaSpec-ULS2048-USB2-UA-50; Avantes, Eerbeek, The Netherlands).

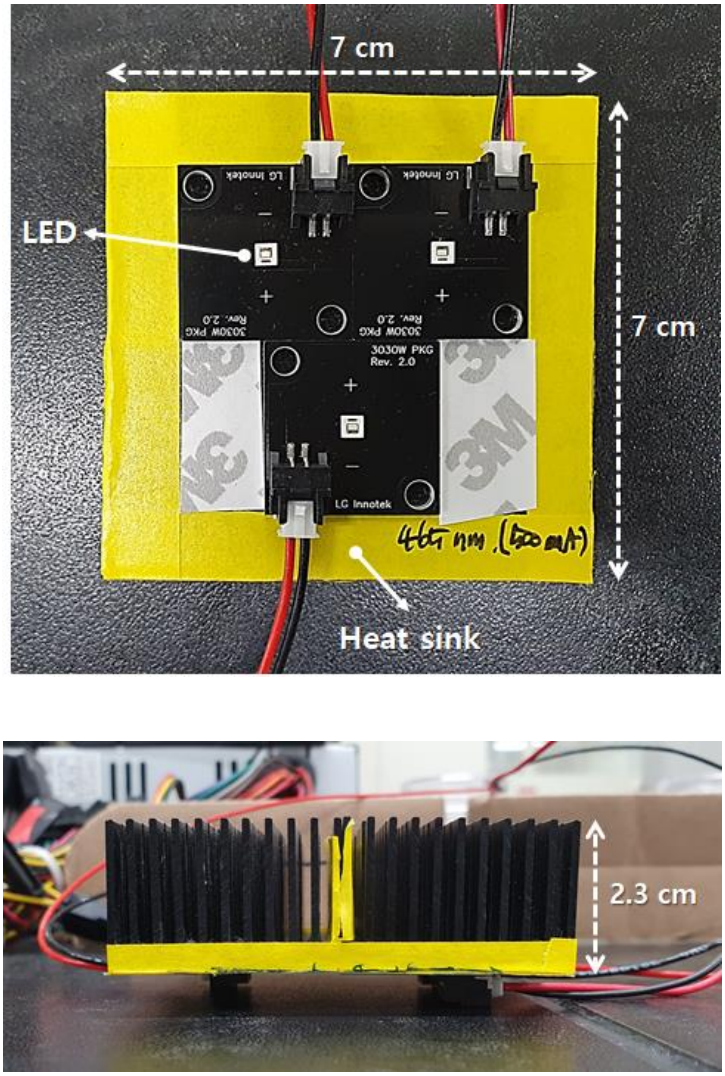


Figure 19. Depiction of blue light-emitting diode array.

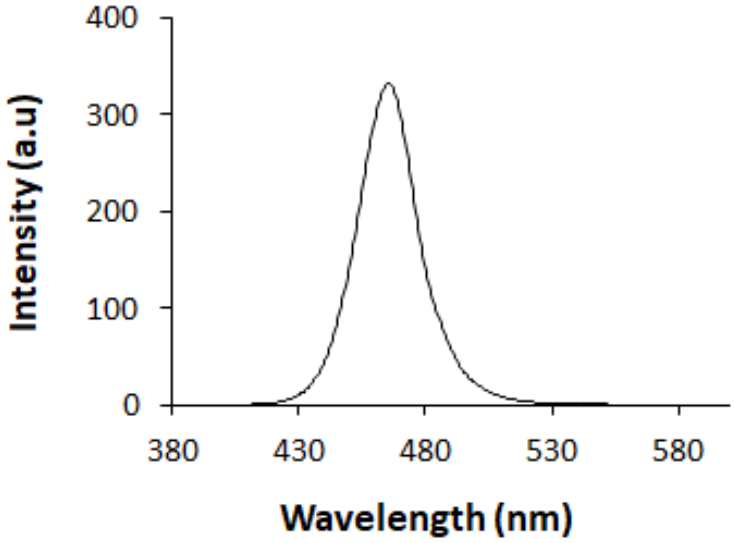


Figure 20. Emission spectrum of blue light-emitting diode (LED).

LED emitted blue light at a center wavelength of 466 nm with a full width at half maximum (FWHM) of 27 nm.

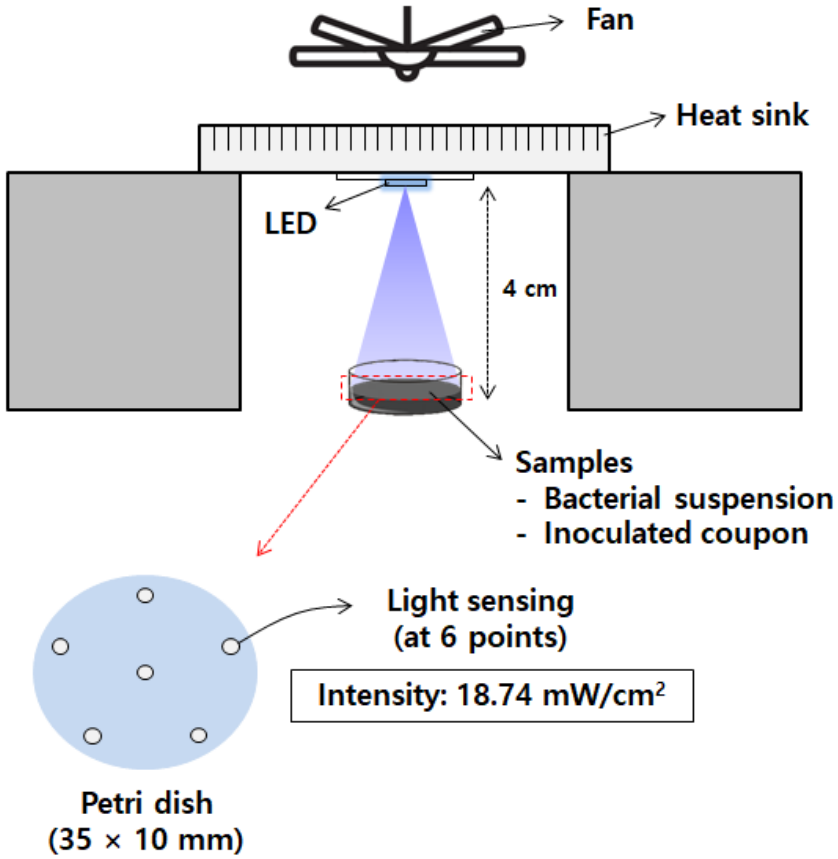


Figure 21. Experimental setup for blue light treatment.

*4.2.3. Encapsulated atmospheric-pressure plasma*

Fig. 22 presents the encapsulated atmospheric pressure plasma generator used in this study. The plasma generator was attached via copper electrodes and a polytetrafluoroethylene (PTFE) dielectric to the inner wall of a plastic container (13.7 × 10.4 × 5.3 cm), along with a removable and attachable lid. The discharge was carried out under 2.2 kHz and 4.2 kV conditions, and atmospheric-pressure air was used as the carrier gas. To measure the amount of gaseous ozone ($O_3$) and nitrogen oxides (NOx), the gas generated under the same operating conditions was collected and analyzed. The concentrations of gaseous $O_3$ and NOx were measured using an $O_3$ analyzer (106-M, 2B Technologies, Boulder, USA) and NO/NOx gas analyzer (nCLD 63, Eco Physics AG, Duernten, Switzerland), respectively. The gas present in the chamber after discharge was replaced with fresh dry air between the analyses.

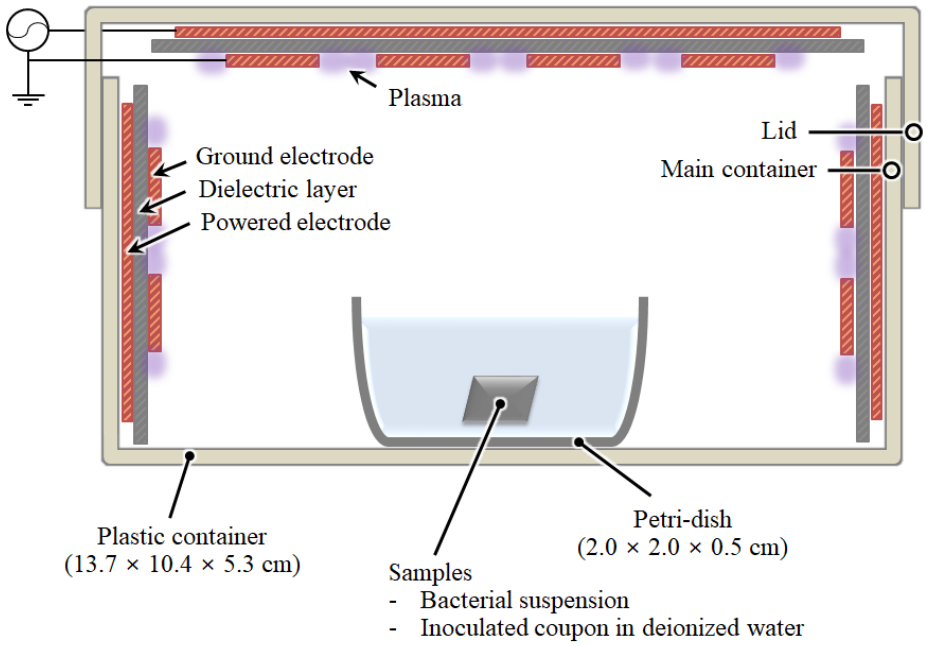


Figure 22. Schematic illustration of an encapsulated atmospheric-pressure dielectric barrier discharge (DBD) plasma generator.

*4.2.4. Synergistic bactericidal effect of blue light and PAW*

*4.2.4.1. Extraction and absorption intensity of carotenoids*

STX was extracted as previous reported (Dong et al., 2019). Ten milliliters of bacterial suspension was added into a 50 mL centrifuge tube and centrifuged at 4,000 *g* for 10 min. After removing the supernatant, 20 mL of methanol (HPLC grade, ≥99.9%) was added, and the cells were vortexed and re-suspended. STX pigments were extracted by treating the cells at 55℃ for 20 min using a digital precise water bath (WB-22; Daihan Scientific Co., Ltd., Korea). Following centrifugation, the supernatant containing STX pigments was collected and 5 mL was added into a petri-dish (35 × 10 mm); then, 466 nm blue light was applied at various dosages (0, 30, 60, 90, and 150 J/cm$^2$). The absorption intensity of the STX pigment at 460 nm was analyzed using a UV/Vis spectrophotometer (X-ma 3100, Human Co. Ltd, Seoul, Korea). In addition, a bacterial suspension ($OD_{600}$=0.2) was prepared without extraction process and treated under 150 J/cm$^2$ condition to examine changes in the absorbance intensity of the bacterial cells.

*4.2.4.2. Assessment of synergy between blue light and PAW*

The overall flow diagram for single and combined treatments of blue light and PAW is shown in Fig. 23. Five milliliters of *S. aureus* suspension was added into a petri-dish (35 × 10 mm) and treated with 466 nm blue light at a dosage of 150 J/cm$^2$. Following the treatment, the bacterial suspension was collected and mixed uniformly. Three milliliters of untreated or blue light-treated bacteria were added to a petri-dish (35 × 10 mm) and treated with

plasma for 10 min. In addition, the bactericidal effect of PAW was investigated by leaving the lid of the petri-dish closed for 10 min after plasma treatment. After all the treatments, the surviving population of bacteria was measured using the viable plate count method. An aliquot (1 mL) of the sample was decimally diluted serially in sterile 0.85% saline, and each diluent (100 μL) was spread on Baird-Parker agar (Difco) plates containing egg yolk tellurite enrichment (Difco), and incubated at 37℃ for 24 h. Considering the additional recovery of bacterial cells, the results of incubation time up to 72 h were confirmed, and the number of colonies was expressed as log CFU/mL.

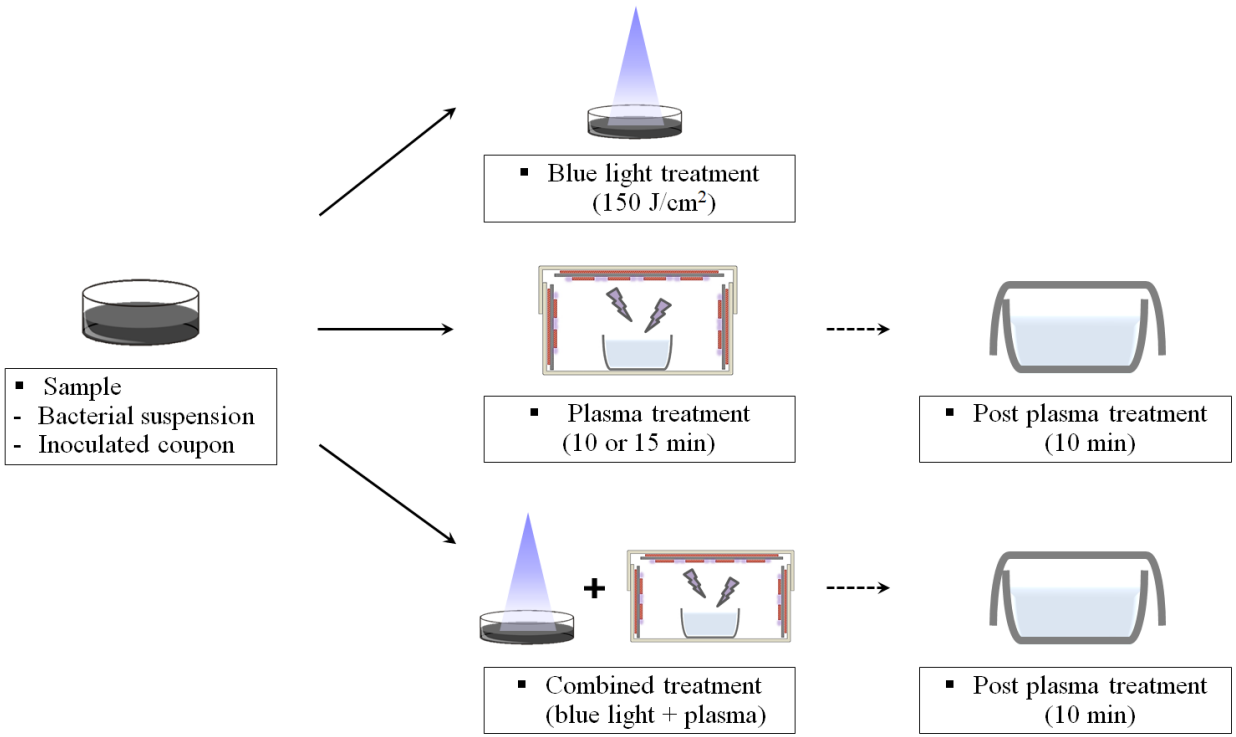


Figure 23. Flow diagram of the experimental procedure for examining synergy between blue light and plasma-activated water.

*4.2.4.3. Measurement of nucleic acid and protein leakage*

The leakage of nucleic acid and protein from single- or combined-treated *S. aureus* was measured by UV absorption according to a previous study (Yoo et al., 2021) with slight modifications. After single or combined treatment with blue light (150 J/cm$^2$) and plasma (10 min), supernatants were obtained by centrifugation of the bacterial suspension at 12,000 *g* for 3 min (Combi R515, Hanil Scientific Inc.). The amount of nucleic acid and protein released into the cell suspension was analyzed using a UV/Vis spectrophotometer (X-ma 3100, Human Co.) by measuring the absorbance of the supernatants at 260 and 280 nm, respectively.

*4.2.4.4. Determination of cell membrane integrity*

A SYTOX$^{TM}$ green (S7020; Invitrogen, USA) was used to evaluate cell membrane integrity. Green fluorescence indicates membrane-damaged bacteria. After 150 J/cm$^2$ of blue light treatment, the bacteria were immediately centrifuged at 12,000 *g* for 3 min (Combi R515, Hanil Scientific Inc.), and re-suspended in 1 mL of sterile deionized water, as SYTOX$^{TM}$ green showed the best performance in buffer without phosphate. The dye (2 μL) was dripped into 1 mL of the bacterial suspension, mixed, and incubated for 10 min at room temperature. Each sample (5 μL) was dripped onto a glass slide (Paul Marienfeld GmbH & Co. KG, Laud-Königshofen, Germany) and covered. A confocal laser scanning microscope (Leica TCS SP8 X, Wetzlar, Germany) was used with appropriate filters for excitation/emission wavelengths at 488/523 nm for SYTOX$^{TM}$ green.

*4.2.5. Synergistic bactericidal effect of blue light and PAW on coupons*

*4.2.5.1. Preparation and inoculation of surfaces*

Stainless steel coupons (2.0 × 2.0 × 0.1 cm) were used as test surfaces. Prior to inoculation, each coupon was washed with 70% ethanol, rinsed with deionized water, and autoclaved at 121℃ for 15 min. Each coupon was dried in a laminar flow clean bench for 1 h to evaporate the residual moisture. A 100 μL aliquot of *S. aureus* suspension was dropped at 9 different points on the coupon, and spread with a sterile spreader for even distribution and attachment. The inoculated coupons were dried for 2 h on a clean bench.

*4.2.5.2. Bactericidal effects of blue light and PAW on coupon*

Inoculated coupons were treated with 466 nm blue light at dosage of 150 J/cm$^2$. Following treatment, an untreated or blue light-treated coupon was added into a petri-dish (60 × 15 mm), which contained 10 mL of sterile deionized water, and treated with plasma for 15 min. The washing effect of the soaking was corrected by the blank that excluded plasma treatment only.

*4.2.5.3. Microbial analysis*

Immediately after treatment, each coupon was transferred to 50 mL centrifuge tube containing 20 mL of 0.1 M phosphate-buffered saline (PBS, pH 7.4) and 2.0 g of glass beads (425-600 μm; Sigma-Aldrich, St. Louis, MO, USA). The sample was vortexed for 2 min. An aliquot (1 mL) of the sample was decimally diluted serially in sterile 0.85% saline, and each diluent (100 μL) was spread on Baird-Parker agar (Difco) plates containing egg yolk

tellurite enrichment (Difco), and incubated at 37℃ for 24 h. Considering the additional recovery of bacterial cells, the results of incubation time up to 72 h were confirmed, and the number of colonies was expressed as log CFU/$cm^2$.

*4.2.6. Statistical analysis*

All experiments were conducted in triplicates. SAS statistical software (version 9.4, SAS Institute Inc., Cary, NC, USA) was used to analyze the data. Student's *t*-test and Tukey's multiple comparison test were used for statistical analyses. Significant differences among the mean values were established at a significance level of $p<0.05$.

## 4.3. Results and discussion

### *4.3.1. Reactive species in gas phase*

The concentration of gas phase reactive species according to plasma discharge time is shown in Fig. 24. During the discharge, gaseous $O_3$ concentration increased to about 1,350 ppm within 2 min, and tended to decrease as the discharge time increased. Park et al. (2018) reported that the rapidly generated $O_3$ at the early stage of discharge was eventually quenched by NO, resulting in the dominance of NO and $NO_2$, and that gas temperature ($N_2$ vibrational temperature) is one of the important factors in this transition. In this experiment, the concentration of NOx increased, as that of $O_3$ gas decreased, to about 15 and 76 ppm during 10 and 15 min of discharge, respectively. Since high concentrations of $O_3$ gas occur during plasma treatment to solutions (Fig. 24) and can be harmful to humans (Brodowska et al., 2018; Guzel-Seydim et al., 2004), safe and proper way should be considered to decompose or release residual $O_3$ gas for industrial application.

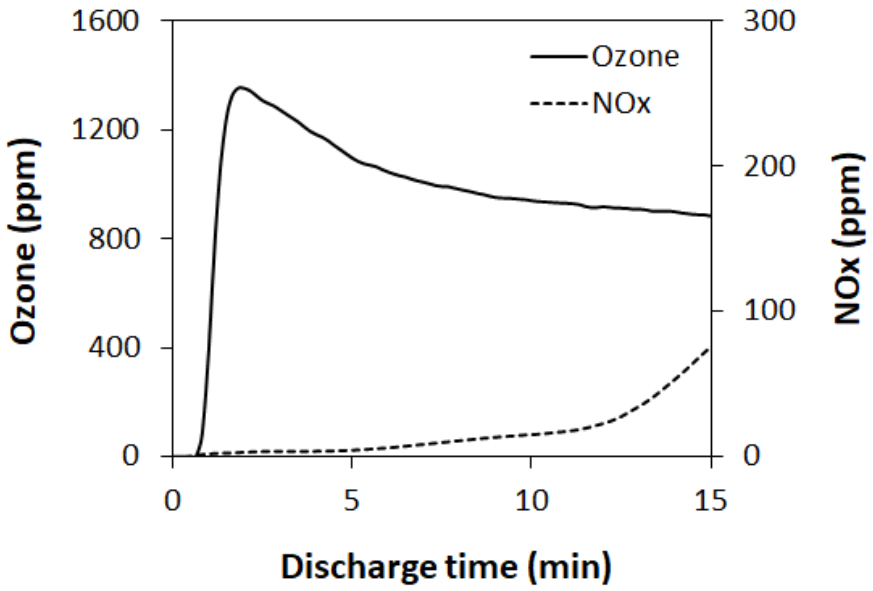


Figure 24. Gaseous ozone ($O_3$) and nitrogen oxides (NOx) concentration in dielectric barrier discharge plasma generator during discharge.

*4.3.2. Photobleaching of STX extract and S. aureus*

Fig. 25 and 26 shows the absorption intensity of crude STX extract and *S. aureus* at 460 nm. The untreated extract showed relatively stronger absorption at 460 nm compared to the blue light-treated samples. When the STX extract was treated with blue light, the absorbance value at 460 nm significantly decreased ($p<0.05$) in a dose-dependent manner, and the extract became completely transparent when treated above 150 J/cm$^2$ (Fig. 25). These results confirmed that the STX pigments might lose their inherent golden color as photolysis occurs due to exposure to 466 nm blue light, which is similar to the findings presented by Dong et al. (2019). Moreover, the absorbance at 460 nm decreased when *S. aureus* cells were treated directly at 150 J/cm$^2$, which caused the highest photolysis in the STX extract (Fig. 26). Jusuf et al. (2020) suggested that exposure of microbial cells to blue light could result in a relatively less effective in measuring photolysis compared to that of STX extracts, owing to the various biological components contained in cells. Despite this phenomenon, blue light treatment (150 J/cm$^2$) induced photolysis of STX in *S. aureus* cells, which was confirmed by the fading of the intense yellow color of the bacterial suspension (Fig. 26). For the subsequent experiments, a dosage of 150 J/cm$^2$ was chosen as the optimal condition as it induced the highest STX photobleaching.

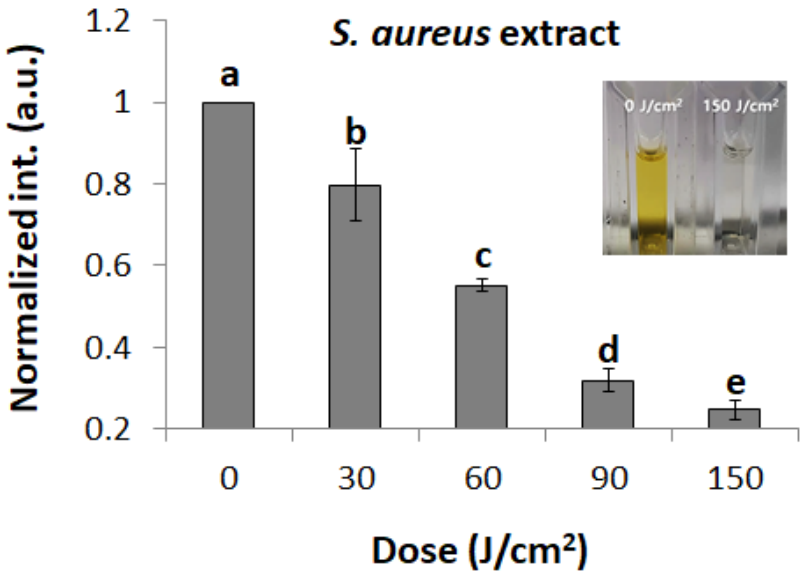


Figure 25. Absorption intensity of crude staphyloxanthin (STX) pigment at 460 nm following treatment to 0, 30, 60, 90, and 150 J/cm$^2$ of 466 nm blue light.

Error bars denote standard deviation.

[a-e]Different letters indicate significant differences ($p$<0.05).

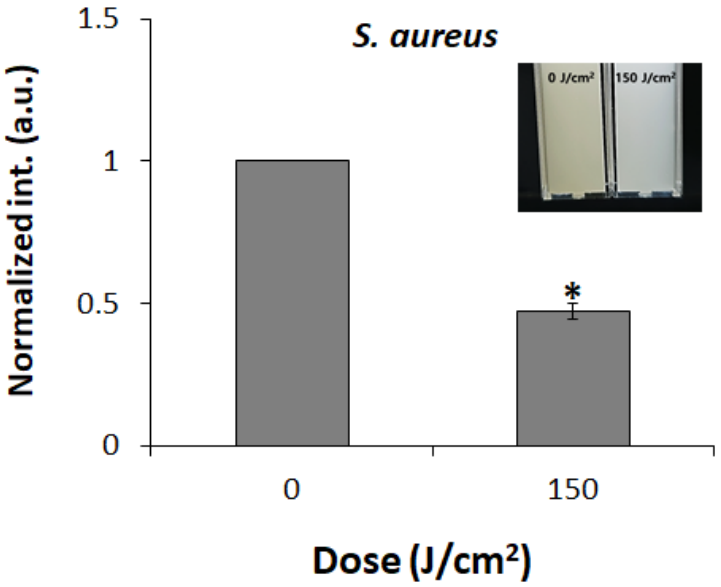


Figure 26. Absorption intensity of *S. aureus* at 460 nm following treatment to 150 J/cm$^2$ of 466 nm blue light.

Error bars denote standard deviation.

Student's *t*-test; $^*$, $p<0.05$ with respect to the untreated control.

*4.3.3. Bactericidal effects of individual and combined treatment of blue light and PAW*

Fig. 27 shows the bactericidal effects of individual and combined treatments of 466 nm blue light (150 J/cm$^2$) and PAW (10 min) against *S. aureus* cells. Blue light (150 J/cm$^2$) did not show any significant bactericidal effect. Although studies have suggested that blue light exhibit bactericidal properties, this depends on the target bacterial strain and treatment conditions (Amin et al., 2016; Hui et al., 2020; Hyun et al., 2020); Dong et al. (2019) have demonstrated the possibility that blue light-treated *S. aureus* can be recovered with limited damages. The number of *S. aureus* cells decreased by 1.07 log CFU/mL when treated for 10 min with plasma alone ($p$<0.05). However, the combined treatment with blue light and plasma showed a bactericidal effect of 2.70 log CFU/mL, which was about 40 times greater than that of the individual plasma treatment (Fig. 27). This may be due to the fact that 466 nm blue light (150 J/cm$^2$) induced photolysis of STX (Fig. 25 and 26). The photolysis of STX may have reduced the specific antioxidant activities of *S. aureus*, and may have increased sensitivity to various reactive species in PAW due to perturbation of the cell membrane wherein STX was present. The same pattern could be identified when the sample were left for an additional 10 min after single and combined treatments to observe the post-treatment effects. In particular, when the combined treatment group was left for 10 min, the reduction in the viable *S. aureus* population was more than 6.66 log CFU/mL compared to that in the control group, resulting in non-detectable levels (detection limit: 1 log CFU/mL) (Fig. 27).

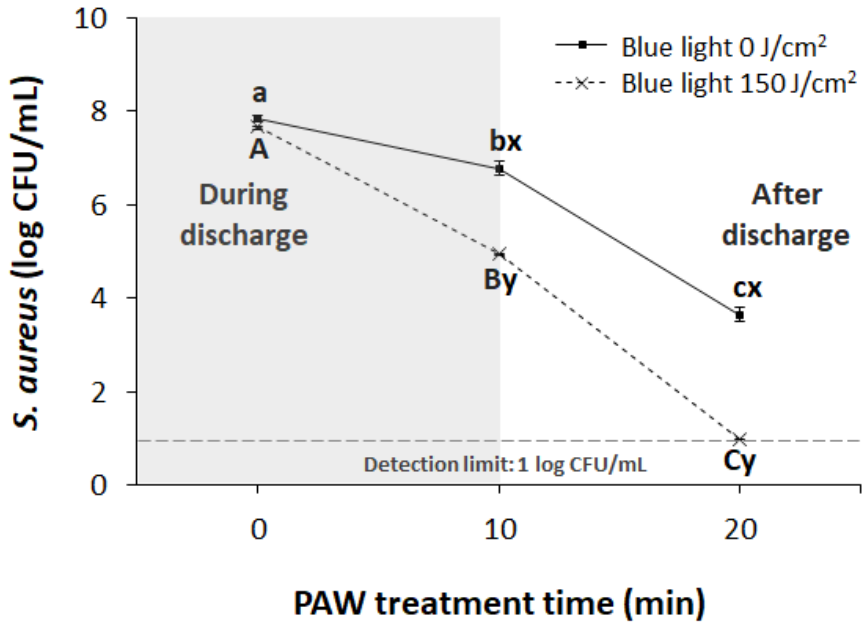


Figure 27. Surviving population (log CFU/mL) of *S. aureus* after single or combined treatment with 466 nm blue light (150 J/cm$^2$) and PAW (10 min).

The bacteria were left for 10 min after the discharge was terminated.

Error bars denote standard deviation.

$^{a\text{-}c}$Different letters within the same blue light treatment group indicate significant differences ($p$<0.05).

$^{A\text{-}C}$Different letters within the same blue light treatment group indicate significant differences ($p$<0.05).

$^{x,y}$Different letters within the same PAW treatment time group indicate significant differences ($p$<0.05).

*4.3.4. Leakage of intracellular nucleic acids and proteins*

The leakage of intracellular nucleic acids and proteins from bacterial cells is a general indicator of cell membrane damage in microorganism (Xiang et al., 2018). As shown in Fig. 28, the untreated bacteria (control) showed the lowest absorbance values at 260 and 280 nm, indicating that there were relatively lower extracellular nucleic acid and protein levels in the bacterial suspension than those in other treated bacteria. Both single and combined blue light (150 J/cm$^2$) and plasma (10 min) treatment resulted in a rapid increase in the absorbance values at 260 and 280 nm. Individual plasma treatment (10 min) against *S. aureus* resulted in an approximately 1.07 log reduction (Fig. 27). However, individual blue light treatment (150 J/cm$^2$) also resulted in intracellular nucleic acid and protein leakage, although it did not show a significant bactericidal effect (Fig. 27). These results indicate the possibility of damage to microbial cell membranes caused by blue light at levels that do not cause bactericidal action. Depending on the results (Fig. 28), the release of small or large cytoplasmic components of cells by structural and functional perturbation of bacterial membranes may be proposed (Ajiboye et al., 2016). The combined treatment of blue light (150J/cm$^2$) and plasma (10 min), which had the best bactericidal effect, resulted in the highest absorbance values at both 260 and 280 nm, indicating relatively large amounts of intracellular nucleic acid and protein leakage.

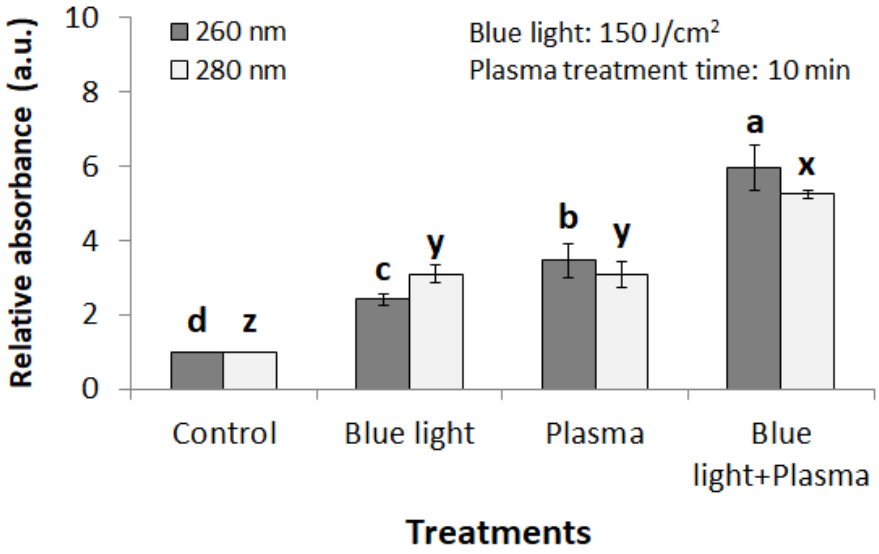


Figure 28. The absorbance intensities of intracellular nucleic acid (260 nm) and protein (280 nm) leakage from *S. aureus* after single or combined treatment with 466 nm blue light (150 J/cm$^2$) and PAW (10 min).

Error bars denote standard deviation.

[a-d]Different letters within the same wavelengths differ significantly ($p$<0.05).

[x-z]Different letters within the same wavelengths differ significantly ($p$<0.05).

*4.3.5. Determination of bacterial cell membrane damage*

The fluorescence images and corresponding transmission images of *S. aureus* are shown in Fig. 29. Transmission images can be used to indirectly identify the proportion of fluorescent cells to the whole cell in the corresponding section. SYTOX$^{TM}$ green can be used to verify the perturbation of cell membranes as it binds with nucleic acids upon passing through damaged cell membranes (McKenzie et al., 2016). Treatment with 150 J/cm$^2$ of blue light increased the number of fluorescence signals from the entire cell compared to that of the control group. Hui et al. (2020) suggested that the 460 nm laser treatment (46 J/cm$^2$) for *S. aureus* can increase cell membrane permeability via STX photolysis, allowing small-molecule antibiotics to penetrate into the cell. This is also be supported by the changes in the value of 460 nm absorbance of the STX extract and *S. aureus* cells after 150 J/cm$^2$ blue light treatment (Fig. 25 and 26).

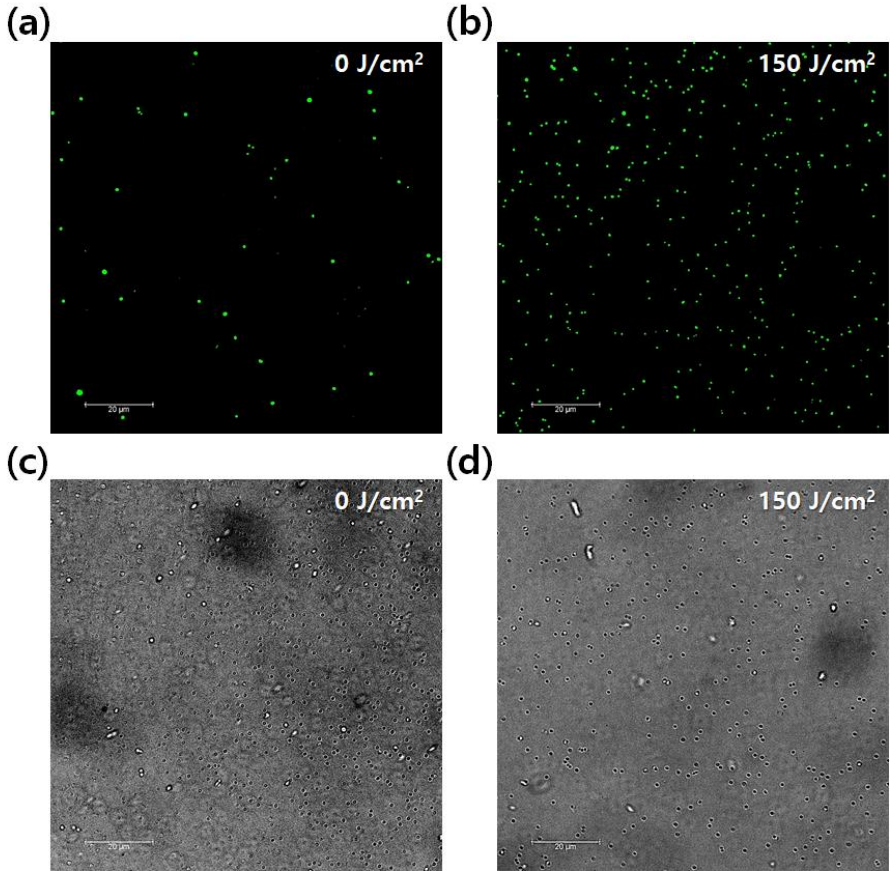


Figure 29. Confocal fluorescence images (upper) and corresponding transmission images (bottom) of intracellular uptake of SYTOX™ green by *S. aureus* cells without (a, c) or with (b, d) 466 nm blue light treatment (150 J/cm$^2$).

*4.3.6. Bactericidal effects of blue light and PAW on stainless steel coupons*

A stainless steel coupon was used as a model to assess the practicality of the synergic bactericidal action of blue light and PAW. When the coupon was treated with plasma alone for 15 min, no significant bactericidal effect on *S. aureus* cells present on the coupon was observed (Fig. 30). Unlike the bacterial suspension, bacterial cells inoculated on the surface of a coupon do not float in the solution and have relatively less chance of contact with the reactive species in PAW, especially in the case of some short-lived reactive species that have a low penetration depth and decompose in a short period of time (Burns et al., 2012; Kondeti et al., 2018; Møller et al., 2007). At this time, long-lived reactive species, a variety of secondary products, should contribute to bactericidal action (Kondeti et al., 2018); however, a single treatment of plasma for 15 min did not show a valid bactericidal effect under the current conditions. Nevertheless, the number of *S. aureus* cells on the coupon significantly reduced by 3.33 log CFU/cm$^2$ when 150 J/cm$^2$ of blue light was applied to the inoculated coupon prior to the 15 min of plasma treatment ($p$<0.05). These results suggest that the sensitivity of *S. aureus* cells to the reactive species increased upon treatment with 466 nm blue light (150 J/cm$^2$), which in turn could have shown a synergistic bactericidal effect with PAW.

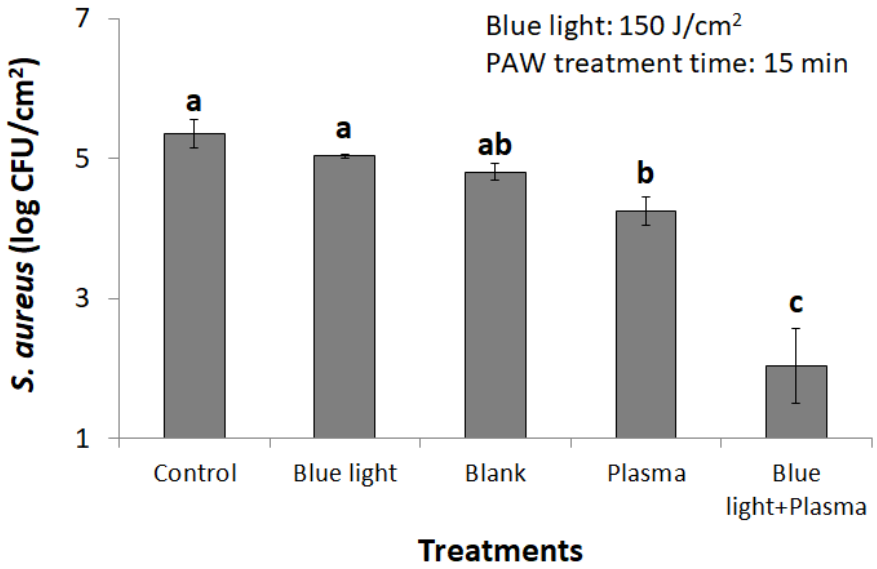


Figure 30. Surviving population (log CFU/cm$^2$) of *S. aureus* on stainless steel surface (2.0 × 2.0 × 0.1 cm) after single or combined treatment of 466 nm blue light (150 J/cm$^2$) and PAW (15 min).

Blank: Immersion treatment excluding plasma discharge.

Error bars denote standard deviation.

[a-c]Different letters indicate significant differences ($p$<0.05).

### 4.4. Conclusion

This study was conducted to investigate whether blue LED treatment could induce STX photolysis in *S. aureus* and consequently promote the bactericidal effect of PAW. The 466 nm blue light treatment for STX extract induced photolysis in a dose-dependent manner, resulting in the perturbation of the *S. aureus* cell membrane. The combined treatment of blue light and PAW for both *S. aureus* suspension and *S. aureus*-inoculated stainless steel surfaces showed a synergistic bactericidal effect, unlike that by the treatment with PAW alone.

**References**

Ajiboye, T. O., Mohammed, A. O., Bello, S. A., Yusuf, I. I., Ibitoye, O. B., Muritala, H. F., & Onajobi, I. B. (2016). Antibacterial activity of *Syzygium aromaticum* seed: Studies on oxidative stress biomarkers and membrane permeability. *Microbial Pathogenesis*, *95*, 208-215.

Amin, R. M., Bhayana, B., Hamblin, M. R., & Dai, T. (2016). Antimicrobial blue light inactivation of *Pseudomonas aeruginosa* by photo-excitation of endogenous porphyrins: In vitro and in vivo studies. *Lasers in Surgery and Medicine*, *48*, 562-568.

Baek, K. H., Heo, Y. S., Park, J. Y., Kang, T., Lee, Y. E., Lim, J., Kim, S. B., & Jo, C. (2020a). Inactivation of *Salmonella* Typhimurium by non-thermal plasma bubbles: Exploring the key reactive species and the influence of organic matter. *Foods*, *9*, 1689.

Baek, K. H., Yong, H. I., Yoo, J. H., Kim, J. W., Byeon, Y. S., Lim, J., Yoon, S. Y., Ryu, S., & Jo, C. (2020b). Antimicrobial effects and mechanism of plasma activated fine droplets produced from arc discharge plasma on planktonic *Listeria monocytogenes* and *Escherichia coli* O157:H7. *Journal of Physics D: Applied Physics*, *53*, 124002.

Bekeschus, S., Favia, P., Robert, E., & von Woedtke, T. (2019). White paper on plasma for medicine and hygiene: Future in plasma health sciences. *Plasma Processes and Polymers*, *16*(1), 1800033.

Ben Belgacem, Z., Carré, G., Charpentier, E., Le-Bras, F., Maho, T., Robert, E., Pouvesle, J. –M., Polidor, F., Gangloff, S. C., Boudifa, M., & Gelle, M. P. (2017). Innovative non-thermal plasma disinfection process inside

sealed bags: Assessment of bactericidal and sporicidal effectiveness in regard to current sterilization norms. *PLoS One*, *12*(6), e0180183.

Brodowska, A. J., Nowak, A., & Śmigielski, K. (2018). Ozone in the food industry: Principles of ozone treatment, mechanisms of action, and applications: An overview. *Critical Reviews in Food Science and Nutrition*, *58*(13), 2176-2201.

Burns, J. M., Cooper, W. J., Ferry, J. L., King, D. W., DiMento, B. P., McNeill, K., Miller, C. J., Miller, W. L., Peake, B. M., Rusak, S. A., Rose, A. L., & Waite, T. D. (2012). Methods for reactive oxygen species (ROS) detection in aqueous environments. *Aquatic Sciences*, *74*, 683-734.

Chen, F., Di, H., Wang, Y., Cao, Q., Xu, B., Zhang, X., Yang, N., Liu, G., Yang, C. -G., Xu, Y., Jiang, H., Lian, F., Zhang, N., Li, J., & Lan, L. (2016). Small-molecule targeting of a diapophytoene desaturase inhibits *S. aureus* virulence. *Nature Chemical Biology*, *12*(3), 174.

Choi, N. –Y., Baek, S. –Y., Yoon, J. –H., Choi, M. –R., Kang, D. –H., & Lee, S. –Y. (2012). Efficacy of aerosolized hydrogen peroxide-based sanitizer on the reduction of pathogenic bacteria on a stainless steel surface. *Food Control*, *27*, 57-63.

Do, J. S., & Bang, W. S. (2013). Bactericidal effect of 461 nm blue light emitting diode on pathogenic bacteria. *Korean Journal of Food Preservation*, *20*, 419-423.

Dong, P. T., Mohammad, H., Hui, J., Leanse, L. G., Li, J., Liang, L., Dai, T., Seleem, M. N., & Cheng, J. X. (2019). Photolysis of staphyloxanthin in

methicillin-resistant *Staphylococcus aureus* potentiates killing by reactive oxygen species. *Advanced Science*, *6*, 1900030.

El Shaer, M., Eldaly, M., Heikal, G., Sharaf, Y., Diab, H., Mobasher, M., & Rousseau, A. (2020). Antibiotics degradation and bacteria inactivation in water by cold atmospheric plasma discharges above and below water surface. *Plasma Chemistry and Plasma Processing, 40,* 971-983.

Fetsch, A., & Johler, S. (2018). *Staphylococcus aureus* as a foodborne pathogen. *Current Clinical Microbiology Reports*, *5*, 88-96.

Guzel-Seydim, Z. B., Greene, A. K., & Seydim, A. C. (2004). Use of ozone in the food industry. *LWT-Food Science and Technology*, *37*(4), 453-460.

Hu, W., Li, C., Dai, J., Cui, H., & Lin, L. (2019). Antibacterial activity and mechanism of Litsea cubeba essential oil against methicillin-resistant *Staphylococcus aureus* (MRSA). *Industrial Crops and Products*, *130*, 34-41.

Hui, J., Dong, P. T., Liang, L., Mandal, T., Li, J., Ulloa, E. R., Zhan, Y., Jusuf, S., Zong, C., Seleem, M, N., Liu, G. Y., Cui, Q., & Liu, G. Y. (2020). Photo-disassembly of membrane microdomains revives conventional antibiotics against MRSA. *Advanced Science*, *7*, 1903117.

Hyun, J. E., Moon, S. K., & Lee, S. Y. (2020). Antibacterial activity and mechanism of 460–470 nm light-emitting diodes against pathogenic bacteria and spoilage bacteria at different temperatures. *Food Control*, 107721.

Ji, S. H., Ki, S. H., Ahn, J. H., Shin, J. H., Hong, E. J., Kim, Y. J., & Choi, E. H. (2018). Inactivation of *Escherichia coli* and *Staphylococcus aureus* on

contaminated perilla leaves by dielectric barrier discharge (DBD) plasma treatment. *Archives of Biochemistry and Biophysics*, *643*, 32-41.

Jusuf, S., Hui, J., Dong, P. T., & Cheng, J. X. (2020). Staphyloxanthin photolysis potentiates low concentration silver nanoparticles in eradication of methicillin-resistant *Staphylococcus aureus*. *The Journal of Physical Chemistry C*, *124*, 5321-5330.

Kim, D. –K., & Kang, D. –H. (2020). Effect of surface characteristics on the bactericidal efficacy of UVC LEDs. *Food Control*, *108*, 106869.

Kondeti, V. S. K., Phan, C. Q., Wende, K., Jablonowski, H., Gangal, U., Granick, J. L., Hunter, R. C., & Bruggeman, P. J. (2018). Long-lived and short-lived reactive species produced by a cold atmospheric pressure plasma jet for the inactivation of *Pseudomonas aeruginosa* and *Staphylococcus aureus*. *Free Radical Biology and Medicine*, *124*, 275-287.

Krewing, M., Stepanek, J. J., Cremers, C., Lackmann, J. W., Schubert, B., Müller, A., Awakowicz, P., Leichert, L. I. O., Jakob, U., & Bandow, J. E. (2019). The molecular chaperone Hsp33 is activated by atmospheric-pressure plasma protecting proteins from aggregation. *Journal of the Royal Society Interface*, *16*, 20180966.

Liao, X., Cullen, P. J., Liu, D., Muhammad, A. I., Chen, S., Ye, X., Wang, J., & Ding, T. (2018). Combating *Staphylococcus aureus* and its methicillin resistance gene (mecA) with cold plasma. *Science of the Total Environment*, *645*, 1287-1295.

Liao, X., Xiang, Q., Cullen, P. J., Su, Y., Chen, S., Ye, X., ... & Ding, T. (2020). Plasma-activated water (PAW) and slightly acidic electrolyzed

water (SAEW) as beef thawing media for enhancing microbiological safety. *LWT*, *117*, 108649.

Liu, D. X., Liu, Z. C., Chen, C., Yang, A. J., Li, D., Rong, M. Z., Chen, H. L., & Kong, M. G. (2016). Aqueous reactive species induced by a surface air discharge: Heterogeneous mass transfer and liquid chemistry pathways. *Scientific Reports*, *6*, 23737.

Liu, Y., Shen, X., Sun, J., Li, P., & Zhang, A. (2019). Treatment of aniline contaminated water by a self-designed dielectric barrier discharge reactor coupling with micro-bubbles: optimization of the system and effects of water matrix. *Journal of Chemical Technology & Biotechnology*, *94*, 494-504.

Mai-Prochnow, A., Clauson, M., Hong, J., & Murphy, A. B. (2016). Gram positive and Gram negative bacteria differ in their sensitivity to cold plasma. *Scientific Reports*, *6*, 38610.

McKenzie, K., Maclean, M., Grant, M. H., Ramakrishnan, P., MacGregor, S. J., & Anderson, J. G. (2016). The effects of 405 nm light on bacterial membrane integrity determined by salt and bile tolerance assays, leakage of UV-absorbing material and SYTOX green labelling. *Microbiology*, *162*, 1680.

Ni, L., Zheng, W., Zhang, Q., Cao, W., & Li, B. (2016). Application of slightly acidic electrolyzed water for decontamination of stainless steel surfaces in animal transport vehicles. *Preventive Veterinary Medicine*, *133*, 42-51.

Møller, I. M., Jensen, P. E., & Hansson, A. (2007). Oxidative modifications to cellular components in plants. *Annual Review of Plant Biology*, *58*, 459-481.

Park, S., Choe, W., & Jo, C. (2018). Interplay among ozone and nitrogen oxides in air plasmas: Rapid change in plasma chemistry. *Chemical Engineering Journal*, *352*, 1014-1021.

Royintarat, T., Choi, E. H., Boonyawan, D., Seesuriyachan, P., & Wattanutchariya, W. (2020). Chemical-free and synergistic interaction of ultrasound combined with plasma-activated water (PAW) to enhance microbial inactivation in chicken meat and skin. *Scientific Reports*, *10*, 1-14.

Wang, J., Han, R., Liao, X., & Ding, T. (2020). Application of Plasma-activated water (PAW) for mitigating methicillin-resistant *Staphylococcus aureus* (MRSA) on cooked chicken surface. *LWT*, 110465.

Xiang, Q., Kang, C., Niu, L., Zhao, D., Li, K., & Bai, Y. (2018). Antibacterial activity and a membrane damage mechanism of plasma-activated water against *Pseudomonas deceptionensis* CM2. *LWT*, *96*, 395-401.

Xiang, Q., Kang, C., Zhao, D., Niu, L., Liu, X., & Bai, Y. (2019). Influence of organic matters on the inactivation efficacy of plasma-activated water against *E. coli* O157:H7 and *S. aureus*. *Food Control*, *99*, 28-33.

Xu, Z., Cheng, C., Shen, J., Lan, Y., Hu, S., Han, W., & Chu, P. K. (2018). In vitro antimicrobial effects and mechanisms of direct current air-liquid discharge plasma on planktonic *Staphylococcus aureus* and *Escherichia coli* in liquids. *Bioelectrochemistry*, *121*, 125-134.

Yang, Y., Wang, H., Zhou, H., Hu, Z., Shang, W., Rao, Y., Peng, H., Zheng, Y., Hu, Q., Zhang, R., Rao, X., & Luo, H. (2020). Protective effect of the golden staphyloxanthin biosynthesis pathway on *Staphylococcus aureus* under cold atmospheric plasma treatment. *Applied and Environmental Microbiology*, *86*, e01998-19.

Yoo, J. H., Baek, K. H., Heo, Y. S., Yong, H. I., & Jo, C. (2020). Synergistic bactericidal effect of clove oil and encapsulated atmospheric pressure plasma against *Escherichia coli* O157:H7 and *Staphylococcus aureus* and its mechanism of action. *Food Microbiology*, *93*, 103611.

Zhang, M., Oh, J. K., Huang, S. –Y., Lin, Y. –R., Liu, Y., Mannan, M. S., Cisneros-Zevallos, L., & Akbulut, M. (2015). Priming with nano-aerosolized water and sequential dip-washing with hydrogen peroxide: An efficient sanitization method to inactivate *Salmonella* Typhimurium LT2 on spinach. *Journal of Food Engineering*, *161*, 8-15.

Zhao, Y., Chen, R., Tian, E., Liu, D., Niu, J., Wang, W., Qi, Z., Xia, Y., Song, Y., & Zhao, Z. (2018). Plasma-activated water treatment of fresh beef: Bacterial inactivation and effects on quality attributes. *IEEE Transactions on Radiation and Plasma Medical Sciences*, *4*, 113-120.

Zhou, R., Zhou, R., Wang, P., Luan, B., Zhang, X., Fang, Z., Xian, Y., Lu, X., Ostrikov, K. K., & Bazaka, K. (2019). Microplasma bubbles: reactive vehicles for biofilm dispersal. *ACS Applied Materials & Interfaces*, *11*, 20660-20669.

Zhou, R., Zhou, R., Wang, P., Xian, Y., Mai-Prochnow, A., Lu, X., Cullen, P. J., Ostrikov, K. K., & Bazaka, K. (2020). Plasma-activated water:

generation, origin of reactive species and biological applications. *Journal of Physics D: Applied Physics*, *53*, 303001

# Chapter V.

# Overall conclusion

PAW could be applied by 1) spraying with arc discharge plasma or 2) bubbling with non-thermal plasma, showing significant bactericidal effect against typical pathogenic microorganisms such as *L. monocytogenes, E. coli* O157:H7, and *S.* Typhimurium. Therefore, PAW has the potential to be applied to various food-related materials or environments where plasma is difficult to access, such as deep inside pipes and areas of equipment or devices. In addition, another non-thermal technique, blue light, could provide synergistic antibacterial activity of PAW against *S. aureus*, by disturbing internal antioxidative mechanism to the pathogen. Such light-based technology has the potential to contribute to the enhancing the utilization of PAW in a wide range without environmental constraints, such as food shelves, disinfection chambers, or slaughterhouses. PAW has different bactericidal efficiency and mechanism for control pathogenic microorganisms. Understanding the mechanism of bactericidal functions both by PAW and other techniques for synergy is important to apply PAW for industry as a promising sanitation method.

# Overall summary in Korean

최근 살균 및 소독제로서 플라즈마 활성수를 다양한 형태로 응용하는 연구들이 진행되고 있다. 특히 실용적인 측면에서 플라즈마 활성수를 스프레이 및 버블 등의 형태로 응용하거나 초음파와 같은 다른 기술들을 접목하여 살균 효율을 증진시키기 위해 노력하고 있다. 따라서, 본 연구에서는 플라즈마 활성수의 활용성을 증진시키기 위한 응용과 각각의 살균 기작을 구명하기 위하여 1) 아크 방전 플라즈마에 의해 생성된 플라즈마 활성 분무액의 병원성 미생물 살균 효과 및 살균 기작을 조사하고, 2) 플라즈마 버블의 살모넬라 티피뮤리움(*Salmonella* Typhimurium) 살균에 기여하는 핵심 활성종과 유기물의 영향을 확인하고, 3) 스테인리스 강 표면에 접종된 황색포도상구균(*Staphylococcus aureus*)에 대하여 청색광과 플라즈마 활성수가 시너지 살균작용을 나타낼 수 있는지를 검증하였다.

실험 I에서는 아크 방전 플라즈마에 의해 생성된 플라즈마 활성 분무액의 리스테리아 모노사이토제네스(*Listeria monocytogenes*) 및 대장균 O157:H7 (*Escherichia coli* O157:H7)에 대한 살균 효과와 살균 기작을 조사하였다. 플라즈마 방전을 위해 0.9% NaCl (w/v) 용액을 급수로 사용하였다. 플라즈마 활성 분무액은 주로 과산화수소와 하이포아염소산이온으로 구성되어 병원성 미생물에 대한 살균작용에 기여하는 것으로 사료된다. *L. monocytogenes*와 *E. coli* O157:H7을 각각 플라즈마 활성 분무액에 반응시킬 경우 5분 이내에 각각 3 및 4 log 수준만큼 살균되었다. 반면, 플라즈마 활성 분무액을 1분 처리하였을 경우 *L. monocytogenes*는 0.58 log 살균되었으나, *E. coli* O157:H7은

4.13 log 살균되어 서로 다른 살균양상을 나타내었다. DNA-결합 형광 염료인 SYTO 9 및 propidium iodide (PI)를 사용하여 미생물 세포막의 온전성 변화를 측정한 결과, 플라즈마 활성 분무액을 5분 처리하였을 경우 대다수의 *L. monocytogenes* 및 *E. coli* O157:H7 세포들이 PI와 반응하여 세포벽과 세포막이 손상되었음을 확인할 수 있었다. 반면, 플라즈마 활성 분무액을 1분 처리하였을 경우에는 *E. coli* O157:H7 세포에 비하여 *L. monocytogenes* 세포의 세포막 손상이 적었다. 투과전자현미경 분석 결과 *L. monocytogenes* 및 *E. coli* O157:H7 모두 플라즈마 활성 분무액 처리에 의하여 세포 내 물질들이 일부 변성되거나 세포 외부로 누출되는 현상의 형태학적 변화를 확인할 수 있었다. 플라즈마 활성 분무액 내 화학종들이 세포 외 구조물을 통과하거나 손상을 입혀 세포 내 물질들에 영향을 미칠 수 있으며 *L. monocytogenes*가 *E. coli* O157:H7과 비교하여 상대적으로 플라즈마 활성 분무액에 덜 민감한 것으로 사료된다.

실험 II에서는 저온 플라즈마 버블의 *S.* Typhimurium 살균작용에 기여하는 핵심 활성종과 유기물의 영향을 조사하였다. 플라즈마는 유전체 장벽 방전을 통해 발생시켰으며, 오존이 주요하게 발생되어 버블의 형태로 용액(400 mL)에 주입되었다. *S.* Typhimurium 생균수는 플라즈마 버블의 처리시간이 늘어남에 따라 유의적으로 감소하여 처리시간 5분 기준으로 약 5.29 log 살균되었다. 핵심 활성종을 구명하기 위하여 오존가스 제거 장치(ozone destruction unit)와 유리기 포촉제(radical scavenger)를 사용하여 검증시험을 진행하였다. 실험 결과, *S.* Typhimurium 살균작용에는 일중항산소가 주요하게 기여하고, 이러한 일중항산소의 생성에는 오존으로부터 생성되는 초과산화물 음이온 라디칼의 존재가 필수적인 것으로 사료된다. 육추출물과 펩톤으

로 구성된 유기물을 농도별(0, 0.005, 0.05, 0.1, 그리고 0.5 g/L)로 준비하여 *S.* Typhimurium을 접종한 후 플라즈마 버블을 5, 10, 15, 20, 25, 그리고 30분 처리한 결과 살균 효율은 유기물 농도 의존적으로 감소하였으나, 일부 농도 조건을 제외하면 더 긴 처리시간을 통하여 성공적인 살균작용을 나타낼 수 있었다.

실험 III에서는 스테인리스 강 표면에 접종된 *S. aureus*에 대하여 청색광 처리가 플라즈마 활성수의 살균 효율을 증진시킬 수 있는지를 조사하였다. 청색광 처리는 발광 다이오드(중심파장, 466 nm; 광도, 18.74 mW/cm$^2$)를 이용하였고, 플라즈마 활성수 처리는 캡슐화된 대기압 플라즈마 발생기(2.2 kHz, 4.2 kV)를 이용하였다. 스타필로잔틴에 청색광을 처리하였을 경우 460 nm 흡광도 값은 조사량(0, 30, 60, 90, 그리고 150 J/cm$^2$)이 증가할수록 유의적으로 감소하였으며, 150 J/cm$^2$ 조건에서 완전히 투명해졌다. 청색광(150 J/cm$^2$)과 플라즈마 활성수(10분)를 *S. aureus* 현탁액에 복합 처리하였을 경우 약 2.70 log 살균되었으며 이는 플라즈마 활성수 단일 처리군과 비교하여 약 40배 수준이었다. 또한, 플라즈마 방전 종료 후 10분간 방치시킨 결과 *S. aureus* 생균수는 복합 처리군에서 검출되지 않아(검출한계, 1 log CFU/mL) 대조군 대비 6.66 log 이상의 살균효과를 나타내었다. *S. aureus* 세포에 대한 청색광(150 J/cm$^2$) 단일처리에 의해 260 및 280 nm 흡광도 값이 증가하여 세포막 섭동에 의한 세포 내 물질의 누출 가능성을 확인하였으며 손상된 세포막만 통과할 수 있는 SYTOX$^{TM}$ green의 침투에 의한 형광 신호의 증가를 마찬가지로 확인할 수 있었다. *S. aureus*가 접종된 스테인리스 강에 대해서도 마찬가지로 청색광(150 J/cm$^2$)과 플라즈마 활성수(15분) 복합 처리에 의한 시너지 살균 효과를 확인할 수 있었다.

본 연구 결과, 병원성 미생물을 제어하기 위하여 플라즈마 활성수를 분무액 및 버블의 형태로 응용할 수 있었고, 또 다른 비가열 기술인 청색광에 응용하여 플라즈마 활성수의 활용성 증진의 가능성을 확인하였고, 각각의 살균 기작을 검증하였다. 플라즈마 활성수는 다양한 형태로 응용될 수 있으며, 병원성 미생물에 대한 플라즈마 활성수의 명확한 살균 기작을 구명함으로써 식품 산업을 포함하여 다양한 분야에서 유망한 살균·소독제로 활용될 수 있을 것으로 사료된다.

# 감사의 글

길다면 길고, 짧다면 짧은 4년 간의 박사과정을 마무리하게 되었습니다. 많은 분들의 도움이 있었기에 가능한 일이었다고 생각하며 이 기회를 빌어 감사의 마음을 전하고자 합니다.

우선, 학위과정 동안 저를 가장 많이 배려해주시고, 또 지도해주신 조철훈 교수님께 존경을 담아 감사의 인사를 올립니다. 교수님께는 학문과 더불어 인생을 살아가는데 있어서 마땅히 배워야 할 많은 것들에 대하여 가르침을 받을 수 있었습니다. 또한, 석사과정 때 저를 지도해주셨던 이성기 교수님의 가르침이 없었다면 저는 박사과정이라는 크나큰 언덕을 오르지조차 못하였을 것이라고 생각합니다. 앞으로도 두 지도교수님의 제자로서 부끄럽지 않은 연구자가 되도록 노력하겠습니다. 코로나로 바쁘고 힘들었을 시기에도 저의 졸업논문을 적극적으로 심사해주신 백명기 교수님, 김영훈 교수님, 김갑돈 교수님, 충남대 정사무엘 교수님께도 깊은 감사의 인사를 올립니다. 교수님들의 세심한 지도를 통해 지금의 학위 논문이 완성될 수 있었습니다. 석사과정 때부터 저를 응원해주셨던 순천대 남기창 교수님, 강원대 장애라 교수님, 건국대 안병기 교수님께 감사 드립니다. 또한, 학부생 시절에 저에게 아낌없이 조언을 해주셨던 강원대 오상집 교수님, 성경일 교수님, 송영한 교수님, 신종서 교수님, 라창식 교수님, 박규현 교수님께 이 기회를 빌어 감사의 인사를 올립니다. 여러 교수님들의 격려와 가르침을 통해 지금의 자리에 도달할 수 있었습니다.

대학원 기간 동안 많은 도움을 주신 분들께도 감사의 마음을 전

합니다. 먼저, 서울대학교 동물성식품학 연구실 모두에게 감사 드립니다. 임동균 박사님, 최주희 박사님, 조은영 선생님, 최은지 선생님을 비롯하여 현정 선배, 해인 선배, 현철, 동진, 다겸, 정연, 소연, 정민, 범진, 상희, 윤지원, 민수, 선진, 지현, 김지원, 예슬, 동헌, 태민, 정아, 민경, 예은, 현준, 성수, 현영, 두연, 조현 모두를 결코 잊지 않겠습니다. 또한, 연구실 생활을 함께 하지 못하였으나 항상 아낌없이 응원해주신 김현주 박사님께 진심으로 감사 드립니다. 학부 동기이자 반추실에서 박사과정을 마무리 중인 정다진솔에게도 고마운 마음을 전합니다. 처음 서울대학교에 진학하였을 때 많은 위로가 되었습니다. 박사과정 중에 함께 연구한 핵융합연구소 김성봉 부장님, 유승민 팀장님을 비롯하여 박상후 연구원님, 박승일 연구원님, 송종석 연구원님, 윤성영 연구원님, 임정현 연구원님, 변용성 연구원님, 홍은정 연구원님, 카이스트 진우씨, 순천대 지영씨, 경기대 송원재 교수님, 위생학실 김도균 박사님, 진영씨, 강원대 혜진, 희진에게도 감사 드립니다.

마지막으로 제가 끝까지 버틸 수 있도록 저를 아껴주시고, 지지해주신 가족들과 친구들에게 진심을 담아 감사의 인사를 올립니다. 어려서부터 저의 모범이 되어주신 부모님과 세상에 단 하나뿐인 형에게 감사합니다. 지금도 집에 돌아오기만을 애타게 기다리고 있을 반려견 해피 정말 너무 사랑해요. 고등학생 때부터 옆에서 힘이 되어준 준재, 상윤, 진영과 더불어 학부 동기인 재영, 재성, 병진, 윤겸, 정훈 모두에게 이 영광을 나누고 싶습니다. 앞으로도 더욱 멋진 연구자가 되도록 정진하겠습니다. 감사합니다.

2021 년 2 월

백 기 호 드림